UNIVERSITY OF CALIFORNIA, SAN DIEGO

Multi-scale Interaction of Drift Wave Turbulence with Large Scale Shear Flows

A dissertation submitted in partial satisfaction of the requirements for the degree of

Doctor of Philosophy

in

Physics

by

Christopher J. McDevitt

Committee in charge:

Patrick H. Diamond, Chair
Glenn R. Ierley
Michael L. Norman
Thomas M. O'Neil
Paolo Padoan
George R. Tynan

2008

The dissertation of Christopher J. McDevitt is approved, and it is acceptable in quality and form for publication on microfilm:

_____

_____

_____

_____

_____

_____

Chair

University of California, San Diego

2008

Contents

List of Figures

List of Tables

Acknowledgements

I gratefully acknowledge the support of my thesis advisor Dr. Patrick Diamond, whose guidance, patience and insistence on understanding a problem from multiple perspectives have been indispensable throughout the completion of this thesis, as well as to my growth as a physicist.

I would also like to thank Dr. Ozgur Gurcan for invaluable help in the early stages of my graduate career, as well as for always being available to provide useful insights and constructive criticism throughout the completion of my thesis work. Also, I would like to show my appreciation to Shane Keating and Dr. Lara Silvers for many stimulating conversations on broader aspects of my thesis topic.

Part of Chapter 2 of this dissertation has been published in Physics of Plasmas, C. J. McDevitt and P. H. Diamond, **14**, 112306 (2007). Chapter 3 has been published in Physics of Plasmas, C. J. McDevitt and P. H. Diamond, **13**, 032302 (2006). C. J. McDevitt was the primary investigator and author of these papers.

Part of Chapter 4 of this dissertation has been published in Physics of Plasmas, P. H. Diamond, C. J. McDevitt, O. D. Gurcan, T. S. Hahm and V. Naulin, **15**, 012303 (2008). C. J. McDevitt was a contributing author to this paper.

Vita, Publications and Fields of Study

Vita

April 1980	Born, San Diego, California
2002	B.A. University of California, Santa Cruz
2002-2003	Teaching Assistant, University of California, San Diego
2003-2008	Research Assistant, University of California, San Diego
2004	M.S. University of California, San Diego
2008	Ph.D. University of California, San Diego

Publications

P. H. Diamond, C. J. McDevitt, O. D. Gurcan, T. S. Hahm and V. Naulin, "Transport of parallel momentum by collisionless drift wave turbulence," Phys. Plasmas **15**, 012303 (2008)

C. J. McDevitt and P. H. Diamond, "Low-q resonances, transport barriers, and secondary electrostatic convective cells," Phys. Plasmas **14**, 112306 (2007)

C. J. McDevitt and P. H. Diamond, "Multiscale interaction of a tearing mode with drift wave turbulence: A minimal self-consistent model," Phys. Plasmas **13**, 032302 (2006)

O. D. Gurcan, P. H. Diamond, C. J. McDevitt and M. Malkov, "Progress in Understanding Multi-Scale Dynamics of Drift Wave Turbulence," Proceedings of the 21st IAEA International Conference on Fusion Energy, Chengdu, China, 2006 (IAEA, Vienna, 2006)

B. Coppi, C. Crabtree, P. H. Diamond, O. G. Gurcan, C. J. McDevitt and V. Roytershteyn, "Interaction of Drift-Tearing (Mesoscopic) Modes with Coherent and Turbulent Microscopic Structures," Proceedings of the 21st IAEA International Conference on Fusion Energy, Chengdu, China, 2006 (IAEA, Vienna, 2006)

Fields of Study

Major Field: Physics

Studies in Theoretical Mechanics
Professor Patrick Diamond

Studies in Mathematical Physics
Professor Donald Fredkin

Studies in Quantum Mechanics
Professor Lu Jeu Sham

Studies in Advanced Classical Electrodynamics
Professor Thomas O'Neil

Studies in Equilibrium Statistical Mechanics
Professor Terence Hwa

Studies in Non-equilibrium Statistical Mechanics
Professor Terence Hwa

Studies in Plasma Physics
Professors Thomas O'Neil, Vitali Shapiro and Ronald Waltz

Studies in Statistical Field Theory
Professor Terence Hwa

Studies in Nonlinear and Non-equilibrium Dynamics of Physical Systems
Professor Patrick Diamond

Studies in Physics of Turbulence
Professor Paolo Padoan

Studies in Nonlinear Plasma Theory
Professor Patrick Diamond

Studies in Galaxies and Galactic Dynamics
Professor Patrick Diamond

ABSTRACT OF THE DISSERTATION

Multi-scale Interaction of Drift Wave Turbulence with Large Scale Shear Flows

by

Christopher J. McDevitt

Doctor of Philosophy in Physics

University of California, San Diego, 2008

Professor Patrick H. Diamond, Chair

Multi-scale methods are utilized within the context of strongly magnetized plasmas to describe the interaction of drift wave turbulence with large scale flow structures. The specific contexts treated correspond to transport barrier formation, magnetic island evolution in the presence of drift wave turbulence, and plasma rotation. Emphasis is placed on identifying critical feedback mechanisms via the study of simple, reduced models, rather than the detailed description of isolated components of the system.

In Chapter 2 a two component self-consistent model is derived to investigate a novel mechanism of transport barrier formation. It is found that intense cellular flow, driven by modulational instability of the background turbulence provides a viable candidate mech-

anism for triggering transport barrier formation in regimes of weak magnetic shear. Similarly, the nonlinear modification of the drift wave phase space topology by the cellular flow is investigated. The presence of a weak non-integrable perturbation in the effective Hamiltonian of the drift wave turbulence, induced by the non-axisymmetric component of the cellular flow, is found to circumvent nonlinear wave trapping as a means of quenching the secondary instability drive of the large scale flow.

In Chapter 3, the interaction of a tearing mode with drift wave turbulence is discussed. Wave kinetics and adiabatic theory are utilized to treat the feedback of tearing mode flows on the drift wave turbulence. The stresses exerted by the self-consistently evolved drift wave population density on the tearing mode are calculated by mean field methods. The principal effect of the drift waves is to pump the resonant low-m mode via a negative viscosity, consistent with the classical notion of an inverse cascade in quasi 2-D turbulence.

In Chapter 4, the multi-scale methods utilized above are extended to describe the transport of parallel momentum. The primarily fluid description employed above is extended to include momentum exchange between waves and resonant particles. A quasi-linear momentum conservation theorem is proven, demonstrating that the total momentum flux can be decomposed into wave and resonant particle fluxes. Quasi-linear expressions for the radial transport of parallel momentum induced both by waves and resonant particles are derived, providing a comprehensive quasi-linear description of parallel momentum transport induced by electrostatic drift wave turbulence.

Chapter 1

General Introduction

Magnetic fusion corresponds to a potentially abundant and environmentally benign source of energy free from many of the constraints that limit the practical usefulness and sustainability of existing technologies. While magnetic fusion presents an attractive energy alternative, strong technological and scientific hurdles must be overcome before this technology can be transformed into an economically viable energy option. More specifically, the success of the magnetic fusion program depends on the ability to produce a deuterium-tritium plasma which satisfies the Lawson criterion, given by $n_i \tau_E \gtrsim 2 \times 10^{20} \mathrm{m}^{-3}\mathrm{s}$, where n_i represents the ion density and τ_E the confinement time. As is clear from the above relation, plasma confinement, and thus an understanding of plasma transport processes are crucial to this endeavor.

Before proceeding further, it is useful to briefly describe some general characteristics of magnetic fusion devices. In particular, an appropriate choice of geometry can strongly limit the avenues for plasma losses, thus facilitating overall plasma confinement. To this end, toroidal vacuum vessels are utilized such that periodic boundary conditions in both the poloidal and toroidal directions are present, leaving only radial fluxes as a means of inducing plasma losses. Furthermore, since the guiding center motion of a charged particle is to lowest order along magnetic field lines, nested magnetic flux surfaces are externally

imposed. In this manner, the rapid loss of particles via motion along magnetic field lines is avoided. Thus, potential plasma loss mechanisms can be separated into two categories:

a.) cross-field transport induced either by collisional or turbulent processes,

b.) spontaneous changes of the magnetic field configuration.

With regard to (a), while collisional processes may in certain cases be significant, and can be understood to set the minimum attainable level of cross-field transport, turbulent processes are typically dominant. Specifically, ubiquitous plasma instabilities, so-called universal modes [1], driven by the strong temperature and density gradients between the dense, hot plasma core and the surrounding vacuum vessel, have been observed to strongly limit the performance of fusion devices. While seminal studies have uncovered regimes of operation which significantly mitigate the detrimental effects of these modes [2], further research into the underlying physics of these regimes is necessary in order to improve upon, and extrapolate these results to the next generation of fusion devices.

Coincident with the practical necessity of understanding the level of cross-field transport induced by universal modes, is the interesting scientific challenge posed by providing a detailed description of their nonlinear evolution. That this problem is interesting, and distinct from classic studies of 3-D neutral fluid turbulence [3, 4], can be most clearly illustrated by briefly reviewing two essential characteristics to the self-consistent description of modes endemic to strongly magnetized plasmas. First, unlike classic studies of 3-D neutral fluid turbulence, where one hypothesizes the presence of a given forcing function, and seeks to compute the spectral evolution and subsequent statistical steady state, universal modes, or so-called drift waves, are driven by the temperature and density profiles present within the plasma. These in turn must be self-consistently calculated based on the level of cross-field transport present within the system, which is largely set by the intensity of the drift wave turbulence. The presence of this nonlinear feedback mechanism, allows bifurcations to occur in the saturated spectrum of the underlying turbulence and the mean

field profiles of the system. Indeed, the significant improvement in confinement alluded to above corresponds to a well known example of such a bifurcation.

Second, aside from the dynamics of the turbulence drive, obtaining a detailed understanding of the nonlinear saturated state of the turbulent fluctuations has proven to be a non-trivial and fertile area of ongoing research. Of critical importance to this line of research has been the study of self-organization within the context of strongly magnetized plasmas. Recently, seminal studies performed by multiple authors, and reviewed in Ref. [5], have demonstrated that the same insidious modes responsible for limiting reactor performance, are capable of inducing the formation of intense axisymmetric shear flows. These spontaneously generated flows, so called zonal flows, are generated by modulational instability of the background turbulence and have the attractive feature of suppressing turbulent eddies via shear decorrelation [6] without themselves driving any net radial transport. Hence, zonal flows provide an effective means of triggering bifurcations into regimes of low transport. Thus, introducing the possibility of a self-regulating system whereby energy extracted from the pressure profile by the background turbulence is ultimately transferred to (benign) large scale flows.

More generally, the phenomenon of self-organization, or more specifically turbulent structure formation, has been observed in a disparate array of systems ranging from dynamo action [7] to Rayleigh-Benard convection [8]. Of particular relevance to strongly magnetized plasmas, whose variations parallel to the magnetic field are typically weak in comparison to cross field variations, is the case of two-dimensional, or so called "quasi" two-dimensional turbulent systems [9]. Indeed, drift wave turbulence corresponds to one example from a fairly broad set of problems collectively referred to as (quasi) 2-D turbulence. This family of problems is distinguished from more general turbulence phenomena due to their unique statistical properties. Central to this distinction is the addition of one or more added constraints to the equations of motion, most notably enstrophy conserva-

tion [10] (integrated square of vorticity). Other examples from this family of problems include Rossby waves, (incompressible) 2-D hydrodynamics, and 2-D magnetohydrodynamics (MHD). These four examples, while instructive to consider together, contain significant differences. The last of the four mentioned (2-D MHD), while often grouped with the former three, can be immediately seen to be fundamentally distinct. This follows since the presence of $\mathbf{J} \times \mathbf{B}$ forcing removes the added constraint of enstrophy conservation. 2-D hydrodynamic turbulence, on the other hand, while conserving enstrophy along with the other two remaining examples, is incapable of supporting waves, and thus can only be described by so called "eddy" turbulence or strong turbulence theory. This is in contrast to Rossby waves and drift waves which may, to varying degrees, be described via "wave" turbulence or weak turbulence theory.

In spite of these differences, remarkable similarities in their descriptions remain. Namely, the first three examples (exempting MHD) all demonstrate a condensation of energy on the largest scale present within the system. The presence of energy condensation at the largest available scale necessitates the use of multi-scale techniques in order to self-consistently model the evolution of the condensate flow and the underlying turbulence. Adiabatic theory provides a tractable means of exploiting the space and time separations between these two components, thus providing a mathematically tractable self-consistent description. Remarkably, for each of the examples cited above, exempting MHD, potential enstrophy density is found to be adiabatically conserved under slow modulations by the condensate flow [11, 12, 13]. Furthermore, the non-local transfer of energy to the condensate flow can be recovered from modulation instability of the underlying turbulence, which can be shown to follow straightforwardly from the form of the adiabatic invariant (see text below). Thus, in spite of the striking physical differences between these three systems (eddy versus wave turbulence, nonlinearities due to: polarization drift, Coriolis force, and vorticity advection), they share critical elements of their dynamics.

Turning now to item (b), while operating regimes which avoid explosive ideal MHD instabilities have been found, and are widely implemented in modern magnetic confinement devices, slower resistive MHD instabilities continue to hinder reactor performance. In particular, magnetic islands created by the spontaneous reconnection of magnetic field lines [14, 15], have been observed to provide a (soft) upper beta limit (ratio of plasma pressure to magnetic field pressure) attainable in numerous tokamak experiments. Hence, a detailed description of the formation and evolution of magnetic islands is essential for the improvement of reactor performance.

Historically, obtaining a comprehensive description of magnetic island evolution has been obstructed by the tacit assumption that processes (a) and (b) can be effectively decoupled from one another. This assumption is typically justified by invoking the temporal scale separation between the rapidly fluctuating turbulence, and the slow changes in magnetic field topology induced by magnetic reconnection. Following this reasoning, drift wave turbulence is often "modelled" via the introduction of turbulently enhanced collsional transport coefficients. These transport coefficients in turn play a critical role in determining the stability of the magnetic island [16]. That this turbulence "model" is unsatisfactory, can be most clearly seen by considering that:

i.) the turbulent drive, and thus intensity of the drift wave turbulence, is strongly affected as the magnetic topology is changed, thus leading to the presence of dynamic transport coefficients,

ii.) large scale flow structures, nonlinearly driven by the background turbulence, can strongly affect the reconnection process.

Both of these processes can be easily seen to be extensions of the two processes discussed above: Item (i) corresponds to feedback on the growth rate of the drift wave turbulence via profile modification, with the added degree of freedom of a self-consistently evolving

magnetic island. Item (ii) is a generalization of turbulent structure formation, but with the addition of a temporally evolving, non-trivial magnetic field topology. Thus, the problem of magnetic island evolution, traditionally confined within the MHD community, can be seen to be in many ways an extension of classic problems in transport physics. Similarly, due to the scale separation that exists between the magnetic island and the drift wave turbulence, adiabatic theory provides a useful tool in simplifying its description. Thus, an analogous theoretical description may be employed in describing magnetic island evolution, albeit with the addition of non-trivial feedback mechanisms absent from the classic turbulent transport problem discussed above.

In this thesis, multi-scale techniques are implemented in the specific contexts of transport barrier formation, magnetic island evolution and plasma rotation. In Chapter 2, a simple model is introduced to investigate a novel mechanism of transport barrier formation. Emphasis is placed on the impact of turbulent structure formation in triggering the transition to improved confinement regimes, as well as identifying critical nonlinear feedback mechanisms, which are investigated via simple reduced models. These include the impact of secondary structure formation on the phase space topology of the drift wave turbulence, and a simple model describing the self-consistent evolution of mean profiles, $\mathbf{E} \times \mathbf{B}$ driven flows, Reynolds stress driven flows, and turbulence intensity.

In Chapter 3, a minimal self-consistent model is introduced in order to explore the evolution of a thin magnetic island in a background of drift wave turbulence. Various nonlinear feedback loops are identified, however emphasis is placed on a secondary instability arising due to modulational instability of the ambient turbulence. A simple closure scheme is implemented, where the non-local transfer of energy from the drift wave turbulence to the large scale flows is manifested by a negative viscosity. Modifications to the dynamics of the thin magnetic island by the drift wave turbulence are subsequently investigated.

Chapter 4 contains a derivation of parallel momentum transport in a strongly magne-

tized plasma. While methods analogous to those implemented in Chapters 2 and 3 are utilized, extensions to include kinetic effects are implemented. A momentum conservation theorem is proven demonstrating momentum conservation between waves and resonant particles, and expressions describing the structure of momentum transport induced by these components are derived.

1.1 Derivation of Multi-scale Model

A minimal description of the multi-scale problem described above requires two components:

a.) a dynamic model for the small scale drift wave turbulence evolving in the presence of the large scale mean fields,

b.) a model for the evolution of the mean fields, accounting for stresses induced by the small scale turbulence.

Gyrokinetics provides a useful framework to begin our description, since both the small scale dynamics of the drift wave turbulence, as well as the large scale mean field dynamics can be obtained as different limiting forms of the generalized gyrokinetic equation. Before proceeding further, we note that our emphasis here is not on the technical elements of the mathematically cumbersome field of modern gyrokinetics (the interested reader is referred to Ref. [17] for a review), but instead on clearly outlining the physics contained within the model equations which will be utilized below. Furthermore, we note that detailed studies of the linear properties of drift wave turbulence in various regimes have been extensively studied (see Ref. [1] for a review). Our objective here is to consider an absolutely minimal model for the linear dynamics of both the small scale and large scale modes, and to instead focus on their self-consistent nonlinear evolution.

The gyrokinetic equation in slab geometry can be written as [18]

$$\begin{aligned} 0 &= \frac{\partial f_s^{tot}}{\partial t} + \left\{ U\hat{\mathbf{b}} + \frac{c}{B}\hat{\mathbf{b}} \times \nabla J_0(\lambda) \left(\phi - \frac{U}{c} A_\parallel \right) \right\} \cdot \nabla f_s^{tot} \\ &- \frac{q_s}{m_s} J_0(\lambda) \left(\hat{\mathbf{b}} \cdot \nabla \phi + \frac{1}{c} \frac{\partial A_\parallel}{\partial t} \right) \frac{\partial f_s^{tot}}{\partial U}, \end{aligned} \tag{1.1}$$

where f_s^{tot} represents the total gyrocenter distribution function for a given particle species s, $\lambda \equiv k_\perp \rho_\perp$, ϕ and $A_\parallel$ represent the scalar potential and the parallel component of the vector potential respectively, and we have neglected magnetic perturbations parallel to the magnetic field for simplicity. Eq. (1.1) can be seen to describe the evolution of the gyrocenter distribution function in the five dimensional phase space given by $(\mathbf{x}, \mu, U)$ (note that the magnetic moment $\mu \equiv m_s v_\perp^2 / 2\omega_{cs}$ is an adiabatic invariant such that $\dot{\mu} \approx 0$, and hence the dimensionality of the system is effectively further reduced). This description is convenient as it both reduces the dimensionality in comparison to the six dimensional Vlasov equation, as well as integrates out the rapid gyro motions of the charged particles about the magnetic field. The latter simplification is particularly convenient as both the drift wave turbulence as well as the secondary structures which we will be interested in describing evolve on scales slow in comparison to the gyro motion of the particles.

Separating the gyrocenter distribution function into $f_s^{tot} = F_{0s} + f_s$, where F_{0s} represents a Maxwellian distribution, Eq. (1.1) can be written as

$$\begin{aligned} &\frac{\partial f_s}{\partial t} + \left\{ U\hat{\mathbf{b}} + \frac{c}{B}\hat{\mathbf{b}} \times \nabla J_0(\lambda) \left(\phi - \frac{U}{c} A_\parallel \right) \right\} \cdot \nabla f_s - \frac{q_s}{m_s} J_0(\lambda) \left(\hat{\mathbf{b}} \cdot \nabla \phi + \frac{1}{c} \frac{\partial A_\parallel}{\partial t} \right) \frac{\partial f_s}{\partial U} \\ &= -\frac{c}{B}\hat{\mathbf{b}} \times \nabla J_0(\lambda) \left(\phi - \frac{U}{c} A_\parallel \right) \cdot \nabla F_{0s} + \frac{q_s}{m_s} J_0(\lambda) \left(\hat{\mathbf{b}} \cdot \nabla \phi + \frac{1}{c} \frac{\partial A_\parallel}{\partial t} \right) \frac{\partial F_{0s}}{\partial U}. \end{aligned} \tag{1.2}$$

Here it is useful to separate the fields f_s, ϕ, and $A_\parallel$ into a slowly fluctuating component and a small scale rapidly fluctuating piece, such that $\psi = \langle \psi \rangle + \delta\psi$. Introducing this

scale separation, equations for the large scale mean field component, and the small scale fluctuating component can be easily derived as:

$$\begin{aligned}\left(\frac{\partial}{\partial t}+U\hat{\mathbf{b}}\cdot\nabla\right)\langle f_s\rangle = &-\frac{c}{B}\hat{\mathbf{b}}\times\nabla J_0(\lambda)\left(\langle\phi\rangle-\frac{U}{c}\langle A_\parallel\rangle\right)\cdot\nabla F_{0s}\\ &+\frac{q_s}{m_s}J_0(\lambda)\left(\hat{\mathbf{b}}\cdot\nabla\langle\phi\rangle+\frac{1}{c}\frac{\partial\langle A_\parallel\rangle}{\partial t}\right)\frac{\partial F_{0s}}{\partial U}\\ &-\frac{c}{B}\left\langle\hat{\mathbf{b}}\times\nabla J_0(\lambda)\left(\delta\phi-\frac{U}{c}\delta A_\parallel\right)\cdot\nabla\delta f_s\right\rangle\\ &+\frac{q_s}{m_s}\left\langle J_0(\lambda)\left(\hat{\mathbf{b}}\cdot\nabla\delta\phi+\frac{1}{c}\frac{\partial\delta A_\parallel}{\partial t}\right)\frac{\partial\delta f_s}{\partial U}\right\rangle. \end{aligned}\tag{1.3}$$

and

$$\left(\frac{\partial}{\partial t}+U\hat{\mathbf{b}}\cdot\nabla\right)\delta f_s = S_1+S_2+S_3,\tag{1.4}$$

where

$$S_1\equiv-\frac{c}{B}\hat{\mathbf{b}}\times\nabla J_0\left(\delta\phi-\frac{U}{c}\delta A_\parallel\right)\cdot\nabla F_{0s}+\frac{q_s}{m_s}J_0\left(\hat{\mathbf{b}}\cdot\nabla\delta\phi+\frac{1}{c}\frac{\partial\delta A_\parallel}{\partial t}\right)\frac{\partial F_{0s}}{\partial U},$$

$$\begin{aligned}S_2 \equiv\ & -\frac{c}{B}\hat{\mathbf{b}}\times\nabla J_0\left(\delta\phi-\frac{U}{c}\delta A_\parallel\right)\cdot\nabla\langle f_s\rangle-\frac{c}{B}\hat{\mathbf{b}}\times\nabla J_0\left(\langle\phi\rangle-\frac{U}{c}\langle A_\parallel\rangle\right)\cdot\nabla\delta f_s\\ +\ & \frac{q_s}{m_s}J_0\left(\hat{\mathbf{b}}\cdot\nabla\delta\phi+\frac{1}{c}\frac{\partial\delta A_\parallel}{\partial t}\right)\frac{\partial\langle f_s\rangle}{\partial U}+\frac{q_s}{m_s}J_0\left(\hat{\mathbf{b}}\cdot\nabla\langle\phi\rangle+\frac{1}{c}\frac{\partial\langle A_\parallel\rangle}{\partial t}\right)\frac{\partial\delta f_s}{\partial U},\end{aligned}$$

$$\begin{aligned}S_3 \equiv\ & -\frac{c}{B}\hat{\mathbf{b}}\times\nabla J_0\left(\delta\phi-\frac{U}{c}\delta A_\parallel\right)\cdot\nabla\delta f_s+\frac{c}{B}\left\langle\hat{\mathbf{b}}\times\nabla J_0\left(\delta\phi-\frac{U}{c}\delta A_\parallel\right)\cdot\nabla\delta f_s\right\rangle\\ +\ & \frac{q_s}{m_s}J_0\left(\hat{\mathbf{b}}\cdot\nabla\delta\phi+\frac{1}{c}\frac{\partial\delta A_\parallel}{\partial t}\right)\frac{\partial\delta f_s}{\partial U}-\frac{q_s}{m_s}\left\langle J_0\left(\hat{\mathbf{b}}\cdot\nabla\delta\phi+\frac{1}{c}\frac{\partial\delta A_\parallel}{\partial t}\right)\frac{\partial\delta f_s}{\partial U}\right\rangle.\end{aligned}$$

Since we are primarily interested in the excitation of secondary structures, the mean field nonlinearities in Eq. (1.3) have been neglected in favor of non-local interactions with the

small scale fluctuations. Considering the fluctuation equation [Eq. (1.4)], the terms on the rhs can be grouped into three categories. The first, defined by S_1, represent purely linear phenomena induced either by inhomogeneities in the equilibrium distribution function (first term in S_1), or momentum and energy exchange between waves and resonant particles (second term in S_1). The second category of terms, denoted by S_2, corresponds to nonlocal interactions with the large scale mean fields. This interaction, as discussed below, can both allow for the exchange of energy between the small scale drift waves and the large scale mean fields, as well as modify the linear characteristics of the small scale modes such as the introduction of a nonlinear correction to the diamagnetic drift through mean field density or pressure fluctuations. Finally, the last set of terms, contained in S_3, correspond to local nonlinear interactions among the drift wave modes. These terms allow for energy and momentum to be exchanged among the small scale modes.

1.1.1 Drift Wave Evolution

Eqs. (1.3) and (1.4) can be simplified significantly. First, considering the equation for small scale fluctuations [Eq. (1.4)], and taking the low β limit, allows for magnetic fluctuations to be neglected. Thus, the zeroth order velocity moment of Eq. (1.4) can be rewritten as

$$\begin{aligned}
\frac{\partial \delta N_i}{\partial t} + c_s \nabla \cdot \left(\hat{\mathbf{b}} \delta V_{\parallel i} \right) &= v_{thi} \rho_i \left(\hat{\mathbf{b}} \times \nabla \ln n_0 \right) \cdot \nabla \left(1 - \frac{1}{2} \eta_i b \right) e^{-\frac{1}{2} b} \frac{e \delta \phi}{T_i} \\
&- \frac{c}{B} \left[\hat{\mathbf{b}} \times \nabla \left(1 + \frac{1}{2} b \right) e^{-\frac{1}{2} b} \delta \phi \right] \cdot \nabla \left\langle N_i \right\rangle \\
&- \frac{c}{B} \left[\hat{\mathbf{b}} \times \nabla \left(1 + \frac{1}{2} b \right) e^{-\frac{1}{2} b} \left\langle \phi \right\rangle \right] \cdot \nabla \delta N_i \\
&+ \frac{1}{2} \frac{c}{B} \left(\hat{\mathbf{b}} \times \nabla b e^{-\frac{1}{2} b} \delta \phi \right) \cdot \nabla \left\langle P_{\perp i} \right\rangle \\
&+ \frac{1}{2} \frac{c}{B} \left(\hat{\mathbf{b}} \times \nabla b e^{-\frac{1}{2} b} \left\langle \phi \right\rangle \right) \cdot \nabla \delta P_{\perp i} + \int d^3 \bar{v} S_3, \qquad (1.5)
\end{aligned}$$

where $\int d^3\bar{v} \equiv 2\pi \int d\mu dU \, (\omega_{ci}/m_i)$, $b \equiv k_\perp^2 \rho_\perp^2$ and we have introduced the normalizations:

$$\left(N_i, V_{\parallel i}, P_{\perp i}\right) \rightarrow \left(\frac{N_i}{n_0}, \frac{V_{\parallel i}}{c_s}, \frac{P_{\perp i}}{p_{0\perp i}}\right).$$

A subtle, but critical characteristic of the gyrokinetic description is that the distribution function describes the distribution of gyrocenters and not the instantaneous particle position within the five dimensional phase space given by $(\mathbf{x}, \mu, U)$. Since the fast gyrocenter motion of the particles is integrated out, rather than describing the evolution of point particles in a six dimensional phase space, one is instead describing the evolution of "rings" in a five dimensional phase space. Thus, the moments of the gyrocenter distribution function (i.e. density, velocity, etc), should be understood to be distinct from the physical moments of particle distributions. Fortunately, the physical particle moments and gyrocenter moments may be related via a set of pull back transformations. Keeping lowest order finite Larmor radius corrections, the relation between gyrocenter moments and particle moments can be written as [18]:

$$N_i = n_i + \frac{1}{2} b \left(p_{\perp i} + 2\frac{e}{T_i}\phi\right), \tag{1.6}$$

$$V_{\parallel i} = \left(1 + \frac{1}{2} b\right) v_{\parallel i}, \tag{1.7}$$

$$P_{\perp i} = p_{\perp i} + b\left(2p_{\perp i} - n_i + 2\frac{e\phi}{T_i}\right). \tag{1.8}$$

Substituting the pull back transformations given by Eqs. (1.6-1.8) into Eq. (1.5), yields:

$$\begin{aligned}
\frac{d}{dt}\left(1 - \rho_s^2 \nabla_\perp^2\right) \frac{e\delta\phi}{T_i} = {} & \tau v_{thi} \rho_i \left(\hat{\mathbf{b}} \times \nabla \ln n_0\right) \cdot \nabla \left(1 + \frac{1}{2}\eta_i \rho_i^2 \nabla_\perp^2\right)\left(1 + \frac{1}{2}\rho_i^2 \nabla_\perp^2\right) \frac{e\delta\phi}{T_i} \\
& + \frac{1}{2}\frac{\partial}{\partial t}\rho_s^2 \nabla_\perp^2 \delta p_{\perp i} + \frac{1}{2}\frac{c}{B}\rho_s^2 \left(\hat{\mathbf{b}} \times \nabla \langle\phi\rangle\right) \cdot \nabla \nabla_\perp^2 \delta p_{\perp i} \\
& - \frac{1}{2}\frac{c}{B}\rho_s^2 \left(\hat{\mathbf{b}} \times \nabla \nabla_\perp^2 \delta\phi\right) \cdot \nabla \langle p_{\perp i}\rangle - \tau \frac{c}{B}\left(\hat{\mathbf{b}} \times \nabla \delta\phi\right) \cdot \nabla \langle n_i \rangle \\
& + \tau \int d^3\bar{v} S_3,
\end{aligned} \tag{1.9}$$

where $d/dt \equiv \partial/\partial t + (c/B)\left(\hat{\mathbf{b}} \times \nabla \langle\phi\rangle\right) \cdot \nabla$, we assume adiabatic electrons, i.e. $\delta n_i = \delta n_e = e\delta\phi/T_e$, and for simplicity we have neglected variations parallel to the magnetic field, as well as finite Larmor radius corrections to the mean fields. Eq. (1.9) can be further simplified by considering the pressure equation for the small scale modes. Operating on Eq. (1.4) with the operator $\int d^3\bar{v}\mu\left(\omega_{ci}/p_{0\perp i}\right)$, the Laplacian of the perpendicular ion pressure can be shown to evolve according to

$$\begin{aligned}
\frac{\partial}{\partial t}\nabla_\perp^2 \delta p_{\perp i} &= \omega_d^*\left(1+\eta_i\right)\nabla_\perp^2 \frac{e\delta\phi}{T_i} + \frac{c}{B}\left(\hat{\mathbf{b}} \times \nabla\nabla_\perp^2\delta\phi\right)\cdot\nabla\langle p_{\perp i}\rangle \\
&- \frac{c}{B}\left(\hat{\mathbf{b}} \times \nabla\langle\phi\rangle\right)\cdot\nabla\nabla_\perp^2\delta p_{\perp i} - 2\frac{c}{B}\nabla\cdot\left[\left(\hat{\mathbf{b}} \times \nabla\nabla\langle\phi\rangle\right)\cdot\nabla\delta p_{\perp i}\right] \\
&- 2\frac{c}{B}\nabla\cdot\left[\left(\hat{\mathbf{b}} \times \nabla\nabla\delta\phi\right)\cdot\nabla\langle p_{\perp i}\rangle\right] + \int d^3\bar{v}\frac{\mu\omega_{ci}}{p_{0\perp i}}\nabla_\perp^2 S_3, \qquad (1.10)
\end{aligned}$$

where we have again dropped finite Larmor radius corrections to the mean fields. Substituting Eq. (1.10) into Eq. (1.9) yields:

$$\begin{aligned}
\frac{d}{dt}\left(1-\rho_s^2\nabla_\perp^2\right)\frac{e\delta\phi}{T_i} &= c_s\rho_s\left(\hat{\mathbf{b}} \times \nabla\ln n_0\right)\cdot\nabla\frac{e\delta\phi}{T_i} \\
&+ \tau^{-1}c_s\rho_s^3\left[\left(\hat{\mathbf{b}} \times \nabla\ln n_0\left(1+\eta_i\right)\right)\right]\cdot\nabla\nabla_\perp^2\frac{e\delta\phi}{T_i} \\
&- \tau\frac{c}{B}\left(\hat{\mathbf{b}} \times \nabla\delta\phi\right)\cdot\nabla\langle n_i\rangle - \frac{c}{B}\rho_s^2\nabla\cdot\left[\left(\hat{\mathbf{b}} \times \nabla\nabla\langle\phi\rangle\right)\cdot\nabla\delta p_{\perp i}\right] \\
&- \frac{c}{B}\rho_s^2\nabla\cdot\left[\left(\hat{\mathbf{b}} \times \nabla\nabla\delta\phi\right)\cdot\nabla\langle p_{\perp i}\rangle\right] \\
&+ \tau\int d^3\bar{v}S_3 + \frac{1}{2}\rho_s^2\int d^3\bar{v}\frac{\mu\omega_{ci}}{p_{0\perp i}}\nabla_\perp^2 S_3. \qquad (1.11)
\end{aligned}$$

Equation (1.11) may be further simplified by noting

$$\begin{aligned}
&\nabla\cdot\left[\left(\hat{\mathbf{b}} \times \nabla\nabla\langle\phi\rangle\right)\cdot\nabla\delta p_{\perp i}\right] + \nabla\cdot\left[\left(\hat{\mathbf{b}} \times \nabla\nabla\delta\phi\right)\cdot\nabla\langle p_{\perp i}\rangle\right] \\
&\approx \left(\hat{\mathbf{b}} \times \nabla\nabla_\perp^2\delta\phi\right)\cdot\nabla\langle p_{\perp i}\rangle = -\left(\hat{\mathbf{b}} \times \nabla\langle p_{\perp i}\rangle\right)\cdot\nabla\nabla_\perp^2\delta\phi,
\end{aligned}$$

where we have used $\nabla \ln \delta\psi > \nabla \ln \langle\psi\rangle$. Thus, Eq. (1.11) can be written in the simplified form:

$$\frac{d}{dt}\left(1-\rho_s^2\nabla_\perp^2\right)\frac{e\delta\phi}{T_i} = c_s\rho_s\left[\hat{\mathbf{b}}\times\nabla\left(\ln n_0+\langle n_i\rangle\right)\right]\cdot\nabla\frac{e\delta\phi}{T_i} + \tau^{-1}c_s\rho_s^3\left[\hat{\mathbf{b}}\times\nabla\left(\ln p_{0\perp i}+\langle p_{\perp i}\rangle\right)\right]\cdot\nabla\nabla_\perp^2\frac{e\delta\phi}{T_i}+\Xi_{nl}, \quad (1.12)$$

where $\Xi_{nl}\equiv\tau\int d^3\bar{v}S_3+(1/2)\,\rho_s^2\nabla_\perp^2\int d^3\bar{v}\mu\left(\omega_{ci}/p_{0\perp i}\right)S_3$ and we note that both $\langle n_i\rangle$ and $\langle p_{\perp i}\rangle$ are both normalized quantities. From the form of Eq. (1.12) it's clear that aside from the convection of potential vorticity, here given by $S\equiv\left(1-\rho_s^2\nabla_\perp^2\right)e\delta\phi/T_e$, mean field fluctuations in density and pressure introduce perturbations to the diamagnetic drift velocity. As an aside, it is useful to note that while the potential vorticity for drift waves is usually defined as $\left(1-\rho_s^2\nabla_\perp^2\right)e\delta\phi/T_e+\ln n_0$, here however it is convenient to use the above definition, since as is shown below, only the nonlinear terms contribute to the form of the adiabatic invariant.

Turning now to local nonlinear interactions, Ξ_{nl} can be written as

$$\begin{aligned}\Xi_{nl} &\equiv \rho_s^2\frac{c}{B}\nabla\cdot\left\{\left[\hat{\mathbf{b}}\times\nabla\left(\frac{e\delta\phi}{T_i}+\delta p_{\perp i}\right)\right]\cdot\nabla_\perp\nabla_\perp\delta\phi\right\}\\ &- \rho_s^2\frac{c}{B}\nabla\cdot\left\langle\left[\hat{\mathbf{b}}\times\nabla\left(\frac{e\delta\phi}{T_i}+\delta p_{\perp i}\right)\right]\cdot\nabla_\perp\nabla_\perp\delta\phi\right\rangle. \quad (1.13)\end{aligned}$$

From Eq. (1.13), it's clear that the local nonlinearity corresponds to the linear combination of $\mathbf{E}\times\mathbf{B}$ convection, plus a diamagnetic drift induced by the pressure fluctuations. As our principle focus is on nonlocal interactions with the large scale mean fields, we neglect the nonlinear diamagnetic term in order to reduce the description of the system of the small scales to a single field. Thus, we approximate local interactions via

$$\Xi_{nl}\equiv\rho_s^2\frac{c}{B}\nabla\cdot\left\{\left(\hat{\mathbf{b}}\times\nabla\frac{e\delta\phi}{T_i}\right)\cdot\nabla_\perp\nabla_\perp\delta\phi\right\}-\rho_s^2\frac{c}{B}\nabla\cdot\left\langle\left(\hat{\mathbf{b}}\times\nabla\frac{e\delta\phi}{T_i}\right)\cdot\nabla_\perp\nabla_\perp\delta\phi\right\rangle. \quad (1.14)$$

Here it is convenient to compare the form of Eq. (1.12) with existing models of drift wave turbulence commonly studied. First, since we are considering electrostatic turbulence, and have neglected variations along the magnetic field, Eq. (1.12) has a structure similar to, but not isomorphic to, classic reduced two-dimensional fluid models such as the Hasegawa-Mima equation [19]. In particular, aside from the addition of a convective nonlinearity of the scalar potential (already noted in Ref. [13]), nonlinear diamagnetic terms due to fluctuations in the large scale density and pressure are also apparent. The latter of these effects is the non-local counterpart of the local pressure nonlinearity well known to exist in reduced models of ion pressure gradient turbulence [20]. The former is typically dropped, due to the local counterpart being proportional to $\delta n_i = \delta n_e \approx e\delta\phi/T_e$, such that aside from non-adiabatic corrections, it goes to zero identically. Also, since in the expansion performed above, instead of taking $\tau = T_e/T_i \rightarrow \infty$, as is usually done in deriving the Hasegawa-Mima equation, we truncate the moment hierarchy after lowest non-trivial order in $b \equiv k_\perp^2 \rho_i^2$. Thus, we also have a correction to the linear dynamics due to the diamagnetic term arising from the equilibrium ion pressure. Finally, while the local nonlinearity [Ξ_{nl}, given by Eq. (1.14)] is the same as that usually studied in the Hasegawa-Mima equation (namely the polarization nonlinearity), this nonlinearity appears as the difference between the unaveraged and averaged contributions. One can formally understand the origin of the averaged term in Eq. (1.14) by considering that in the two scale analysis employed above, we have written a given field as the sum of its mean and rapidly fluctuating components, i.e. $\psi = \langle\psi\rangle + \delta\psi$, where the average in slab geometry may be defined as

$$\langle \cdots \rangle \equiv \int_x^{x+X} \frac{dx}{X} \int_y^{y+Y} \frac{dy}{Y} \int_t^{t+T} \frac{dt}{T} \left(\cdots \right).$$

Here $(\mathbf{X}, T)$ correspond to the spatial and temporal ranges averaged over, and can thus be understood to set the fastest scale on which the mean fields may vary. It then follows that we may write a given field $\psi = \psi\left(\mathbf{x}, t, \mathbf{X}, T\right)$, such that $\langle\psi\rangle = \langle\psi\rangle\left(\mathbf{X}, T\right)$, and

$\delta\psi = \delta\psi\left(\mathbf{x}, t, \mathbf{X}, T\right) = \psi - \langle\psi\rangle$ (where by construction $\langle\delta\psi\rangle = 0$). Hence, modulations due to the large scale mean field component can be seen to induce slow variations in the rapidly fluctuating component. Thus, the second term in Eq. (1.14) can be seen to have the effect of subtracting off slow variations in the local polarization nonlinearity induced by the large scale mean field. In the next section we will use this property in order to derive a set of amplitude equations for the small scale turbulence in which their phase space (both spatial as well as spectral) evolution will be largely set by modulations due to the mean field components.

1.1.2 Wave Kinetic Formulation

Our motivation throughout this work is the self-consistent description of a bath of small scale rapidly oscillating modes evolving in the presence of slowly varying large scale fields. Thus, a minimal description of this system can be seen to be composed of two elements: The first is the modelling of the wave-wave interactions among the small scale modes [Ξ_{nl} in Eq. (1.12)]. Because we are interested in a fairly broad spectrum of dispersive modes, weak turbulence theory provides a suitable method for describing these interactions. The second component corresponds to modelling the effect of slow modulations of the small scale modes due to the large scale fields, and the subsequent back reaction on to the large scale evolution. Here, significant conceptual, as well as mathematical simplification can be made in modelling this interaction via utilizing the presence of any adiabatic invariants which may be present. Indeed, any description of this disparate scale interaction must necessarily respect the added constraints of any adiabatic invariants present within the system.

Fortunately, both of these components may be included within a wave kinetic descrip-

tion. It is convenient to rewrite Eq. (1.12) in Fourier space as

$$\begin{aligned}\frac{\partial}{\partial t}\left(1+k_\perp^2\rho_s^2\right)\delta\varphi_k+i\omega_k\delta\varphi_k &= - \quad c_s\rho_s\sum_{k=k_1+k_2}\left(\hat{\mathbf{b}}\times\mathbf{k}_1\right)\cdot\mathbf{k}_2\left(\langle n\rangle_{k_1}-\langle\varphi\rangle_{k_1}\right)\delta\varphi_{k_2}\\ &+ \quad c_s\rho_s^3\sum_{k=k_1+k_2}\left(\hat{\mathbf{b}}\times\mathbf{k}_1\right)\cdot\mathbf{k}_2k_{\perp 2}^2\left(\langle p\rangle_{k_1}+\langle\varphi\rangle_{k_1}\right)\delta\varphi_{k_2}\\ &+ \quad \Xi_k, \end{aligned} \tag{1.15}$$

and

$$\begin{aligned}\Xi_k &= c_s\rho_s^3\sum_{k=k_1+k_2}\left(\hat{\mathbf{b}}\times\mathbf{k}_1\right)\cdot\mathbf{k}_2k_{\perp 2}^2\delta\varphi_{k_1}\delta\varphi_{k_2}\\ &- c_s\rho_s^3\sum_p\int d\mathbf{x}\left\langle\left(\hat{\mathbf{b}}\times\nabla\frac{e\delta\phi}{T_i}\right)\cdot\nabla_\perp\nabla_\perp\delta\phi\right\rangle_p e^{i(\mathbf{p}-\mathbf{k})\cdot\mathbf{x}},\end{aligned} \tag{1.16}$$

where since any averaged quantity is necessarily a function of the large scale variables $(\mathbf{X},T)$, we have used $\langle\cdots\rangle(\mathbf{X})=\sum_p\langle\cdots\rangle_p\exp(i\mathbf{p}\cdot\mathbf{x})$, and introduced the normalization $\varphi\equiv e\phi/T_e$. Eq. (1.16) can by further simplified as

$$\begin{aligned}\Xi_k &= c_s\rho_s^3\sum_{k=k_1+k_2}\left(\hat{\mathbf{b}}\times\mathbf{k}_1\right)\cdot\mathbf{k}_2k_{\perp 2}^2\delta\varphi_{k_1}\delta\varphi_{k_2}\\ &- c_s\rho_s^3\sum_p\delta_{p,k}\left\langle\left(\hat{\mathbf{b}}\times\nabla\delta\varphi\right)\cdot\nabla_\perp\nabla_\perp\delta\varphi\right\rangle_p,\end{aligned}$$

$$\Xi_k = c_s\rho_s^3\sum_{k=k_1+k_2}\left(\hat{\mathbf{b}}\times\mathbf{k}_1\right)\cdot\mathbf{k}_2k_{\perp 2}^2\delta\varphi_{k_1}\delta\varphi_{k_2}, \tag{1.17}$$

where the last step follows since, by construction $|\mathbf{p}|<|\mathbf{k}|$. From Eq. (1.15) an equation

for the turbulence intensity evolution can be written

$$\begin{aligned}
&\frac{\partial I_k}{\partial t} + i\int d\mathbf{q} e^{i\mathbf{q}\cdot\mathbf{x}} \left(\omega_k + \omega_{-k+q}\right) \left\langle \delta\varphi_k \delta\varphi_{-k+q}\right\rangle \\
&\quad = -c_s\rho_s \int d\mathbf{q} e^{i\mathbf{q}\cdot\mathbf{x}} \sum_{k=k_1+k_2} L_{k_1,k_2,k} \left(\left\langle n\right\rangle_{k_1} - \left\langle \varphi\right\rangle_{k_1}\right) \left\langle \delta\varphi_{k_2}\delta\varphi_{-k+q}\right\rangle \\
&\quad - c_s\rho_s \int d\mathbf{q} e^{i\mathbf{q}\cdot\mathbf{x}} \sum_{-k+q=k_1+k_2} L_{k_1,k_2,-k+q} \left(\left\langle n\right\rangle_{k_1} - \left\langle \varphi\right\rangle_{k_1}\right) \left\langle \delta\varphi_{k_2}\delta\varphi_{k}\right\rangle \\
&\quad + c_s\rho_s^3 \int d\mathbf{q} e^{i\mathbf{q}\cdot\mathbf{x}} \sum_{k=k_1+k_2} M_{k_1,k_2,k} \left(\left\langle p\right\rangle_{k_1} + \left\langle \varphi\right\rangle_{k_1}\right) \left\langle \delta\varphi_{k_2}\delta\varphi_{-k+q}\right\rangle \\
&\quad + c_s\rho_s^3 \int d\mathbf{q} e^{i\mathbf{q}\cdot\mathbf{x}} \sum_{-k+q=k_1+k_2} M_{k_1,k_2,-k+q} \left(\left\langle p\right\rangle_{k_1} + \left\langle \varphi\right\rangle_{k_1}\right) \left\langle \delta\varphi_{k_2}\delta\varphi_{k}\right\rangle \\
&\quad + C_k\left[I_k\right], \qquad (1.18)
\end{aligned}$$

where

$$\begin{aligned}
C_k\left[I_k\right] \equiv\ & c_s\rho_s^3 \int d\mathbf{q} e^{i\mathbf{q}\cdot\mathbf{x}} \sum_{k=k_1+k_2} M_{k_1,k_2,k} \left\langle \delta\varphi_{-k+q}\delta\varphi_{k_1}\delta\varphi_{k_2}\right\rangle \\
& - c_s\rho_s^3 \int d\mathbf{q} e^{i\mathbf{q}\cdot\mathbf{x}} \sum_{-k+q=k_1+k_2} M_{k_1,k_2,-k+q} \left\langle \delta\varphi_{k}\delta\varphi_{k_1}\delta\varphi_{k_2}\right\rangle ,
\end{aligned}$$

$$L_{k_1,k_2,k} \equiv \frac{\left(\mathbf{k}_1\times\mathbf{k}_2\right)_z}{1+k_\perp^2\rho_s^2},$$

$$M_{k_1,k_2,k} \equiv \frac{\left(\mathbf{k}_1\times\mathbf{k}_2\right)_z}{1+k_\perp^2\rho_s^2} k_{\perp 2}^2.$$

Here $I_k \equiv \int d\mathbf{q} e^{i\mathbf{q}\cdot\mathbf{x}} \left\langle \delta\varphi_{k+q}\delta\varphi_{-k}\right\rangle$ is a Wigner function describing the evolution of the turbulence intensity modulated by a slowly varying mean field component, and $\hat{\mathrm{b}}$ has been taken to be along the z axis. Eq. (1.18) may be significantly simplified by utilizing the scale separation between the large scale mean fields and the small scale modes. Also, since for the mean flows which we will consider, the mean pressure and density perturbations are weak relative to electrostatic perturbations, it is useful to consider the simplified limit of

negligible density and pressure fluctuations. This limit is particularly interesting since the nonlinear structure of Eq. (1.18) can be seen to be isomorphic to the 2-D Euler equation, except with a potential vorticity given by $S = (1 + k_\perp^2 \rho_s^2)\, \varphi_k$ instead of $S_H = k_\perp^2 \varphi_k$.

Carrying out the expansion in $|\mathbf{k}_1|$ and $|\mathbf{q}|$, Eq. (1.18) can be written to lowest surviving order as

$$\begin{aligned} \frac{\partial I_k}{\partial t} + \frac{\partial \omega_k}{\partial \mathbf{k}} \cdot \frac{\partial I_k}{\partial \mathbf{x}} &= \frac{-1}{\left(1 + k_\perp^2 \rho_s^2\right)^2} \frac{\partial}{\partial \mathbf{k}} \left(\mathbf{v}_0 \cdot \mathbf{k}_\perp\right) \cdot \frac{\partial}{\partial \mathbf{x}} \left[\left(1 + k_\perp^2 \rho_s^2\right) I_k\right] \\ &+ \frac{1}{\left(1 + k_\perp^2 \rho_s^2\right)^2} \frac{\partial}{\partial \mathbf{x}} \left(\mathbf{v}_0 \cdot \mathbf{k}_\perp\right) \cdot \frac{\partial}{\partial \mathbf{k}} \left[\left(1 + k_\perp^2 \rho_s^2\right) I_k\right] \\ &+ C_k \left[I_k\right], \end{aligned} \tag{1.19}$$

where $\mathbf{v}_0 \equiv c_s \rho_s \left(\hat{\mathbf{z}} \times \nabla \langle \varphi \rangle\right)$. Eq. (1.19) may be written as a conservation law by multiplying by $\left(1 + k_\perp^2 \rho_s^2\right)^2$, yielding [13]:

$$\frac{\partial N_k}{\partial t} + \frac{\partial}{\partial \mathbf{k}} \left(\omega_k + \mathbf{v}_0 \cdot \mathbf{k}_\perp\right) \cdot \frac{\partial N_k}{\partial \mathbf{x}} - \frac{\partial}{\partial \mathbf{x}} \left(\mathbf{v}_0 \cdot \mathbf{k}_\perp\right) \cdot \frac{\partial N_k}{\partial \mathbf{k}} = C_k \left[N_k\right], \tag{1.20}$$

where $N_k \equiv \left(1 + k_\perp^2 \rho_s^2\right)^2 I_k$. Such that, up to local interactions, N_k can be seen to be adiabatically conserved in the presence of slow incompressible flow variations. The form of this adiabatic invariant is not surprising: As mentioned above, for 2-D hydrodynamic turbulence, whose potential vorticity is given by $S_H = k_\perp^2 \varphi$, the potential enstrophy density $N_k^H = k_\perp^4 I_k$ may be shown to be adiabatically invariant in the presence of a slowly varying large scale mean flow. Here, $S = (1 + k_\perp^2 \rho_s^2)\, \varphi_k$, such that for the case of an incompressible flow ($\langle n \rangle_{k_1} \to 0$), it's not surprising that the drift wave potential enstrophy density, $N_k = \left(1 + k_\perp^2 \rho_s^2\right)^2 I_k$ is adiabatically conserved.

1.1.3 Mean Field Evolution

Similarly, from Eq. (1.3) the evolution of the ion and electron particle densities are described by

$$\begin{aligned}
&\frac{\partial \langle n_i \rangle}{\partial t} - \frac{\partial}{\partial t}\rho_i^2 \nabla_\perp^2 \frac{e\langle \phi \rangle}{T_i} + c_s \hat{\mathbf{b}} \cdot \nabla \langle v_{\parallel i} \rangle \\
&\quad = v_{thi}\rho_i \left(\hat{\mathbf{b}} \times \nabla \ln n_0 \right) \cdot \nabla e^{-b/2} \frac{e\langle \phi \rangle}{T_i} - \left\langle \frac{c}{B} \left(\hat{\mathbf{b}} \times \nabla \delta\phi \right) \cdot \nabla \delta n_i \right\rangle \\
&\quad + \frac{c}{B}\rho_i^2 \left\langle \left(\hat{\mathbf{b}} \times \nabla \delta\phi \right) \cdot \nabla \nabla \frac{e\delta\phi}{T_i} \right\rangle + \frac{1}{2}\frac{\partial}{\partial t}\rho_i^2 \nabla_\perp^2 \langle p_{\perp i} \rangle \\
&\quad + \frac{1}{2}\frac{c}{B}\rho_i^2 \left\langle \left(\hat{\mathbf{b}} \times \nabla \delta\phi \right) \cdot \nabla \nabla_\perp^2 \delta p_{\perp i} \right\rangle - \frac{1}{2}\frac{c}{B}\rho_i^2 \left\langle \left(\hat{\mathbf{b}} \times \nabla \nabla_\perp^2 \delta\phi \right) \cdot \nabla \delta p_{\perp i} \right\rangle ,
\end{aligned} \tag{1.21}$$

and

$$\frac{\partial \langle n_e \rangle}{\partial t} + c_s \hat{\mathbf{b}} \cdot \nabla \langle v_{\parallel e} \rangle = \frac{c}{B} \left(\hat{\mathbf{b}} \times \nabla \ln n_0 \right) \cdot \nabla \langle \phi \rangle - \frac{c}{B} \left\langle \left(\hat{\mathbf{b}} \times \nabla \delta\phi \right) \cdot \nabla \delta n_e \right\rangle , \tag{1.22}$$

where we have assumed the small scale component to be well approximated as electrostatic, and we have neglected mean field nonlinearities. Subtracting Eq. (1.22) from Eq. (1.21) yields the vorticity equation given by:

$$\begin{aligned}
\frac{\partial}{\partial t}\rho_i^2 \nabla_\perp^2 \frac{e\langle \phi \rangle}{T_i} &= \frac{v_A^2}{c}\rho_i^2 \hat{\mathbf{b}} \cdot \nabla \nabla_\perp^2 \langle A_\parallel \rangle + \frac{1}{2} v_{thi}\rho_i \left(\hat{\mathbf{b}} \times \nabla \ln n_0 \right) \cdot \nabla \nabla_\perp^2 \frac{e\langle \phi \rangle}{T_i} \\
&- \frac{c}{B}\rho_i^2 \nabla \cdot \left\langle \left[\hat{\mathbf{b}} \times \nabla \left(\frac{e\delta\phi}{T_i} + \delta p_{\perp i} \right) \right] \cdot \nabla_\perp \nabla_\perp \delta\phi \right\rangle .
\end{aligned} \tag{1.23}$$

As discussed above, for simplicity we will drop the flux induced by the nonlinear diamagnetic component, yielding

$$\begin{aligned}
\frac{\partial}{\partial t}\rho_i^2 \nabla_\perp^2 \frac{e\langle \phi \rangle}{T_i} &= \frac{v_A^2}{c}\rho_i^2 \hat{\mathbf{b}} \cdot \nabla \nabla_\perp^2 \frac{e\langle A_\parallel \rangle}{T_i} + \frac{1}{2} v_{thi}\rho_i \left(\hat{\mathbf{b}} \times \nabla \ln n_0 \right) \cdot \nabla \nabla_\perp^2 \frac{e\langle \phi \rangle}{T_i} \\
&- \frac{c}{B}\rho_i^2 \nabla \cdot \left\langle \left(\hat{\mathbf{b}} \times \nabla \frac{e\delta\phi}{T_i} \right) \cdot \nabla_\perp \nabla_\perp \delta\phi \right\rangle .
\end{aligned} \tag{1.24}$$

Ohm's law can be obtained from the parallel velocity moment of the electron equation, yielding:

$$\begin{aligned} \frac{v_A}{c}\frac{\partial}{\partial t}\frac{e\left\langle A_\parallel\right\rangle}{T_e} &+ v_A\hat{\mathbf{b}}\cdot\nabla\left(\frac{e\left\langle\phi\right\rangle}{T_e}-\frac{\left\langle p_{\parallel e}\right\rangle}{n_0T_e}\right)+\frac{v_A}{B}\left(\hat{\mathbf{b}}\times\nabla\left\langle A_\parallel\right\rangle\right)\cdot\nabla\ln P_\parallel^{(0)} \\ &= \frac{v_A}{c}\eta\nabla_\perp^2\frac{e\left\langle A_\parallel\right\rangle}{T_e}, \end{aligned} \tag{1.25}$$

where we have introduced a collisional resistivity such that large scale resistive instabilities may be treated. Neglecting finite Larmor radius effects, Eq. (1.25) can be reduced to

$$\frac{v_A}{c}\frac{\partial}{\partial t}\left\langle A_\parallel\right\rangle + v_A\hat{\mathbf{b}}\cdot\nabla\left\langle\phi\right\rangle = \frac{v_A}{c}\eta\nabla_\perp^2\left\langle A_\parallel\right\rangle. \tag{1.26}$$

Equations (1.20), (1.24) and (1.26) can be closed by noting that

$$\nabla_\perp\cdot\left\langle\left(\hat{b}\times\nabla\delta\varphi\right)\cdot\nabla_\perp\nabla_\perp\delta\varphi\right\rangle \approx -\frac{\partial^2}{\partial x^2}\sum_k\frac{k_xk_y}{\left(1+\rho_s^2k_\perp^2\right)^2}N_k, \tag{1.27}$$

such that the mean field equations are coupled to the turbulence evolution. Equations (1.20), (1.24) and (1.26) provide a simple tractable set of equations for describing a variety of multi-scale phenomena. Contained as limiting cases of the above equations are the reduced MHD (RMHD) equations obtained by setting $N_k \to 0$ and neglecting diamagnetic corrections, as well as secondary instabilities such as zonal flows (i.e. $\hat{b}\cdot\nabla \to 0$). Before proceeding further, it is useful to briefly review regimes in which different closures of Eq. (1.20) are appropriate.

1.2 Phase Space Dynamics

It is instructive to rewrite Eq. (1.20) in the following form

$$\frac{dN_k}{dt} \equiv \frac{\partial N_k}{\partial t} + \frac{d\mathbf{x}}{dt} \cdot \frac{\partial N_k}{\partial \mathbf{x}} + \frac{d\mathbf{k}}{dt} \cdot \frac{\partial N_k}{\partial \mathbf{k}} = C\left[N_k\right], \tag{1.28}$$

where

$$\frac{d\mathbf{k}}{dt} = -\frac{\partial}{\partial \mathbf{x}}\left(\omega_k + \mathbf{v}_0 \cdot \mathbf{k}\right), \tag{1.29}$$

$$\frac{d\mathbf{x}}{dt} = \frac{\partial}{\partial \mathbf{k}}\left(\omega_k + \mathbf{v}_0 \cdot \mathbf{k}\right). \tag{1.30}$$

A number of observations can be immediately made from the structure of Eq. (1.28). The first is that Eq. (1.28) can be easily seen to have a form reminiscent of the Boltzmann equation, where the rhs can be understood to correspond to a wave collisional operator. This analogy is however imperfect. While particle collisional operators must necessarily conserve particle number, momentum, and energy, the rhs of Eq. (1.28) only conserves the latter two. This result may be easily seen to follow from the well known Manley-Rowe relations. Furthermore, while the wave collisional operator undoubtedly plays a strong role in many regimes, particularly those of weak flow shear, since we are primarily interested in multi-scale interactions, it is convenient to consider the collisionless limit such that only non-local interactions are kept. Equation (1.28) may then be written as:

$$\frac{\partial N_k}{\partial t} + \frac{\partial}{\partial \mathbf{x}} \cdot \left[\frac{\partial}{\partial \mathbf{k}}\left(\omega_k + \mathbf{v}_0 \cdot \mathbf{k}\right) N_k\right] + \frac{\partial}{\partial \mathbf{k}} \cdot \left[-\frac{\partial}{\partial \mathbf{x}}\left(\omega_k + \mathbf{v}_0 \cdot \mathbf{k}\right) N_k\right] = 0. \tag{1.31}$$

From Eq. (1.31) it's clear that in this limit the potential enstrophy density evolves as an incompressible fluid in a four dimensional phase space given by $(\mathbf{x}, \mathbf{k})$. This conservation law can be easily seen to significantly impact the dynamics of both the large scale flow and the small scale turbulence. This follows since the potential enstrophy density may be written as $N_k = \left(1 + k_\perp^2 \rho_s^2\right) E_k$, where E_k is the energy of the small scale turbulence.

Thus, any variation in $k_\perp$ induced by non-local interaction with the large scale flow, must necessarily induce a transfer of energy between the large scale flow and the small scale turbulence, in order to preserve the adiabatic constraint. In particular, any increase in $k_\perp$ will necessarily transport energy to the large scale flow. Thus, an understanding of the phase space dynamics of the drift wave turbulence in the presence of a large scale shear flow pattern, can provide insight into the direction and strength of non-local energy transfer between these two components. In the following sections, we consider idealized flow patterns where either statistical or exact solutions of Eq. (1.31) can be found.

1.2.1 Stationary Shear Flow Pattern

Considering the trivial limit of a constant shear flow pattern given by $\mathbf{v}_0 = \hat{\mathbf{y}} v'_{0y} x$, where $\hat{\mathbf{y}}$ is taken to be in the poloidal direction, and $\hat{\mathbf{x}}$ is in the radial direction. From Eq. (1.29), the time evolution can be trivially solved, yielding [5]:

$$k_x = k_{0x} - k_{0y} v'_{0y} t, \quad k_y = k_{0y}, \tag{1.32}$$

such that $|k_x| \rightarrow \infty$ as $t \rightarrow \infty$, and energy is necessarily transferred to the large scale flow. This solution can be seen to be valid in two regimes: for stationary shear flows strong enough to drive the turbulence into the damped region (not explicitly included here) before the wave packet displaces a distance comparable to the correlation length of the shear flow, or for a drift wave packet moving resonantly with the shear flow pattern. Here, the term resonance, is used to indicate a wave packet whose radial group velocity is equivalent to the radial phase velocity of a poloidally symmetric shear flow structure with frequency Ω and radial wave number q_x. For the latter scenario, Eq. (1.32) can be easily seen to correspond to a poor approximation to the dynamics of the wave packet. This follows, since the radial group velocity of the wave packet is also a function of k_x, such that an initially resonant

wave packet will be rapidly pushed off resonance.

1.2.2 Wave Trapping

A somewhat more realistic model corresponds to a stationary poloidally symmetric shear flow pattern undergoing oscillations in the radial direction. This model may be easily generalized to flow structures with a finite radial phase velocity by transforming to a frame uniformly moving in the radial direction. From Eqs. (1.29) and (1.30), it can be easily shown [21]:

$$\frac{dk_x}{dx} = -k_y \frac{c}{B} \frac{1}{v_{grx}} \frac{\partial^2 \bar{\phi}}{\partial x^2}, \tag{1.33}$$

$$k_y = \text{const} = k_y^0. \tag{1.34}$$

Upon integration an expression for the trajectory of k_x can be written as

$$\begin{aligned}(k_x \rho_s)^2 = & \frac{\left[1 + \left(k_y^{(0)} \rho_s\right)^2\right] \left[1 + \left(k_\perp^{(0)} \rho_s\right)^2\right]}{1 - \left(v_{0y}/v_e^*\right) \left[1 + \left(k_\perp^{(0)} \rho_s\right)^2\right]} \\ & \cdot \left\{ \frac{v_{0y}}{v_e^*} + \frac{\left(k_x^{(0)} \rho_s\right)^2}{\left[1 + \left(k_\perp^{(0)} \rho_s\right)^2\right] \left[1 + \left(k_y^{(0)} \rho_s\right)^2\right]} \right\},\end{aligned} \tag{1.35}$$

where $k_x^{(0)}$ and $k_y^{(0)}$ correspond to the value of k_x and k_y at $v_{0y}\,(x = 0)$ respectively [where $v_{0y}\,(x = 0)$ is taken to be zero for simplicity], and we assume $|v_{0y}/v_e^*| < \left[1 + \left(k_\perp^{(0)} \rho_s\right)^2\right]^{-1}$, such that the denominator before the braces in Eq. (1.35) is nonzero and positive (well satisfied in most applications). From this expression it's clear the trajectories of the wave quanta can be separated into two categories:

a.) trapped: wave quanta whose k_x passes through zero, and are thus reflected by the shear flow,

b.) passing: wave packets whose group velocity is large enough such that the shear flow is incapable of reversing their direction.

A trapping criterion for a given quasi-particle can be easily derived from Eq. (1.35), yielding

$$\left|\frac{v_{0y}}{v_e^*}\right| = \frac{v_y}{c_s}\frac{L_n}{\rho_s} > \frac{\left(k_x^{(0)}\rho_s\right)^2}{\left[1+\left(k_\perp^{(0)}\rho_s\right)^2\right]\left[1+\left(k_y^{(0)}\rho_s\right)^2\right]}, \tag{1.36}$$

where v_y is the amplitude of the oscillatory shear flow. Note that a trapped wave packet undergoes closed orbits in phase space, such that no net energy is transferred to the large scale flow.

1.2.3 Stochastic Regime

In the previous section the trajectories of wave quanta in the presence of a shear flow pattern composed of a single mode with a given Ω and q_x were considered. Here, it is useful to consider the more general case of a spectrum of large scale modes.

The presence of multiple modes can qualitatively alter the trajectories of the drift wave packets. This follows, since as the phase space islands associated with different modes begin to overlap, the previously integral orbits become stochastic, necessitating a statistical description of the drift wave packet's orbits. In order to estimate when a statistical description is appropriate, it is convenient to introduce an effective Chirikov parameter [22] defined by $K_{ch} = \Delta v_{grx}/\Delta\left(\Omega/q_x\right)$, where Δv_{grx} is the range of wave packet group velocities trapped by a given island (i.e. island width), and $\Delta\left(\Omega/q_x\right)$ is the spacing between between islands. Assuming $\left(k_\perp^{(0)}\rho_s\right)^2 < 1$, the width of the phase space islands may be approximated from Eq. (1.36), i.e. $\Delta v_{grx} \approx 2v_e^* k_y^{(0)} \Delta k_x \rho_s^2$, and $\Delta k_x \rho_s \approx \sqrt{v_{0y}/v_e^*}$, such that $\Delta v_{grx} \approx 2\sqrt{v_e^* v_{0y}} k_y^{(0)} \rho_s$. For $K_{ch} > 1$ the trajectories of the wave packets can be well approximated as stochastic, and for $K_{ch} < 1$, the system will remain largely integral, such that the results from the previous section remain valid. Considering the limit $K_{ch} > 1$,

quasi-linear theory provides a useful means of describing the evolution of the drift wave packets. Separating N_k into a mean and fluctuating piece, i.e. $N_k = \langle N_k \rangle + \tilde{N}_k$, and averaging Eq. (1.31), yields:

$$\frac{\partial \langle N_k \rangle}{\partial t} + \mathbf{v}_{gr} \cdot \frac{\partial}{\partial \mathbf{x}} \langle N_k \rangle + \frac{\partial}{\partial \mathbf{x}} \cdot \left\langle \mathbf{v}_0 \tilde{N}_k \right\rangle - \frac{\partial}{\partial \mathbf{k}} \cdot \left\langle \frac{\partial}{\partial \mathbf{x}} \left(\mathbf{k} \cdot \mathbf{v}_0 \right) \tilde{N}_k \right\rangle = 0, \tag{1.37}$$

where the system may be closed via the fluctuation equation:

$$\tilde{N}_k = \frac{-i}{\Omega - \mathbf{v}_{gr} \cdot \mathbf{q}} \left\{ \mathbf{k} \cdot \left(\hat{z} \times \mathbf{q} \right) \mathbf{q} \cdot \frac{\partial \langle N_k \rangle}{\partial \mathbf{k}} + i \left(\hat{z} \times \mathbf{q} \right) \cdot \frac{\partial \langle N_k \rangle}{\partial \mathbf{x}} \right\} \bar{\phi}_q. \tag{1.38}$$

The general form of the mean field equation can thus be seen to contain both real space and k-space diffusion contributions, as well as cross terms. For simplicity, we introduce the limit $q_x \gg q_y$, such that the lowest order expression may be written as [5]

$$\frac{\partial \langle N_k \rangle}{\partial t} + v_{grx} \frac{\partial}{\partial x} \langle N_k \rangle = \frac{\partial}{\partial k_x} \left(D_k \frac{\partial \langle N_k \rangle}{\partial k_x} \right). \tag{1.39}$$

The term on the right hand side of Eq. (1.39) corresponds to k-space diffusion introduced via non-local interaction with the mesoscale flow, with a diffusion coefficient of the form $D_k = k_y^2 \sum_q R\left(\Omega, q\right) q_x^4 \left|\bar{\phi}_q\right|^2$, and the response function $R\left(q_x, \Omega\right) = \pi \delta \left(\Omega - v_{grx} q_x\right)$, where for simplicity the growth rate of the large scale mode has been assumed to be small such that the non-resonant contribution to the response function is negligible. Thus, within this regime, a robust transfer of energy to the large scale flows can be seen to exist.

Chapter 2

Low-q resonances, transport barriers, and secondary electrostatic convective cells

2.1 Introduction

A detailed theoretical understanding of the physical mechanism triggering internal transport barrier formation near low-q resonant surfaces remains elusive. This topic is particularly relevant, as the power input required for inducing an internal transport barrier depends sensitively on the mean current distribution and the presence of integer q surfaces. Note that a standard paradigm often employed to describe transport barrier formation – Reynolds stress driven shear flow inducing a local steepening of the pressure gradient, thus triggering a transport bifurcation via equilibrium $\mathbf{E} \times \mathbf{B}$ flow shear – may not be sufficient, since this phenomenology by itself does not uniquely specify the spatial location of the transport barrier. Thus, a necessary component of any theory of ITB formation must be to *link* the ITB triggering mechanism to the presence of the low-q surface. Many candidate

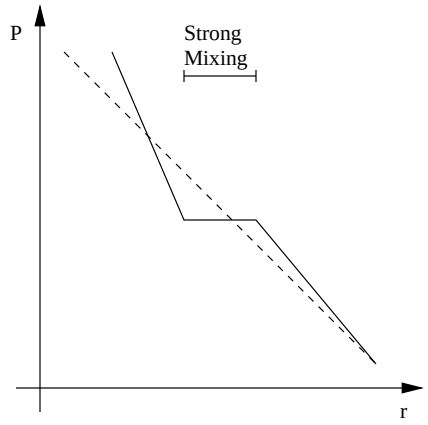

Figure 2.1: Sketch of pressure profile in presence of convective mode. Broken line corresponds to original pressure profile and the solid line corresponds to corrugated profile.

mechanisms have been proposed. These include, but are not limited to (see Ref. [23] for a review): magnetic islands creating local, sharp gradients in profiles [24], sheared electric fields responding to magnetic topology changes or energetic particle dynamics [25], or "rarefaction" of resonant surfaces and its effect on global (i.e. ballooning) modes [26, 27] (also, see Ref. [28] for a discussion of parallel velocity affects). However, in light of recent experimental observations [29], a major challenge to any model of ITB formation at low-q resonances is the need to simultaneously explain *all* of the experimental observations:

a.) the possibility of a purely *electrostatic* trigger mechanism, since magnetic perturbations are not observed in some cases

b.) a region of profile flattening (i.e. "corrugation") *at* the resonant surface, which suggests strong, but localized, mixing or transport in that region

c.) the appearance of a transport barrier, due to strong $\mathbf{E} \times \mathbf{B}$ shear flow, in the region immediately *nearby* the low-q resonance (sketched in Fig. 2.1).

As a means of explaining the experimental observations a.) - c.), detailed gyrokinetic simulations [30] have been performed to support the hypothesis of zonal flows being generated near "gaps" in the density of rational surfaces localized in the vicinity of low-q resonances.

However, any ITB theory based on zonal flow formation alone is inherently unable to satisfy observations b.) and c.). In particular, a self-consistent description of transport near low-q surfaces requires the simultaneous evolution of *both* the Reynolds stress driven shear flows, *and* the underlying micro-turbulence intensity *profile*. This suggests that a critical element linking shear flows to low-q surfaces is the spatial profile of the turbulence intensity and its response to the appearance of a low-q surface. We note that considering the numerous studies of complex nonlinear spatial dynamics of drift wave turbulence, considerations of the linear properties of the micro-turbulence near a low-q surface are not sufficient to determine its saturated nonlinear structure. Furthermore, observations b.) and c.) can be seen to be compatible, since strong localized mixing can induce the formation of $\mathbf{E} \times \mathbf{B}$ shear flows in the layer where ∇P and ∇n steepen immediately adjacent to the mixing zone [31]. In addition, Reynolds stress driven shear flows are necessarily strongest in regions of large fluctuation intensity gradient. Considered together, this further reinforces the necessity of understanding how low-q resonances 'structure' *both* the turbulence intensity *and* the shear flow profiles. For example, a local peak in the intensity profile at the resonant-q surface could lead to the formation of a dipolar shear layer *around* the resonant-q surface, as well as driving localized mixing *a*t the resonant surface [32]. Together, these could steepen the profiles immediately adjacent to the surface.

An equally important element in describing transport near low-q surfaces, is the structure of the shear flow profile. In particular, while Reynolds stress driven axisymmetric shear flows, coupled with a description of the micro-turbulence dynamics, presents a possible route toward a description of transport near low-q surfaces, a more natural and direct approach is to instead consider the impact of *weakly non-axisymmetric shear flows*. Indeed the breaking of axisymmetry by a large scale shear flow has the advantage of introducing *both* local profile relaxation via the intrinsic mixing of the flow, as well as introducing strong shear flows in the adjacent regions. Furthermore, since non-axisymmetric shear

flows are strongly inhibited by magnetic shear, this mechanism would tightly link their appearance to regions of weak magnetic shear, thus providing a simple explanation for why ITBs are often observed to form in OAMq profiles, which typically have weak magnetic shear.

The specific physical mechanism which we propose is a low-m secondary cell, driven by nonlocal transfer of energy form high-k, radially co-located drift wave turbulence. This structure is a finite m, n analogue of the zonal flow (which has $m = n = 0$), and is somewhat similar in concept to the idea of a “convective cell" originally proposed by Dawson and Sagdeev [33, 34]. These secondary cells are strongly localized near resonant surfaces, and damped by friction (as are zonal flows), field line bending, viscosity, Landau resonance, etc. In normal shear discharges they usually have negligibly small width, but become broader and stronger in regimes of weak magnetic shear, which are characteristic of the regimes of OAMq plasmas we consider. In contrast to zonal flows, convective cells combine *both* strong mixing at the resonant surface *and* the generation of shear flows nearby, thus constituting a simple mechanism for satisfying critical elements of the above observations.

In the following, a simple dynamical model describing the self-consistent evolution of a low-m secondary convective cell driven by drift wave turbulence is developed and analyzed. The paper is organized as follows: Section II introduces the model equations, in Section III the cell excitation criterion is derived, Section IV discusses nonlinear properties of the drift wave-convective cell system, Section V presents a simplified transport model, and Section VI presents the conclusions and a discussion of future work.

2.2 Basic Equations

Similar to zonal flows, secondary convective cells are mesoscale phenomena, i.e. they evolve on larger (slower) spatial (temporal) scales compared to the microscopic scales, but

smaller (faster) in comparison to those on which the equilibrium profiles vary. This scale separation, allows the description of the system to be separated into two elements, namely:

a.) a dynamical model of the large scales which incorporates stresses induced by small scales,

b.) a model of the turbulence and how it responds to large scale cellular flow.

In the following, a description of both the large and small scale models are presented. Emphasis is placed on clearly delineating the regime in which convective cells are most likely to be excited, as well as on the critical physical elements which determine their evolution.

2.2.1 Dynamical Model of Mean Field Evolution

Here we are interested in deriving an expression describing the evolution of the large scale mean flow in the presence of a background of ambient drift wave turbulence. The gyrokinetic equation for the total distribution function of ion gyrocenters is given by [18]

$$\frac{\partial f_i^{tot}}{\partial t} + \dot{\mathbf{X}} \cdot \frac{\partial f_i^{tot}}{\partial \mathbf{X}} + \dot{U} \frac{\partial f_i^{tot}}{\partial U} = C\left(f_i^{tot}\right), \tag{2.1}$$

where

$$\dot{\mathbf{X}} = U\left(\hat{b} + \frac{\langle \mathbf{B}_\perp \rangle_\alpha}{B}\right) + \mathbf{v}_d + \frac{c}{B}\hat{b} \times \nabla \langle \psi \rangle_\alpha, \tag{2.2}$$

$$\begin{aligned} \dot{U} &= -\frac{e}{m_i c}\frac{\partial \langle A_\parallel \rangle_\alpha}{\partial t} - \frac{e}{m_i}\left(\hat{b} + \frac{\langle \mathbf{B}_\perp \rangle_\alpha}{B}\right) \cdot \nabla \langle \psi \rangle_\alpha - \frac{1}{m_i}\left(\hat{b} + \frac{\langle \mathbf{B}_\perp \rangle_\alpha}{B}\right) \cdot \nabla \left(\mu \omega_{ci}\right) \\ &- \frac{c}{B} U \hat{b} \times \left(\hat{b} \cdot \nabla \hat{b}\right) \cdot \nabla \langle \psi \rangle_\alpha, \end{aligned} \tag{2.3}$$

$$\mathbf{v_d} = \hat{b} \times \left(\frac{\mu}{m_i}\nabla \ln B + U^2 \frac{\hat{b} \cdot \nabla \hat{b}}{\omega_{ci}}\right).$$

Here $C(f)$ is the gyrokinetic collision operator, $\mu \equiv (m_i v_\perp^2)/(2\omega_{ci})$, $\langle \cdots \rangle_\alpha \equiv (2\pi)^{-1} \int_0^{2\pi} d\alpha \, (\cdots)$, $\psi = \phi - (1/c)\, \mathbf{A}_\perp \cdot \mathbf{v}_\perp$, and ϕ, $\mathbf{A}$, and $\mathbf{B}_\perp$ are perturbed quantities. Eq. (2.2) contains the parallel velocity along a general perturbed magnetic field, drifts due to generalized magnetic geometry, and the $\mathbf{E} \times \mathbf{B}$ drift, with finite β corrections. Eq. (2.3) includes both the electrostatic and inductive component of the parallel electric field and the mirror force. Also, the last term in Eq. (2.3) is necessary in order to cancel the finite divergence of the $\mathbf{E} \times \mathbf{B}$ drift in generalized geometry, so that phase space volume is conserved. Finally, we note that the polarization drift appears via the transformation from gyrocenter coordinates to particle coordinates.

The ordering used is similar to the standard gyrokinetic ordering, i.e.:

$$\frac{\partial_t}{\omega_{ce}} \sim \frac{f}{F_0} \sim \frac{e\phi}{T_e} \sim \epsilon$$

where $\epsilon = \rho_i / L_0$ is the gyrokinetic expansion parameter, and L_0 is the smallest equilibrium scale length. In this analysis we are primarily concerned with considering magnetohydrodynamic (MHD) stable, low-q surfaces for which tearing modes, and other electromagnetic instabilities are not present. Thus, we anticipate weak electromagnetic fluctuations, and it is therefore convenient to take the low β limit for which $\beta \sim \epsilon$. Thus, we are left with the remaining parameters ordered as

$$\frac{A_\parallel}{B\rho_i} \sim \frac{A_\perp}{B\rho_i} \sim \beta \frac{\rho_i}{L_0} \sim \epsilon^2,$$

Note that the low β ordering utilized here, will likely be violated after the formation of the transport barrier, however here our primary interest is understanding the *triggering* mechanism for the ITB. Applying this ordering procedure, evaluating the gyro-averages, and writing the distribution function as $f_i^{tot} = F_{0i} + f_i$, where F_{0i} is the equilibrium piece

(assumed to be Maxwellian), and f_i is a fluctuating quantity, Eq. (2.1) yields the expression

$$\begin{aligned}\frac{\partial f_i}{\partial t}+\left\{U\hat{b}+\frac{c}{B}\hat{b}\times J_0\left(\lambda\right)\nabla\phi+\mathbf{v}_d\right\}\cdot\nabla f_i &= -\frac{c}{B}\hat{b}\times J_0\left(\lambda\right)\nabla\phi\cdot\nabla F_{0i}\\ &+ \left\{\frac{e}{m_i}\hat{b}+\frac{c}{B}U\hat{b}\times\left(\hat{b}\cdot\nabla\right)\hat{b}\right\}\\ &\cdot J_0\left(\lambda\right)\nabla\phi\frac{\partial F_{0i}}{\partial U}+C\left(f_i\right). \qquad (2.4)\end{aligned}$$

It is convenient at this point to separate the fields into a slowly evolving mean field component as well as a rapidly fluctuating small scale component (whose evolution is described in the following section). Defining $\psi=\bar{\psi}+\tilde{\psi}$, where $\bar{\psi}$ and $\tilde{\psi}$ represent the slow and rapidly varying portions respectively, and averaging Eq. (2.4) over the fast scales defined as $\langle\cdots\rangle=(XT)^{-1}\int_t^{t+T}\int_x^{x+X}dt'dx'\left(\cdots\right)$, where x is a radial variable, and X and T correspond respectively to meso length and time scales, yields:

$$\begin{aligned}\frac{\partial\bar{f}_i}{\partial t}+\left\{U\hat{b}+\mathbf{v}_d\right\}\cdot\nabla\bar{f}_i &= -\frac{c}{B}\hat{b}\times\nabla\bar{\phi}\cdot J_0\left(\lambda\right)\nabla F_{0i}\\ &+ \left\{\frac{e}{m_i}\hat{b}+\frac{c}{B}U\hat{b}\times\hat{b}\cdot\nabla\hat{b}\right\}\cdot J_0\left(\lambda\right)\nabla\bar{\phi}\frac{\partial F_{0i}}{\partial U}\\ &- \left\langle\frac{c}{B}\hat{b}\times J_0\left(\lambda\right)\nabla\tilde{\phi}\cdot\nabla\tilde{f}_i\right\rangle+C\left(f_i\right), \qquad (2.5)\end{aligned}$$

Here $\nabla\ln\bar{\psi}<\nabla\ln\tilde{\psi}$, such that the mean field nonlinearity is subdominant to the fluctuation nonlinearity. This approximation, while valid for relatively weak mean flows, needs to be reexamined for the case of intense mean flows in which tertiary instabilities may occur. Also note that for the case of convective cells, the mean field nonlinearity requires somewhat more careful attention than for the case of zonal flows. For zonal flows, the mean field nonlinearity is strictly a sink of free energy, i.e. any tertiary instability necessarily results in the break up of the zonal flow. However, for the case of convective cells, for which $m\neq 0$, tertiary instability of a zonal flow, may in fact act as a source of free energy for the convective cell. This introduces the possibility of two mechanisms of excitation of

convective cells [35]: indirect excitation via Kelvin-Helmholtz instability of zonal flows, or direct excitation via modulational instability of drift wave turbulence. Here we focus on the latter, and leave the former for future analysis.

2.2.1.1 Vorticity Equation

Applying the integral $2\pi \int dU d\mu \left(\omega_{ci}/m_i\right)$ to Eq. (2.5), and noting the spatial dependence of the Jacobian, yields an equation for the evolution of the density of gyrocenters given by

$$\begin{aligned}
&\frac{\partial \bar{N}_i}{\partial t} + \nabla \cdot \left(\hat{b} n_0 \bar{V}_{\|i}\right) + \frac{T_i c}{eB}\hat{b} \times \nabla \ln B \cdot \nabla \bar{P}_{\perp i} + \frac{T_i c}{eB}\hat{b} \times \left(\hat{b} \cdot \nabla\right) \hat{b} \cdot \nabla \bar{P}_{\|i} \\
&\quad = \frac{c}{B}\left(\hat{b} \times \nabla \ln N_0\right) \cdot \nabla \left(1 - \eta_i \frac{b}{2}\right) \exp\left(-\frac{b}{2}\right) \bar{\phi} \\
&\quad - \frac{c}{B}\hat{b} \times \ln B \cdot \nabla \left(1 - \frac{b}{2}\right) \exp\left(-\frac{b}{2}\right) \bar{\phi} - \frac{c}{B}\hat{b} \times \left(\hat{b} \cdot \nabla\right) \hat{b} \cdot \nabla \exp\left(-\frac{b}{2}\right) \bar{\phi} \\
&\quad - \frac{c}{B}\left\langle \hat{b} \times \nabla \left(1 + \frac{b}{2}\right) \exp\left(-\frac{b}{2}\right) \tilde{\phi} \cdot \nabla \tilde{N}_i \right\rangle + \frac{c}{B}\left\langle \hat{b} \times \nabla \frac{b}{2} \exp\left(-\frac{b}{2}\right) \tilde{\phi} \cdot \nabla \tilde{P}_{\perp i} \right\rangle,
\end{aligned} \tag{2.6}$$

where $b = k_\perp^2 \rho_i^2$, $\eta_i \equiv L_n/L_T$, L_T and L_n are the ion temperature and density gradients respectively. Note that a rigorous treatment of the gyrokinetic collision operator in generalized geometry, including full neoclassical effects is currently unavailable. Since a detailed treatment of the gyrokinetic collision operator is not the focus of this analysis, it's contributions to the vorticity equation will be temporarily suppressed for simplicity.

At this point it is necessary to transform from gyrocenter moments into particle fluid moments. In order to obtain a simple expression for the evolution of the particle density it is convenient to exploit the smallness of $\left(k_\perp \rho_s\right)^2$ for the mean fields. Keeping terms up to second order in $\left(k_\perp \rho_s\right)^2$, yields the expressions [18]

$$N_i = n_i + \frac{b}{2}\left(p_{\perp i} + 2\frac{e}{T_i}\phi\right), \tag{2.7}$$

$$V_{\|i} = \left(1 + \frac{b}{2}\right) v_{\|i}, \tag{2.8}$$

$$P_{\|i} = p_{\|i} + \frac{b}{2}\left(p_{\|i} + p_{\perp i} - n_i + 2\frac{e\phi}{T_i}\right), \tag{2.9}$$

$$P_{\perp i} = p_{\perp i} + b\left(2p_{\perp i} - n_i + 2\frac{e\phi}{T_i}\right), \tag{2.10}$$

Substitution of Eqs. (2.7-2.10) into Eq. (2.6) and expanding in b, yields a reduced equation for the ion density

$$\begin{aligned}
&\frac{\partial \bar{n}_i}{\partial t} + \nabla\cdot\left(\hat{b}\bar{v}_{\|i}\right) + \omega_{d\nabla}\bar{p}_{\perp i} + \omega_{d\kappa}\bar{p}_{\|i} - \frac{1}{2}\rho_i^2\frac{\partial}{\partial t}\nabla_\perp^2\bar{p}_{\perp i} - \rho_i^2\frac{\partial}{\partial t}\nabla_\perp^2\frac{e\bar{\phi}}{T_i} - \frac{1}{2}\rho_i^2\nabla\cdot\left(\hat{b}\nabla_\perp^2\bar{v}_{\|i}\right)\\
&\quad = \omega_d^*\frac{e\bar{\phi}}{T_i} - \frac{1}{2}\rho_i^2\omega_d^*\left(1+\eta_i\right)\nabla_\perp^2\frac{e\bar{\phi}}{T_i} - \left(\omega_{d\nabla}+\omega_{d\kappa}\right)\frac{e\bar{\phi}}{T_i} - \frac{c}{B}\left\langle\hat{b}\times\nabla\tilde{\phi}\cdot\nabla\tilde{n}_i\right\rangle\\
&\quad - \frac{c}{B}\rho_i^2\left\langle\hat{b}\times\nabla\tilde{\phi}\cdot\nabla\nabla_\perp^2\frac{e\tilde{\phi}}{T_i}\right\rangle - \frac{1}{2}\frac{c}{B}\rho_i^2\left\langle\hat{b}\times\nabla\tilde{\phi}\cdot\nabla\nabla_\perp^2\tilde{p}_{\perp i}\right\rangle\\
&\quad - \frac{1}{2}\frac{c}{B}\rho_i^2\left\langle\hat{b}\times\nabla\nabla_\perp^2\tilde{\phi}\cdot\nabla\tilde{p}_{\perp i}\right\rangle,
\end{aligned} \tag{2.11}$$

where $p_{\perp i} \to p_{\perp i}/p_{\perp oi}$, $p_{\|i} \to p_{\|i}/p_{\|0i}$, $n_i \to n_i/n_0$, and the drifts are defined as

$$\omega_d^* = v_{thi}\rho_i\hat{b}\times\nabla\ln n_0\cdot\nabla,$$

$$\omega_{d\kappa} = v_{thi}\rho_i\hat{b}\times\left(\hat{b}\cdot\nabla\right)\hat{b}\cdot\nabla,$$

$$\omega_{d\nabla} = v_{thi}\rho_i\hat{b}\times\nabla\ln B\cdot\nabla,$$

and $v_{thi} \equiv \sqrt{T_i/m_i}$. Similarly, the electrons are described by the nonlinear drift kinetic equation

$$\begin{aligned}
&\left\{\frac{\partial}{\partial t} + \left(\mathbf{v_d} + \frac{c}{B}\hat{b}\times\nabla\phi + U\hat{b}\right)\cdot\nabla\right\} f_e^{tot}\\
&+\left(\frac{e}{m_e}\hat{b}\cdot\nabla\phi - \mu\frac{\omega_{ce}}{m_e}\hat{b}\cdot\nabla\ln B - \frac{c}{B}U\hat{b}\times\left(\hat{b}\cdot\nabla\hat{b}\right)\cdot\nabla\phi\right)\frac{\partial f_e^{tot}}{\partial U} = C\left(f_e^{tot}\right),
\end{aligned} \tag{2.12}$$

A similar calculation gives the evolution equation for the density of electrons as

$$\frac{\partial \bar{n}_e}{\partial t} + \nabla \cdot \left(\hat{b} \bar{v}_{\parallel e} \right) + \omega_{d\nabla} \bar{p}_{\perp e} + \omega_{d\kappa} \bar{p}_{\parallel e} = \omega_d^* \frac{e\bar{\phi}}{T_i} - \left(\omega_{d\nabla} + \omega_{d\kappa} \right) \frac{e\bar{\phi}}{T_i} - \frac{c}{B} \left\langle \hat{b} \times \nabla \tilde{\phi} \cdot \nabla \tilde{n}_e \right\rangle, \tag{2.13}$$

where $\bar{p}_{\parallel e} \rightarrow \bar{p}_{\parallel e}/p_{0e}$ and $\bar{p}_{\perp e} \rightarrow \bar{p}_{\perp e}/p_{0e}$. Taking the difference between Eqs. (2.11) and (2.13), applying Eq. (2.15), and utilizing quasi-neutrality then yields

$$\begin{aligned} \frac{\partial}{\partial t} \nabla_\perp^2 \frac{e\bar{\phi}}{T_i} = & -v_A \frac{e}{T_i} \hat{b} \cdot \nabla \nabla_\perp^2 \bar{A}_\parallel - \frac{\omega_{d\nabla}}{\rho_i^2} \bar{p}_\perp - \frac{\omega_{d\kappa}}{\rho_i^2} \bar{p}_\parallel - \frac{1}{2} \omega_d^* \left(1 + \eta_i \right) \nabla_\perp^2 \frac{e\bar{\phi}}{T_i} - \frac{1}{2} \hat{b} \cdot \nabla \nabla_\perp^2 \bar{v}_{\parallel i} \\ & - \frac{c}{B} \left\langle \hat{b} \times \nabla \tilde{\phi} \cdot \nabla \nabla_\perp^2 \frac{e\tilde{\phi}}{T_i} \right\rangle - \frac{1}{2} \frac{\partial}{\partial t} \nabla_\perp^2 \bar{p}_{\perp i} - \frac{1}{2} \frac{c}{B} \left\langle \hat{b} \times \nabla \tilde{\phi} \cdot \nabla \nabla_\perp^2 \tilde{p}_{\perp i} \right\rangle \\ & + \frac{1}{2} \frac{c}{B} \left\langle \hat{b} \times \nabla \nabla_\perp^2 \tilde{\phi} \cdot \nabla \tilde{p}_{\perp i} \right\rangle, \end{aligned} \tag{2.14}$$

where $p_\perp$ and $p_\parallel$ represent the total perpendicular and parallel pressure, $A_\parallel \rightarrow \left(v_A/c \right) A_\parallel$, the $\nabla \cdot \hat{b} = -\hat{b} \cdot \nabla \ln B$ terms are neglected, and Ampere's law, given by

$$v_{\parallel i} - v_{\parallel e} = -\frac{c}{4\pi n_0 e} \nabla_\perp^2 A_\parallel, \tag{2.15}$$

has been used to eliminate the parallel velocity components. Eq. (2.14) provides a description of vorticity evolution appropriate for mesoscale phenomena.

2.2.1.2 Ohm's Law

In contrast to zonal flows, convective cells, while poloidally extended, have a weak but finite radial component of velocity. This weak spatial asymmetry necessitates the inclusion of resistivity in order to allow the plasma to diffuse through the magnetic field. Hence, in this section it is convenient to model the role of collisions via the explicit inclusion of parallel resistivity.

Taking the first order moment of Eq. (2.12), yields the expression

$$v_A \hat{b} \cdot \nabla \left(\bar{p}_{\parallel e} \tau - \frac{e\bar{\phi}}{T_i} \right) = -\frac{e}{T_i} \eta \nabla_\perp^2 \bar{A}_\parallel, \tag{2.16}$$

where $\eta \equiv \eta_\parallel$ is the parallel collisional resistivity, and $\tau \equiv T_e/T_i$. Here we consider the evolution of mesoscale phenomena (large in comparison to the electron skin depth), such that electron inertia may be ignored. We have also again neglected terms proportional to $\hat{b} \cdot \nabla \ln B$. This expression for Ohm's law interpolates between two well known regimes. For large scale dynamics in which finite Larmor corrections may be neglected, Eq. (2.16) reduces to $v_A \hat{b} \cdot \nabla \bar{\phi} = \eta \nabla_\perp^2 \bar{A}_\parallel$, which corresponds to the electrostatic limit of the resistive MHD Ohm's Law. Also, for scales in which $k_\perp \rho_s \approx 1$, in the low collisionality limit, and in the absence of temperature fluctuations, Eq. (2.16) reduces to the adiabatic response limit $\bar{n}/n_0 = e\bar{\phi}/T_e$. Here, however, since convective cells correspond to mesoscale phenomena, and collisions play an essential role in allowing the convective cell to diffuse through the magnetic field, we are interested in considering the more generalized form given by Eq. (2.16).

2.2.1.3 Pressure and Ion Parallel Velocity Evolution

In order to close the system given by Eqs. (2.14) and (2.16), it is necessary to derive expressions for the evolution of the electron and ion pressure, as well as the parallel ion velocity. In the following, since we consider the limit of weak magnetic inhomogeneity and $b < 1$, we will only keep the lowest order contributions. Thus, the perpendicular and parallel ion pressure equations can be written as

$$\frac{\partial p_{\perp i}}{\partial t} + \hat{b} \cdot \nabla v_{\parallel i} = \omega_d^* \left(1 + \eta_i\right) \frac{e\phi}{T_i} - \frac{c}{B} \hat{b} \times \nabla \phi \cdot \nabla p_{\perp i}, \tag{2.17}$$

$$\frac{\partial p_{\parallel i}}{\partial t} + 3\hat{b} \cdot \nabla v_{\parallel i} = \omega_d^* \left(1 + \eta_i\right) \frac{e\phi}{T_i} - \frac{c}{B} \hat{b} \times \nabla \phi \cdot \nabla p_{\parallel i}, \tag{2.18}$$

where again collisions have been temporarily suppressed. Similarly for electrons

$$\frac{\partial p_{\perp e}}{\partial t} + \hat{b}\cdot\nabla v_{\parallel e} = \omega_d^*\left(1+\eta_i\right)\tau^{-1}\frac{e\phi}{T_i} - \frac{c}{B}\hat{b}\times\nabla\phi\cdot\nabla p_{\perp e}, \tag{2.19}$$

$$\frac{\partial p_{\parallel e}}{\partial t} + 3\hat{b}\cdot\nabla v_{\parallel e} = \omega_d^*\left(1+\eta_i\right)\tau^{-1}\frac{e\phi}{T_i} - \frac{c}{B}\hat{b}\times\nabla\phi\cdot\nabla p_{\parallel e}. \tag{2.20}$$

Also, an equation for the ion parallel velocity can be easily derived by taking the parallel velocity moment of Eq. (2.5):

$$\frac{\partial v_{\parallel i}}{\partial t} = -v_{thi}^2\hat{b}\cdot\nabla\left(\frac{e\phi}{T_i} + p_{\parallel i}\right) - \frac{c}{B}\hat{b}\times\nabla\phi\cdot\nabla v_{\parallel i}, \tag{2.21}$$

Eqs. (2.14,2.16,2.17-2.21) form a closed set of equations describing the evolution of the convective cell. In the next section, these equations will be simplified into a single equation, providing a simple and intuitive description of the large scale mean flow.

2.2.1.4 Equation for Convective Cell Evolution

Here we seek to simplify the system given by Eqs. (2.14,2.16,2.17-2.21). Eq. (2.14) can be simplified by taking the Laplacian of Eq. (2.17)

$$\begin{aligned}\frac{\partial}{\partial t}\nabla_\perp^2 p_{\perp i} + \hat{b}\cdot\nabla\nabla_\perp^2 v_{\parallel i} = \omega_d^*\left(1+\eta_i\right)\nabla_\perp^2\frac{e\phi}{T_i} + \frac{c}{B}\left(\hat{b}\times\nabla\nabla_\perp^2\phi\right)\cdot\nabla p_{\perp i} \\ - \frac{c}{B}\left(\hat{b}\times\nabla\phi\right)\cdot\nabla\nabla_\perp^2 p_{\perp i} - 2\frac{c}{B}\nabla\cdot\left[\left(\hat{b}\times\nabla\nabla\phi\right)\cdot\nabla p_{\perp i}\right],\end{aligned} \tag{2.22}$$

where we have used the approximation

$$\begin{aligned}\nabla_\perp^2\left[\left(\hat{b}\times\nabla\phi\right)\cdot\nabla p_{\perp i}\right] \approx -\left(\hat{b}\times\nabla\nabla_\perp^2\phi\right)\cdot\nabla p_{\perp i} + \left(\hat{b}\times\nabla\phi\right)\cdot\nabla\nabla_\perp^2 p_{\perp i} \\ + 2\nabla\cdot\left[\left(\hat{b}\times\nabla\nabla\phi\right)\cdot\nabla p_{\perp i}\right].\end{aligned} \tag{2.23}$$

Performing an average over the rapid spatial and temporal scales on Eq. (2.22), and inserting the result into Eq. (2.14) yields:

$$\frac{\partial}{\partial t}\nabla_\perp^2\frac{e\bar{\phi}}{T_i} = \frac{v_A^2}{\eta}\left(\hat{b}\cdot\nabla\right)^2\left(\bar{p}_{\parallel e}\tau - \frac{e\bar{\phi}}{T_i}\right) - \frac{\omega_{d\nabla}}{\rho_i^2}\bar{p}_\perp - \frac{\omega_{d\kappa}}{\rho_i^2}\bar{p}_\parallel - \omega_d^*\left(1+\eta_i\right)\nabla_\perp^2\frac{e\bar{\phi}}{T_i} - \frac{c}{B}\left\langle\hat{b}\times\nabla\tilde{\phi}\cdot\nabla\nabla_\perp^2\frac{e\tilde{\phi}}{T_i}\right\rangle, \tag{2.24}$$

where the last term on the right of Eq. (2.22) has been dropped as discussed in Chapter 1, and Eq. (2.16) has been used to eliminate the $\nabla_\perp^2\bar{A}_\perp$ term. In order to further simplify Eq. (2.24), we calculate the linear response of Eqs. (2.18) and (2.20), to obtain

$$\bar{p}_{\parallel e} = -3i\frac{\hat{b}\cdot\nabla}{\omega}\bar{v}_{\parallel e} + i\frac{\omega_d^*}{\omega}\left(1+\eta_i\right)\tau^{-1}\frac{e\bar{\phi}}{T_i}, \tag{2.25}$$

$$\bar{p}_{\parallel i} = -3i\frac{\hat{b}\cdot\nabla}{\omega}\bar{v}_{\parallel i} + i\frac{\omega_d^*}{\omega}\left(1+\eta_i\right)\frac{e\bar{\phi}}{T_i}. \tag{2.26}$$

$\bar{v}_{\parallel e}$ can be obtained from Eqs. (2.15) and (2.16), and is

$$\bar{v}_{\parallel e} = \bar{v}_{\parallel i} - \frac{v_A^2\rho_i^2}{\eta}\hat{b}\cdot\nabla\left(\tau\bar{p}_{\parallel e} - \frac{e\bar{\phi}}{T_i}\right). \tag{2.27}$$

Similarly for $\bar{v}_{\parallel i}$, we find

$$\bar{v}_{\parallel i} = -i\frac{v_{thi}^2}{\omega}\hat{b}\cdot\nabla\left(\frac{e\bar{\phi}}{T_i} + \bar{p}_{\parallel i}\right). \tag{2.28}$$

Utilizing Eq. (2.26), Eq. (2.28) can be written in terms of $\bar{\phi}$, yielding:

$$\bar{v}_{\parallel i} = -\frac{iv_{thi}^2}{\omega}\left[1 + \frac{3v_{thi}^2}{\omega^2}\left(\hat{b}\cdot\nabla\right)^2\right]^{-1}\hat{b}\cdot\nabla\left\{1 + i\frac{\omega_d^*}{\omega}\left(1+\eta_i\right)\right\}\frac{e\bar{\phi}}{T_i}. \tag{2.29}$$

The second term in the denominator, can be estimated as

$$\frac{3v_{thi}^2}{\omega^2}\left(\hat{b}\cdot\nabla\right)^2 \sim m^2\left(\frac{\omega_{ci}}{\omega}\right)^2\left(\frac{\rho_i}{a}\right)^2\left(\frac{\Delta x}{L_s}\right)^2,$$

where m is the poloidal mode number of the cell, a is the minor radius, and Δx is the radial extent of the cell. For realistic parameters, in regimes of weak magnetic shear, this term is negligible. Thus, Eq. (2.29) may be reduced to

$$\bar{v}_{\parallel i} = -\frac{iv_{thi}^2}{\omega}\hat{b}\cdot\nabla\left\{1+i\frac{\omega_d^*}{\omega}\left(1+\eta_i\right)\right\}\frac{e\bar{\phi}}{T_i}. \tag{2.30}$$

Similarly, $\bar{v}_{\parallel e}$ can be written as

$$\begin{aligned}\bar{v}_{\parallel e} = &\left[1-3i\tau\frac{v_A^2\rho_i^2}{\eta\omega}\left(\hat{b}\cdot\nabla\right)^2\right]^{-1}\\ &\cdot\hat{b}\cdot\nabla\left\{\frac{v_A^2\rho_i^2}{\eta}\left[1-i\frac{\omega_d^*}{\omega}\left(1+\eta_i\right)\right]-i\frac{v_{thi}^2}{\omega}\left[1+i\frac{\omega_d^*}{\omega}\left(1+\eta_i\right)\right]\right\}\frac{e\bar{\phi}}{T_i},\end{aligned} \tag{2.31}$$

where the second term in the denominator can be estimated as

$$3\tau\frac{v_A^2\rho_i^2}{\eta\omega}\left(\hat{b}\cdot\nabla\right)^2 \sim m^2\tau S\left(\frac{\omega_{ci}}{\omega}\right)\left(\frac{\rho_i}{a}\right)^3\beta_i^{1/2}\left(\frac{\Delta x}{L_s}\right)^2.$$

Here β_i is evaluated using the ion temperature, and S is the Lundquist number defined as $S \equiv (v_A a/\eta)$. This term is negligible for realistic parameters, so Eq. (2.31) can be approximated as

$$\bar{v}_{\parallel e} = \hat{b}\cdot\nabla\left\{\frac{v_A^2\rho_i^2}{\eta}\left[1-i\frac{\omega_d^*}{\omega}\left(1+\eta_i\right)\right]-i\frac{v_{thi}^2}{\omega}\left[1+i\frac{\omega_d^*}{\omega}\left(1+\eta_i\right)\right]\right\}\frac{e\bar{\phi}}{T_i}. \tag{2.32}$$

Hence, from Eq. (2.25) the electron parallel pressure can be written as

$$\bar{p}_{\|e} = -3i\frac{v_A^2\rho_i^2}{\eta\omega}\left(\hat{b}\cdot\nabla\right)^2\left\{1 - i\left(\frac{v_{thi}}{v_A}\right)^2\frac{\eta}{\omega\rho_i^2}\right\}\frac{e\bar{\phi}}{T_i} + i\frac{\omega_d^*}{\omega}\left(1+\eta_i\right)\tau^{-1}\frac{e\bar{\phi}}{T_i}, \tag{2.33}$$

where we have dropped the $i\left(\omega_e^*/\omega\right)\left(1+\eta_i\right)$ terms inside the brackets in Eq (2.32), since they are smaller than the second term in Eq. (2.33) by factors of $3\left(v_A k_\| \rho_i\right)^2/\left(\eta\omega\right)$ and $3v_{thi}^2 k_\|^2/\omega^2$ respectively. Employing analogous approximations for the perpendicular electron and ion pressure, Eq. (2.24) can then be written as

$$\begin{aligned}\frac{\partial}{\partial t}\nabla_\perp^2\bar{\phi} = &-\frac{v_A^2}{\eta}\left\{1 - i\frac{\omega_d^*}{\omega}\left(1+\eta_i\right) - i\frac{\omega_{d\nabla}+3\omega_{d\kappa}}{\omega}\left[1 - 2i\left(\frac{v_{thi}}{v_A}\right)^2\frac{\eta}{\omega\rho_i^2}\right]\right\}\nabla_\|^2\bar{\phi} \\ &- i\frac{\omega_d^*}{\omega}\frac{\omega_{d\kappa}+\omega_{d\nabla}}{\rho_i^2}\left(1+\eta_i\right)\left(1+\tau^{-1}\right)\bar{\phi} - \omega_d^*\left(1+\eta_i\right)\nabla_\perp^2\bar{\phi} \\ &- \frac{c}{B}\left\langle\hat{b}\times\nabla\tilde{\phi}\cdot\nabla\nabla_\perp^2\tilde{\phi}\right\rangle - \gamma_d\nabla_\perp^2\bar{\phi} + \nu_c\nabla_\perp^2\nabla_\perp^2\bar{\phi},\end{aligned} \tag{2.34}$$

where $\nabla_\| \equiv \hat{b}\cdot\nabla$, and fourth order terms of $\nabla_\|$ have been neglected. The terms on the right hand side of Eq. (2.34) correspond to field line bending, coupling to the equilibrium pressure gradient in generalized magnetic geometry, diamagnetic drift, Reynolds stresses induced by the micro-turbulence, and the last two terms correspond to generic forms for neoclassical friction and classical viscosity. While corrections due to finite Larmor radius effects and generalized magnetic geometry perturb the mode structure and the growth rate of the cell, the three critical elements within this description correspond to magnetic field line bending, collisional damping, and Reynold's stresses. In the simplest picture, these three elements combine to set the radial width of the mode, the magnitude of the large scale damping, as well as the strength of the instability drive. More explicitly, resistive field line bending plays a dual role: acting in combination with collisional viscosity as a mechanism for large scale damping, as well as setting the radial extent of the convective cell. Both of these properties are critical elements within the description, since the radial

extent of the mode determines the width over which the cell mixes and, in analogy with the drift wave-zonal flow system, large scale damping is expected to determine how well the cell regulates the turbulence intensity. Another necessary component within our description corresponds to the Reynolds stresses exerted by the small scale micro-turbulence. This term provides the mechanism for spectral transfer of energy from small to large scales, and is the dominant mechanism of cell drive.

2.2.2 Model of Turbulence Intensity Evolution

Wave kinetics provides the simplest framework for describing the evolution of the small scales. This description provides both easy visualization of the drift wave dynamics, as well as a simple mathematical framework to self-consistently incorporate multi-scale interactions. The wave kinetic equation for drift wave turbulence is given by [13]

$$\frac{\partial N_k}{\partial t} + \frac{\partial}{\partial \mathbf{k}} \left(\omega_k + \mathbf{v}_0 \cdot \mathbf{k} \right) \cdot \frac{\partial N_k}{\partial \mathbf{x}} - \frac{\partial}{\partial \mathbf{x}} \left(\omega_k + \mathbf{v}_0 \cdot \mathbf{k} \right) \cdot \frac{\partial N_k}{\partial \mathbf{k}} = \gamma_k N_k - \Delta \omega_k N_k^2, \quad (2.35)$$

where N_k is the wave quanta population, defined by $N_k \equiv \left(1 + k_\perp^2 \rho_s^2\right)^2 I_k$, I_k is a Wigner function defined as $I_k = \int d\mathbf{q} e^{i\mathbf{q}\cdot\mathbf{x}} \left\langle \tilde{\phi}_{k+q} \tilde{\phi}_{-k} \right\rangle$, (where the averaging is over the fast temporal scales), ω_k is the linear frequency, and $\mathbf{v}_{gr} = d\omega_k / d\mathbf{k}$ is the group velocity. Here, nonlocal interactions between the large scale shear flow and the drift wave turbulence are described by the advection and refraction of the drift wave packets, corresponding to the second and third terms respectively on the left hand side of Eq. (2.35). The right hand side of Eq. (2.35) has the form of an effective collision operator, where the first and second terms represent growth and local self-saturation, respectively. From Eq. (2.35) an expression for the the evolution of the mean turbulence intensity in the presence of a large scale

shear flow can be easily derived as [5]

$$\frac{\partial \langle N \rangle}{\partial t} + v_{grx} \frac{\partial \langle N \rangle}{\partial x} = \frac{\partial}{\partial k_x} \left(D_k \frac{\partial \langle N \rangle}{\partial k_x} \right) + \gamma_k \langle N \rangle - \Delta\omega_k \langle N \rangle^2 . \tag{2.36}$$

The first term on the right hand side of Eq. (2.36) corresponds to k-space diffusion introduced via nonlocal interaction with the convective cell (i.e. random shearing), the second term corresponds to spatial mixing of the turbulence intensity profile by the convective cell. The k-space diffusion coefficient has the form $D_k = k_y^2 \sum_q R(k,q)\, q_x^4 \left|\bar{\phi}_q\right|^2$, where the resonance function is $R(k,q) = \gamma_k / \left(\gamma_k^2 + (\omega_q - v_{grx} q_x)^2\right)$. Here, q_x corresponds to the radial wave number of the large scale mode, ω_q is the frequency of the large scale mode, and γ_k is understood to represent the drift wave self-decorrelation rate set by the condition of quasi-stationary turbulence $\gamma_k N_k - \Delta\omega_k N_k^2 \approx 0$. Note that this broadened form of the response function interpolates between the case of weak local interactions where the response function asymptotes to $R(k,q) \rightarrow \pi\delta(\omega_q - v_{gr} q_x)$, as well as the case of strong local interactions in which the broadening of the resonance is significant.

2.2.3 Self-Consistent Model

Eqs. (2.34) and (2.35) provide a self-consistent description of the coupled dynamics of the drift wave-convective cell system. Here, we are interested in formally closing the system of equations. This can be easily done by utilizing the expression

$$\left\langle \hat{b} \times \nabla\tilde{\phi} \cdot \nabla\nabla_\perp^2 \tilde{\phi} \right\rangle \approx -\frac{\partial^2}{\partial x^2} \sum_k \frac{k_x k_y}{\left(1 + \rho_s^2 k_\perp^2\right)^2} N_k. \tag{2.37}$$

From Eqs. (2.37) and (2.34), one can follow the two-scale, adiabatic closure used in Refs. [5, 36] to derive a Fourier transformed evolution equation for the convective cell

$$\frac{v_A^2 q_y^2}{\eta L_s^2} \left(1 - i\frac{\omega_d^*}{\omega}\right) \frac{d^2\phi_q}{dq_x^2} = \left\{ \left[\nu_c + \nu_T(q_x)\right] q_x^2 + \left[\gamma_d - i(\omega - \omega_d^*)\right] \right\} q_x^2 \phi_q, \tag{2.38}$$

where the magnetic curvature terms have been dropped and

$$\nu_T = c_s^2 \sum_k R\left(k,q\right) \frac{\rho_s^2 k_y^2}{\left(1+\rho_s^2 k_\perp^2\right)^2} k_x \frac{\partial \left\langle N \right\rangle}{\partial k_x}. \tag{2.39}$$

Here, $\rho_s = c_s/\omega_{ci}$, $c_s = \sqrt{T_e/m_i}$ and $(1+\eta_i)$ has been absorbed into ω_d^*. For $\partial \left\langle N \right\rangle / \partial k_x < 0$ (true for all practical cases), the turbulent viscosity will be *negative*, and thus correspond to a source of free energy for the mean flow, a result familiar from previous studies of the drift wave-zonal flow system. Note that the inclusion of magnetic curvature would allow the cell to couple directly to the free energy contained within the pressure gradient, and thus admit additional unstable roots. Here, for simplicity, we choose to focus exclusively on unstable roots associated with modulation instability of the drift wave turbulence, as this will allow for an uncluttered presentation of the physics underlying the convective cell. Finally, Eq. (2.38) is derived using $q_\parallel = q_y\left(x/L_s\right)$, where $x = r - r_{m,n}$, and $r_{m,n}$ is the m,n rational surface.

Eqs. (2.36) and (2.38) constitute a closed, self-consistent description of the dynamics of a low-m, electrostatic vortical cell evolving in the presence of drift wave turbulence. Unlike zonal flows, the resonant finite-m convective cell drives radial transport (since $\tilde{v}_r \neq 0$) and also is damped by field line bending and collisional viscosity, as well as by friction between trapped and untrapped particles. Thus, the convective cell is more strongly damped than the zonal flow, which is (linearly) damped *only* by collisional friction and viscosity. The width of the cell is determined by the interplay between field line bending (i.e. proportional to magnetic shear!) and viscosity. Thus, finite m, n convective cells are always localized at $\mathbf{k}\cdot\mathbf{B} = 0$ resonances and are more damped than zonal flows, and so are usually subdominant to zonal flows. *However, in the weak shear regimes characteristic of OAMq plasmas, they can be considerably broader and more robust than in normal shear regimes.*

2.3 Excitation criterion

Here, we are interested in identifying the excitation criterion for the convective cell. In order to simplify the notation throughout the analysis, Eq. (2.39) is approximated as:

$$\left|\nu_T\left(q_x\right)\right| \approx c_s^2 \frac{\gamma_k}{\gamma_k^2 + \left(q_x v_{gr}\right)^2} \left\langle N \right\rangle \approx \frac{4 D_{GB}}{1 + \left(4\rho_s q_x\right)^2} \frac{\left\langle N \right\rangle}{N_{ML}} \,, \tag{2.40}$$

where $v_{gr}/\gamma_k \approx 4 v_e^*/\omega_e^* \approx 4\rho_s$, $N_{ML} = \left(\rho_s/L_n\right)^2$, and $D_{GB} = \left(\rho_s/L_n\right) c_s \rho_s$. A solution to Eq. (2.38) can be found using a WKB analysis. We require convergent solutions for $\Re q_x \rightarrow \infty$, and since the potential of Eq. (2.38) has a double well structure, we apply $\phi_q\left(0\right) = 0$ for odd modes, and $\phi_q'\left(0\right) = 0$ for even modes. The rhs of Eq. (2.38) has six zeros in the coefficient of ϕ_q, resulting in singularities in the WKB solution. Thus, we must find a solution near these regions and match to the surrounding WKB solutions. Performing the asymptotic analysis yields the eigenvalue conditions for the odd and even modes (respectively) as (details contained in Appendix A):

$$\Delta x \int_{q_1}^{q_2} dq_x \sqrt{\Xi\left(q_x\right)} = \pi \left(l_o - \frac{1}{2}\right) \,, \tag{2.41a}$$

$$\Delta x \int_{q_1}^{q_2} dq_x \sqrt{\Xi\left(q_x\right)} = \pi \left(l_e - \frac{1}{2}\right) + \delta \,, \tag{2.41b}$$

$$\tan\delta = -\frac{1}{\sqrt{2}} \exp\left(-\frac{4}{3}\Delta x \left(-\frac{d\Xi}{dq_x}|_{q=q_1}\right)^{1/2} q_1^{3/2}\right) \,, \tag{2.42a}$$

$$\Xi\left(q_x\right) \equiv \left(1 - i\frac{\omega_d^*}{\omega}\right)^{-1} \left[\left(\frac{\nu_c - \left|\nu_T\left(q_x\right)\right|}{\left|\nu_T\left(0\right)\right|}\right) \Delta x^2 q_x^2 + \frac{\Delta x^2}{\left|\nu_T\left(0\right)\right|} \left[\gamma_d - i\left(\omega - \omega_d^*\right)\right]\right] \Delta x^2 q_x^2 \,. \tag{2.42b}$$

Here, l_o and l_e are integers ≥ 1, $\Delta x \equiv \left(\left|\nu_T\left(0\right)\right| \eta\right)^{1/6} \left(L_s/\left(v_A q_y\right)\right)^{1/3}$, and q_1 and q_2 are the roots (in the complex plane) of Eq. (2.42b) with $|q_1| < |q_2|$. A branch cut is made between q_1 and q_2, in order to ensure the kernel of Eqs. (2.41a) and (2.41b) is single valued, and

the contour of integration is chosen to run just below this branch cut. Note that since the real piece of δ is negative definite, the even mode with $l_e = 1$ is always the most unstable solution. Thus, for the remainder of this analysis we will focus exclusively on this mode, although the general properties of other modes would not differ significantly. At this point it is convenient to introduce the following definitions

$$N \equiv \frac{\langle N \rangle}{N_{ML}}, \quad \hat{\nu}_c \equiv \frac{\nu_c}{D_{GB}}, \quad \Gamma \equiv \frac{1}{\gamma_k}\left[\gamma_d - i\left(\omega - \omega_d^*\right)\right], \quad \zeta \equiv \frac{1}{8}\left(\frac{N-\Gamma}{\hat{\nu}_c} - \frac{1}{4}\right) + \frac{1}{16}\,.$$

Making the change of variables, $z = \rho_s^2 q_x^2 - (1/8)\left(N - \Gamma - \hat{\nu}_c/4\right)/\hat{\nu}_c$, Eq. (2.41b) can be rewritten as:

$$\frac{1}{2}\sqrt{\frac{\nu_c}{|\nu_T(0)|}}\left(\frac{\Delta x}{\rho_s}\right)^3\left(1 - i\frac{\omega_d^*}{\omega}\right)^{-1/2}\int_{-z_c}^{z_c} dz\sqrt{\frac{(z_c - z)(z_c + z)}{z + \zeta}} = \frac{\pi}{2} + \delta\,, \tag{2.43}$$

$$z_c = \frac{1}{8}\sqrt{\left(\frac{N-\Gamma}{\hat{\nu}_c} - \frac{1}{4}\right)^2 - \frac{\Gamma}{\hat{\nu}_c}}\,, \tag{2.44}$$

and $|\zeta| > |z_c|$. Evaluating the integral in Eq. (2.43) then yields:

$$\frac{\pi}{2} + \delta = \frac{2}{3}\sqrt{\frac{\nu_c}{|\nu_T(0)|}}\left(\frac{\Delta x}{\rho_s}\right)^3\left(1 - i\frac{\omega_d^*}{\omega}\right)^{-1/2}\sqrt{z_c + \zeta}\left\{\zeta \mathrm{E}\left(\frac{2z_c}{z_c + \zeta}\right) - (\zeta - z_c)\,\mathrm{K}\left(\frac{2z_c}{z_c + \zeta}\right)\right\}. \tag{2.45}$$

Here K and E are complete elliptical integrals of the first and second kind respectively [37]. Expanding this expression to first order in $\hat{\nu}_c$, yields a recursive expression for the growth rate of the mode

$$\Gamma \approx N - \left(\frac{\frac{3\pi}{2} + \delta}{1 - \epsilon}\right)^{2/3}\frac{\nu_c^{2/3}}{\eta^{1/3}}\left(\frac{v_A q_y}{L_s}\right)^{2/3}\left(1 - i\frac{\omega_d^*}{\omega}\right)^{1/3}\frac{1}{\gamma_k}\,, \tag{2.46}$$

$$\epsilon \equiv \frac{3}{4}\alpha\left(\ln\left(\frac{16}{\alpha}\right) - \frac{N-2\Gamma}{N-\Gamma}\right) ,$$

$$\alpha \equiv \frac{1}{4}\frac{N}{(N-\Gamma)^2}\hat{\nu}_c .$$

In order to obtain a simple excitation criterion for the convective cell, it is useful to neglect the ω_d^* dependence in the second term in Eq. (2.46) (a higher order ω_d^* correction), then the lowest order imaginary component of yields $\omega \approx \omega_d^*$. Thus, Eq. (2.46) becomes

$$N \approx \frac{\gamma_d}{\gamma_k} + \left(\frac{\frac{3\pi}{2}+\delta}{1-\epsilon}\right)^{2/3}\frac{\nu_c^{2/3}}{\eta^{1/3}}\left(\frac{v_A q_y}{L_s}\right)^{2/3}\frac{1}{\gamma_k} . \tag{2.47}$$

Here, since we are interested in an excitation criterion, the growth rate has been taken to zero, and ϵ is defined above, except with $\Gamma \rightarrow \gamma_d/\gamma_k$. The first term in Eq. (2.47) is the contribution from scale-independent collisional damping, familiar from descriptions of zonal flows, and the second term corresponds to damping due to magnetic shear (field line bending) and collisional viscosity. Note that although $\nu_c/D_{GB} \ll 1$ for all practical cases, α may still be significant due to the factor of $(N-\Gamma)^2$ in the denominator. This surprisingly strong dependence on the collisional viscosity and field line bending can be understood by considering the coupled effect of these two damping mechanisms. As shown below, stronger field line bending leads to more localized modes in real space, so the rapid variation of the mode structure will then enhance the contribution from collisional viscosity (note that the anomalous viscosity possesses scale dependence!), leading to a stronger stabilizing effect. Furthermore, since the mode is ultimately localized by the presence of collisional viscosity, it's clear that even for modest values, the saturated turbulence intensity can be strongly affected.

A numerical solution of Eq. (2.45) [with $\omega_d^* = 0$, in order to compare with Eq. (2.47)] is plotted in Figs. 2.2 and 2.3. As can be seen from examination of Figs. 2.2 and 2.3, or Eq. (2.47), for strong magnetic shear or viscosity the cell is strongly damped, so it

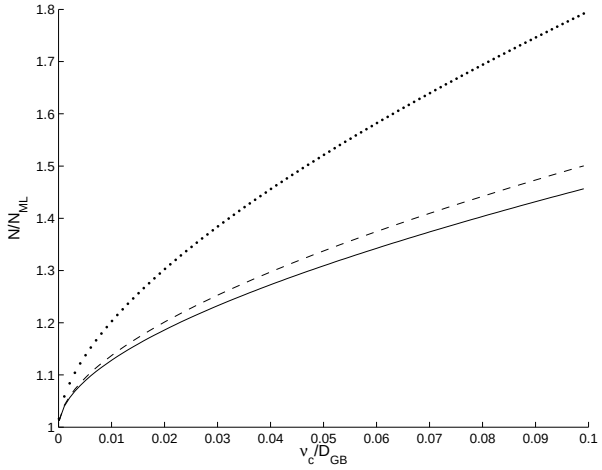

Figure 2.2: Saturated intensity of drift wave turbulence for three values of magnetic shear with the parameters $\gamma_d/\gamma_k = 1$, $\eta/D_{GB} = 1/10$, $\beta = 1/20$, $m = 2$, and $\rho^* = 0.01$. The solid curve corresponds to $L_s/L_n = 20$, the broken curve to $L_s/L_n = 10$, and the last curve to $L_s/L_n = 1$.

plays no role in regulating turbulence levels. In the opposite limit, the damping effects of field line bending and collisional viscosity are limited, thus leading to a lower level of saturated turbulence, and an increase in cell size (which determines the extent of cell-induced mixing), and flow shear. Thus in this limit, the approximate scaling of the excitation threshold of the turbulence intensity in the presence of the convective cell will roughly scale as $\langle N \rangle / N_{ML} \sim \gamma_d/\gamma_k$ plus a small correction. This scaling is similar to the results from previous drift wave-zonal flow studies. Thus, while low-m convective cells may *exist* for normal q profiles, they can be expected to be much broader and more active (i.e. with higher flow velocities and stronger flow shear) in regimes of weak magnetic shear. Associated fluctuation levels will be concomitantly reduced in such weak shear regimes, as well. This leads us to the important conclusion that l*ow-m convective cells are most important in regions of weak magnetic shear*, such as often exist for OAMq profiles.

Here it is useful to consider the structure and properties of the convective cell. In real space, an approximate form of the cell structure can be calculated by inverse Fourier transforming Eq. (2.38). This procedure is complicated by the scale dependence of $\nu_T(q_x)$,

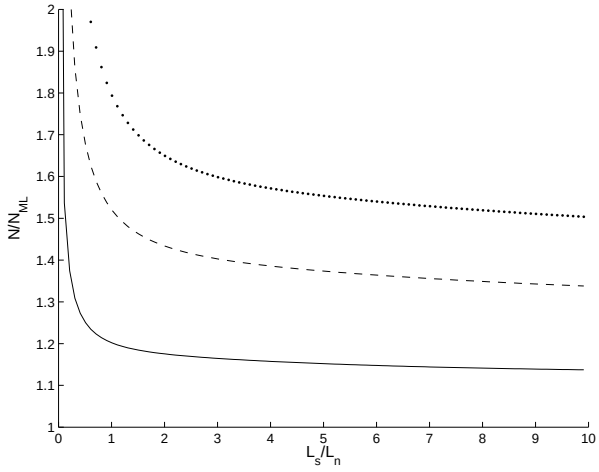

Figure 2.3: Saturated intensity of drift wave turbulence for three values of viscosity for the parameters $\gamma_d/\gamma_k = 1$, $\eta/D_{GB} = 1/10$, $\beta = 1/20$, $m = 2$, and $\rho^* = 0.01$. The solid curve corresponds to $\nu_c/D_{GB} = 0.01$, the broken curve to $\nu_c/D_{GB} = 0.05$, and the last curve to $\nu_c/D_{GB} = 0.1$.

which prevents $\nu_T(q_x)$ from behaving like a simple diffusion coefficient. A crude estimate can be obtained by solving Eq. (2.38) (in real space) for the case of $\nu_T(q_x) \approx \nu_T(0) =$ const. The asymptotic form of the radial cell profile is then given by

$$\phi(x) \sim \frac{1}{x^{3/4}} \exp\left(i\frac{2}{3}\left(\frac{x}{\Delta x}\right)^{3/2}\right) . \tag{2.48}$$

A more detailed asymptotic calculation of the convective cell potential profile is shown in Fig. 2.4. The width of the cell, which sets the scale of the flat spot or corrugation over which profiles are mixed, scales as $\Delta x \equiv (|\nu_T(0)|\,\eta)^{1/6}\,(L_s/(v_A q_y))^{1/3}$, and increases with L_s.

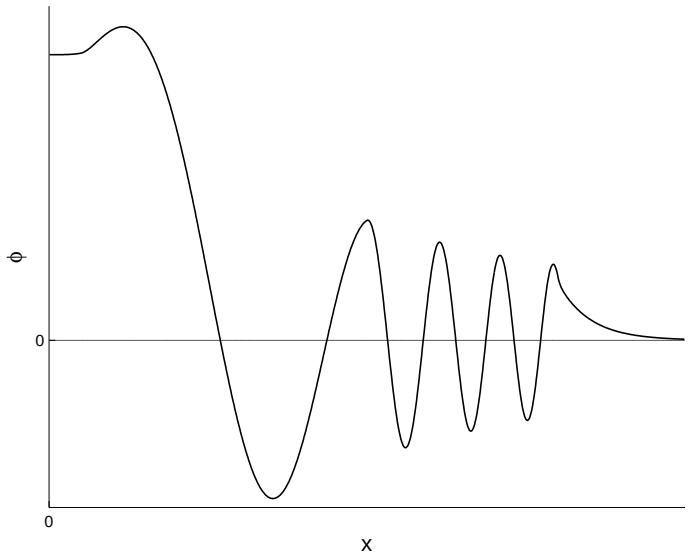

Figure 2.4: Sketch of radial eigenmode of convective cell.

Another observation that can be made from Eq. (2.48) is that, while ϕ decays algebraically, the strength of the *flow shear increases* as $\left|v_y'\right| \sim x^{1/4}$. Thus, the magnitude of D_k in Eq. (2.36) is stronger away from the rational surface, suggesting that the convective cell will suppress turbulence *away* from the resonant surface more strongly than it will affect turbulence *at* the resonant surface. This appears consistent with the dual observations of persistent transport or mixing at the surface (needed for the local flat spot) along with flow shear suppression of turbulence *nearby* the surface. Note that shear suppression by both $m \neq 0$ flow components and $m = 0$ zonal flows, has been observed in simulations [38].

We also note that this mechanism has a power threshold determined by the critical fluctuation intensity level (N_{crit}) required to drive the convective flow against damping due to friction, line bending and viscosity, as shown in Eq. (2.47). Using a simple, standard model of ITG turbulence [39] to relate heat flux to turbulence intensity, along with power balance, yields:

$$Q_{\text{crit}} = -\chi_{\text{crit}} \frac{\partial T_i}{\partial r} \approx v_{thi} T_i \eta_i \epsilon_T^{-1/2} \tau^2 N_{\text{crit}}, \tag{2.49}$$

$$P_{\text{in}} \sim R r_b Q_{\text{crit}} \sim R r_b v_{thi} T_i \eta_i \epsilon_T^{-1/2} \tau^2 N_{\text{crit}}, \tag{2.50}$$

where

$$N_{crit} \approx \Gamma + \left(\frac{\frac{3\pi}{2}+\delta}{1-\epsilon}\right)^{2/3} \frac{\nu_c^{2/3}}{\eta^{1/3}} \left(\frac{v_A q_y}{L_s}\right)^{2/3} \frac{1}{\gamma_k}\,.$$

Here, $\epsilon_T \equiv L_T/R$, R is the major radius, and r_b is the radius of the barrier. The power threshold clearly increases for stronger friction, and decreases for weaker magnetic shear.

2.4 Nonlinear evolution of convective cell

In the above discussion, an estimate of the excitation criterion for the destabilization of the convective cell was presented. That analysis provided insight into the regimes in which a convective cell is likely to be active, as well as the scale over which it is expected to mix. Here we discuss purely nonlinear properties of the drift wave-convective cell system which are not easily incorporated into the quasi-linear analysis. Specifically, we focus on the role of trapping/detrapping of wave packets (quasi-particles) as they propagate in the cell field. As discussed further below, this topic is critical as the presence of a significant population of trapped quasi-particles can substantially impact the quasi-linear analysis utilized above [40].

One of the utilities of the wave kinetic description is that it allows for the simple visualization of micro-turbulence dynamics via the phase space evolution of drift wave packets. More specifically, instability of secondary structures requires transport of micro-turbulence to high-$k_\perp$. Within the above description, this transport is induced via quasi-linear diffusion of the drift wave turbulence by the large scale shear flow (random refraction). A necessary condition for the validity of this quasi-linear description, is that the phase space trajectories of the quasi-particles be stochastic. In the limit of small Kubo number (defined as the ratio of the autocorrelation time of the shear flow structure to the shearing time $\tau_{cc}^{-1} = v'_{0y}$), this condition can be satisfied via resonance overlap in phase space (Chirikov criterion). The

resulting ray chaos induces diffusive transport of the quasi-particles to high-$k_\perp$, which can be approximated via the k-space quasi-linear diffusion coefficient appearing in Eq. (2.36). Alternatively, for a temporally stationary but spatially chaotic shear flow pattern of low amplitude (conditions under which use of the quasi-linear equation is strictly justified), diffusion in k-space follows directly.

For the important case of finite amplitude flows in the limit of large Kubo number (i.e. stationary shear flow structures), purely integrable orbits may form in phase space due to the strong nonlinear modification of quasi-particle orbits. These coherent structures are not compatible with the quasi-linear description, since they are capable of 'impeding' the transport of quasi-particles to high-k. One particular phase space structure which is of interest here is that of trapped quasi-particles, which can be induced by velocity wells in the shear flow pattern. Due to trapped quasi-particles undergoing closed orbits in phase space, no net energy need be transferred from the trapped quasi-particle population to the large scale shear flow. This is in contrast to the case of untrapped quasi-particles. They are instead exposed to the global shear flow pattern, allowing them to be transported to higher $k_\perp$. Thus, quasi-particle trapping suggests a means by which intense shear flow patterns may be nonlinearly saturated [5].

Our motivation in considering this topic is that in order to understand which types of flow patterns are likely to be dominant near low-q surfaces, it's necessary to consider the "competition" between different Reynolds stress driven flow structures (i.e. $m = 0$ vs. finite-m). Criteria which provide insight into the importance or relevance of a given flow pattern can be divided into two categories. The first is the stability threshold, as this criterion must necessarily be satisfied for a particular flow pattern to be established. Thus, it provides insight into the parameter regimes in which a specific flow pattern is likely to be observed. In the above, we have already noted that for the case of weak magnetic shear, the stability threshold for convective cells asymptotes to that of zonal flows. Hence, for

reversed magnetic shear configurations, zonal flows have only a marginal advantage over convective cells with regards to their respective excitation criterion. Also, in contrast to zonal flows, the mean field nonlinearity within the vorticity equation can act as *both* a sink or a source of energy for a finite-m flow, allowing for dual mechanisms of excitation (note that tertiary instabilities are most important in regimes of weak magnetic shear).

Nonlinear saturation mechanisms define a second property which yields insight into the relative importance of a specific flow structure. This property is critical, as once a flow pattern is excited, the efficiency of the flow in regulating the turbulence intensity will depend sensitively on its saturation mechanism. As noted above, for the case of weak magnetic shear, magnetic field line bending plays only a marginal role in damping convective cells, hence the collisional saturated intensity of ($m \neq 0$) convective cells is only mildly reduced in comparison to zonal flows. To this we add that as shown below, due to the finite mixing present within a convective cell (see Fig. 2.5) quasi-particles can be detrapped by the large scale convection. This can easily be seen by considering that the "depth" of a shear well increases in proportion to the strength of the shear flow. Hence, for the case of a purely poloidal flow, the fraction of trapped quasi-particles will increase as the shear flow intensifies. However, for the case of a finite-m flow, as the strength of the shear flow increases, *both* the strength of the shear wells, as well as the efficiency of radial convective transport increase, allowing the cell to circumvent quasi-particle trapping as a means of nonlinear saturation.

2.4.1 Nonlinear wave trapping

Here we discuss two independent wave trapping mechanisms which may be induced by a shear flow structure. The first mechanism which we consider corresponds to the classic zonal flow trapping mechanism discussed in Ref. [21]. This solution is pertinent to this analysis since, as alluded to above, it is strongly modified for the case of weakly non-

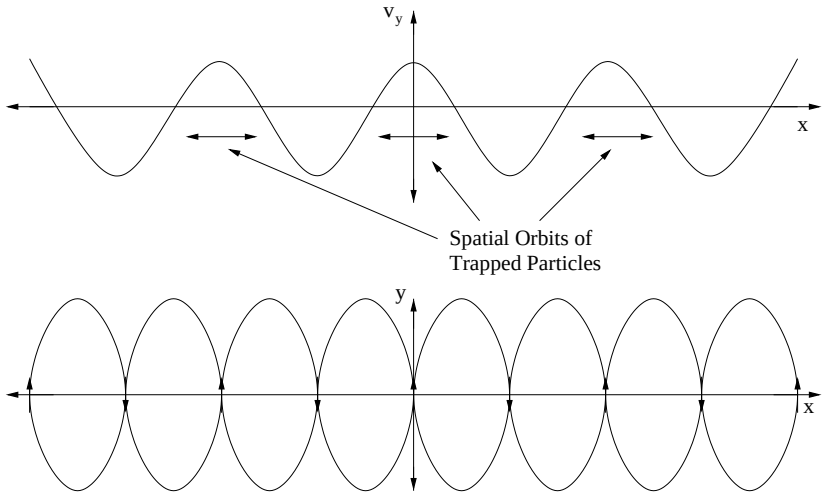

Figure 2.5: The top figure shows a sketch of an oscillating shear profile. The locations of the orbits of the trapped quasiparticles are indicated. The bottom figure shows a sketch of velocity contours in the perpendicular plane, with arrows indicating the direction of the velocity flow. The cells clearly provide a mechanism for the quasiparticles to be transported between shear wells.

axisymmetric flows. Similarly, we demonstrate the existence of a novel wave trapping mechanism, relevant in the limit of strongly non-axisymmetric flow structures, or strongly anisotropic turbulence.

We begin by briefly reviewing the derivation of a simple trapping mechanism for the case of $m = 0$ flows. Considering the characteristics of the W.K.E. given by Eqs. (1.28) and (1.29), for the general case of $m \neq 0$, an equation for the evolution of k_x can be derived as

$$\frac{d^2 k_x}{dt^2} = -k_y \frac{d\mathbf{x}}{dt} \cdot \frac{\partial v_y'}{\partial \mathbf{x}} - v_y' \frac{dk_y}{dt} - k_x \frac{d\mathbf{x}}{dt} \cdot \frac{\partial v_x'}{\partial \mathbf{x}} - v_x' \frac{dk_x}{dt}. \tag{2.51}$$

As discussed in the next section, the solutions to Eq. (2.51) are in general chaotic. However, here we are able to identify two simple solutions which are particularly pertinent to our analysis. The first solution corresponds to the classic zonal flow wave trapping solution discussed above (see also [21]), which may easily be recovered by setting $\partial/\partial y = 0$ and

substituting Eqs. (1.28) and (1.28) into Eq. (2.51)

$$\frac{d^2k_x}{dt^2} = 2v_e^* \frac{\left(k_y\rho_s\right)^2}{\left(1+\left(k_\perp\rho_s\right)^2\right)^2}\frac{\partial v_y'}{\partial x}k_x \approx 2v_e^*\left(k_y\rho_s\right)^2\frac{\partial v_y'}{\partial x}k_x, \tag{2.52}$$

where for $v_e^*\partial v_y'/\partial x \approx \text{const} < 0$ (note the dependence on the branch of micro-turbulence) can be recognized as the equation for a harmonic oscillator, with a bounce frequency given by $\omega_b = \sqrt{2v_e^* v_y''}\left(k_y\rho_s\right)$.

The second solution which we consider is a novel wave trapping mechanism, induced by the finite radial component of the non-axisymmetric shear flow. Due to the non-axisymmetric nature of this solution, it will be necessary to simultaneously solve the four coupled equations given by Eqs. (1.28) and (1.29). For simplicity, we consider purely non-axisymmetric stationary flows with only a single harmonic present. Note that this second trapping mechanism will be composed of two distinct components. The first is an oscillation of the orbits of the wave quanta induced by the mesoscale flow. These oscillations – which vary on a time scale given by $\tau_{os}^{-1} \sim q_y v_e^*$ – are quite general to a wide variety of different wave quantum orbits and are simply a result of the sign of the velocity shear seen by the wave quantum flipping as it traverses from one cell to another in the poloidal direction. Thus, this component is present in any solution where $|v_{gry}| > |v_y|$. Because of its generality, this component of the solution will provide very little information about the overall orbit of the wave quantum. The second component which is relevant to this analysis is a drift of wave quanta induced by the shear flow, and varies on a time scale given by $\tau_{cc}^{-1} \sim v_{0y}'$. Whether this net drift is oscillatory or divergent determines if the wave quantum remains trapped by the flow. Utilizing these two time scales, a two scale perturbative analysis may be performed on Eqs. (1.28) and (1.29) (details of the derivation are presented in appendix

B), yielding the bounce frequency

$$\omega_{cc} = v'_{0y}\left(k_{0y}\rho_s\right)\sqrt{2 - \left(\frac{q_x}{q_y}\right)^2 \left(k_{0y}\rho_s\right)^2}, \tag{2.53}$$

which provides a trapping criterion given by

$$\frac{1}{2}\left(\frac{q_x}{q_y}\right)^2 \left(k_{0y}\rho_s\right)^2 < 1. \tag{2.54}$$

Note that while Eq. (2.54) does not contain any explicit dependence on v_{0y}/v_e^*, the width of the separatrix of the islands in the k_x-x plane will depend sensitively on the strength of the shear flow via Eq. (2.B12). Hence, similar to the zonal flow trapping solution, the width of cell induced islands increases as v_{0y}/v_e^* becomes stronger. Furthermore, while Eq. (2.54) places a strong restraint on the value of k_y, it places no restraint on the strength of k_x. Thus, this trapping solution, while of limited applicability for isotropic turbulence, may play a potentially important role for poloidally extended anisotropic turbulence. Also note that, as nonlinear wave trapping is only important in regimes in which the autocorrelation time of the shearing pattern is long in comparison to the bounce frequency of wave quanta, Eq. (2.53) provides an upper bound on the rate in which the shear flow pattern may vary. Finally we note, that while for a generalized mesoscale flow both of these solutions are strongly modified, each solution strongly affects overall transport via the introduction of nontrivial phase space topology.

2.4.2 Convective cell induced ray chaos

As is clear from Eqs. (1.28) and (1.29), this system possesses a Hamiltonian structure where

$$\delta\omega\left(x, y, k_x, k_y\right) = \omega_k + \mathbf{v}_0 \cdot \mathbf{k}, \tag{2.55}$$

acts as the effective Hamiltonian. As noted above, for the axisymmetric case of $q_y = 0$, the quasi-particle orbits which this Hamiltonian describes are particularly simple, i.e. since k_y is a constant of the motion, the contours of $N = N(x, y, k_x, k_y)$ evolve in the three dimensional space given by (x, y, k_x). After applying the constraint $\delta\omega(x, y, k_x, k_y) =$ const, this further restricts the contours to a two dimensional surface within this space. Hence, if a cross section of the phase space is taken at constant y, the orbits of the quasi-particles will necessarily have solutions described by $N = N(\delta\omega(x, k_x), k_y)$. However, considering the more general case of a weakly non-axisymmetric flow with small but finite q_y, k_y will be modulated by the weak radial component of the cell, removing one of the constants of motion. Thus, the space in which the quasi-particle is allowed to wander is increased by one dimension. For arbitrarily small values of q_y many of the surfaces on which the wave packet traversed in the unperturbed system are likely to remain intact. However, as q_y is increased, an increasing number of these surfaces are destroyed, leading to chaotic orbits.

Here we consider a mean electrostatic potential of the form

$$\bar{\phi} = \phi_A \sin(q_x x) + \sum_i \phi_{NA}^{(i)} \sin\left(q_x^{(i)} x + \psi^{(i)}\right) \cos\left(q_y^{(i)}(y - V_{0y} t)\right), \tag{2.56}$$

where ϕ_A and ϕ_{NA} correspond to the axisymmetric and non-axisymmetric components of the flow respectively, ψ is the relative phase of the non-axisymmetric component in comparison to the axisymmetric component, and V_{0y} is the phase velocity of the non-axisymmetric component. This flow, while clearly an idealization, is capable of approximating a wide variety of shear flow structures relevant to laboratory plasmas.

In order to remove the time dependence in Eq. (2.56) it is convenient to transform to a frame moving with the same phase velocity as the shear flow structure. This is most

conveniently done via introducing the generating function given by:

$$S\left(\mathbf{k}', \mathbf{x}, t\right) = \mathbf{k}' \cdot \mathbf{x} - k_y' V_{0y} t, \tag{2.57}$$

where the canonical transformation is then defined as

$$\mathbf{k} = \frac{\partial S\left(\mathbf{k}', \mathbf{x}, t\right)}{\partial \mathbf{x}} = \mathbf{k}', \quad \mathbf{x}' = \frac{\partial S\left(\mathbf{k}', \mathbf{x}, t\right)}{\partial \mathbf{k}'} = \mathbf{x} - V_{0y} t \hat{y}, \tag{2.58}$$

and

$$\delta\omega\left(\mathbf{k}', \mathbf{x}', t\right) = \delta\omega\left(\mathbf{k}, \mathbf{x}, t\right) + \frac{\partial}{\partial t} S\left(\mathbf{k}', \mathbf{x}, t\right), \tag{2.59}$$

which after substituting Eq. (2.58) into the electrostatic potential given by Eq. (2.56), and evaluating the time derivative, Eq. (2.59) can be rewritten as

$$\delta\omega\left(\mathbf{k}', \mathbf{x}'\right) = \mathbf{k}' \cdot \mathbf{v_0}\left(\mathbf{x}'\right) + \frac{k_y'}{1 + k_\perp'^2 \rho_s^2} \left[v_e^* - V_{0y}\left(1 + k_\perp'^2 \rho_s^2\right)\right]. \tag{2.60}$$

Thus, in this frame the Hamiltonian has no explicit time dependence. Note that for co-propagating flow structures with $V_{0y} = v_e^*$, the system approaches the hydrodynamic integrable limit. Thus for this limit, dispersion (along with non-axisymmetry of the shear flow) of the drift wave turbulence introduces the non-integrable perturbation. Alternatively for counter-propagating flows, only non-axisymmetry is required for non-integrability. Thus, in contrast to the purely axisymmetric case, electron and ion branches of drift wave turbulence are likely to interact somewhat differently with non-axisymmetric shear flow structures.

In the following, the phase space structures present for a number of different limits of Eq. (2.60) are discussed. Poincaré surface of sections are computed for constant values of y. These simulations are performed by considering a large number of initial k_x and x values (where $\delta\omega$ is kept constant for each initial condition), and integrating for-

ward in time. The accuracy of the numerical integration is verified both by checking that $\delta\omega$ is constant throughout the integration (to within a relative error of 10^{-6}), and that the simulation results are qualitatively unchanged as the accuracy of the numerical solver is increased. Note that for this section we are primarily concerned with gross properties of the phase space structure, such that while increased accuracy would make the details of phase space structures clearer, for this section such accuracy is not required. However, in subsequent sections where greater resolution is required, the accuracy of the solver will be subsequently increased.

2.4.2.1 Stationary flows

As discussed above, the $q_y = 0$ limit possesses particularly simple solutions. Here we look for solutions of a more general form by considering weakly non-axisymmetric structures, but with $V_{0y} = 0$. In order to minimize the dimensionality of the parameter space of the system, we consider the limit where only a single harmonic is present. A Poincaré surface of section for the parameters $q_y/q_x = 1/20$ and $|v_{0y}|/v_e^* = 0.04$ is plotted in Fig. 2.6(b). In comparison with the $q_y = 0$ zonal flow case shown in Fig. 2.6(a), it's clear that the region of trapped wave quantum orbits has been replaced by a dense area filling stochastic region. The efficiency of non-axisymmetric flows in destroying the trapped particle orbits can be easily understood by considering the two dimensional nature of the structure. For a purely non-axisymmetric flow, O-points smoothly evolve into X-points as wave quanta traverse the poloidal circumference [the $\cos(q_y y)$ term in Eq. (2.56)]. Thus a particle which is initially trapped by an O-point will be scattered by an X-point as it traverses the circumference of the confinement device. In this way, arbitrarily weak non-axisymmetric flows are capable of breaking closed KAM surfaces associated with trapped wave quanta.

Similarly, it is instructive to increase the strength of the shear flow pattern. For the

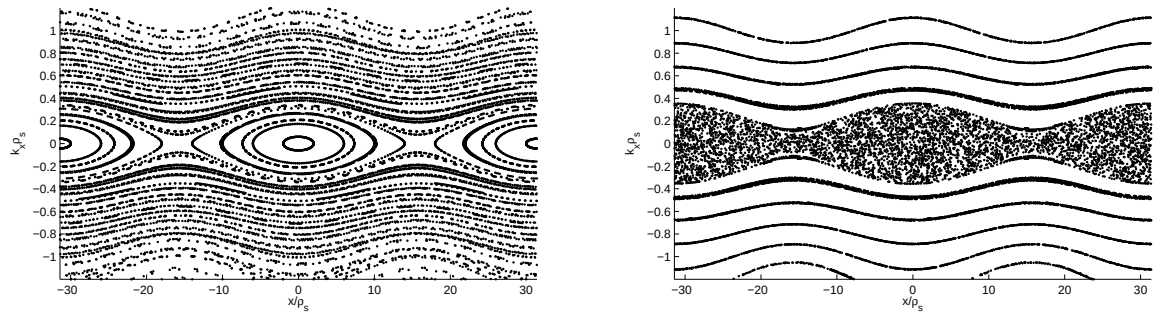

Figure 2.6: Poincaré surface of sections in the k_x-x plane. The plot on the left is for $q_y = 0$. The plot on the right is for the parameters $q_y/q_x = 1/20$ and $|v_{0y}|/v_e^* = 0.04$.

parameters $q_y/q_x = 1/20$ and $|v_{0y}|/v_e^* = 0.2$ (shown in Fig. 2.7), it is clear that while the region inside the separatrix is still largely chaotic, this figure contains a clearly visible region in which integrability has been restored. Note that these closed KAM surfaces, do not correspond to trapped wave quanta, instead they are periodic orbits in which a wave quantum traverses a single velocity well after each rotation around the poloidal circumference (i.e. traversing successive O-points in the radial direction). Also note that the width of the stochastic region has significantly increased, which is simply a result of the width of the separatrix in the $q_y = 0$ integrable region increasing. Note that for both Figs. 2.6(b) and 2.7 the KAM surfaces associated with untrapped wave quanta remain intact. These surfaces may be broken via stronger non-axisymmetry, increased $\mathbf{v_0}$, violation of the strict periodicity utilized in this simple analysis, or as discussed below, the inclusion of a finite phase velocity.

2.4.2.2 Time periodic flows

In the previous section, the Hamiltonian of a stationary flow structure was studied in various limits. Here we find it useful to generalize to a time periodic flow profile, i.e. one moving in the poloidal direction with a constant phase velocity. This limit is interesting as many weakly non-axisymmetric flow structures propagate with a nearly constant poloidal

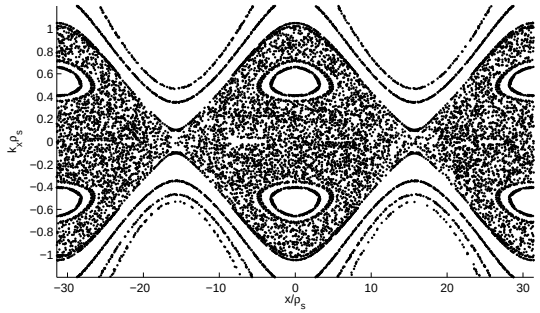

Figure 2.7: Poincaré surface of section in the k_x-x plane. This plot is for $q_y/q_x = 1/20$ and $|v_{0y}|/v_e^* = 0.2$.

phase velocity (drift tearing modes, secondary convective cells, etc). Thus, this analysis can be understood to correspond to a study of coherent non-axisymmetric flow structures with short wavelength drift wave turbulence.

Considering the simple case of $V_{0y} = v_e^*$, Poincaré surface of sections are plotted in Figs. (2.8) and (2.9)(with q_y increased by a factor of two in comparison to the previous section to reduce the run time of the routine). In order to provide a more complete picture of the phase evolution of the system, we have plotted a larger area in phase space, such that the role of integral structures at high-k_x is evident. As can clearly be seen, in comparison with the case of stationary flows, the phase space is significantly more chaotic. While the chaotic region remains localized for small v_{0y}/v_e^*, as the strength of the shear flow is increased, it's clear that nearly all KAM surfaces are destroyed, allowing the system to enter into a state of global chaos.

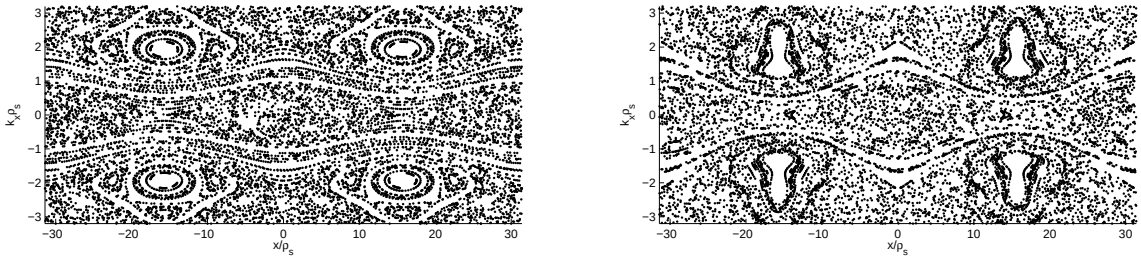

Figure 2.8: Poincaré surface of sections in the k_x-x plane. The plot on the left is for $q_y/q_x = 1/10$ and $|v_{0y}|/v_e^* = 0.1$. The plot on the right is for the parameters $q_y/q_x = 1/10$ and $|v_{0y}|/v_e^* = 0.2$.

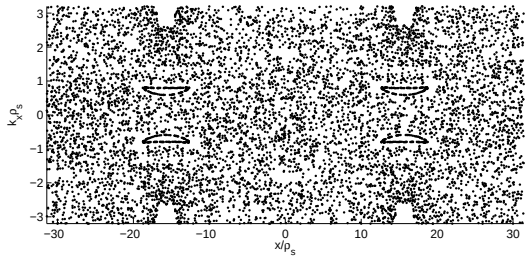

Figure 2.9: Poincaré surface of sections in the k_x-x plane for the parameters $q_y/q_x = 1/10$ and $|v_{0y}|/v_e^* = 0.3$.

The phase space of a counter-rotating mode translating with a constant velocity $V_{0y} = -v_e^*$ is shown in Figs. 2.10 and 2.11. Similar to the co-rotating case, the onset of global chaos occurs for approximately $v_{0y}/v_e^* \approx 0.3$. Note that while the density of points in Fig. 2.11 is much larger in the region of formerly trapped quasi-particles, the exterior KAM surfaces associated with this region have been broken. The increased density of points can instead be understood to correspond to residual correlations of the trapped quasi-particle orbits, or a region of locally small Lyapunov exponents surrounded by one with substantially larger values.

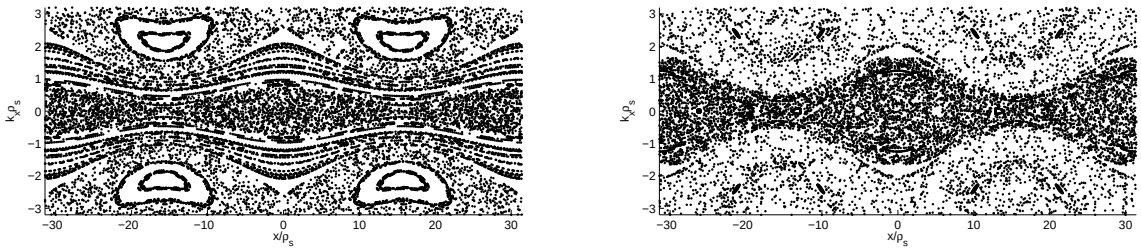

Figure 2.10: Poincaré surface of sections in the k_x-x plane. The plot on the left is for $q_y/q_x = 1/10$ and $|v_{0y}|/v_e^* = 0.1$. The plot on the right is for the parameters $q_y/q_x = 1/10$ and $|v_{0y}|/v_e^* = 0.2$.

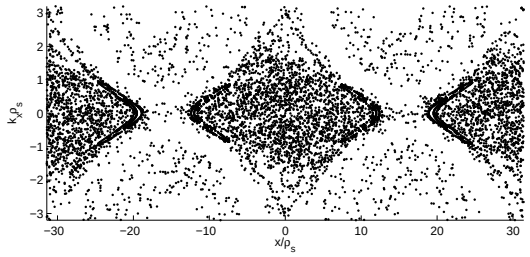

Figure 2.11: Poincaré surface of sections in the k_x-x plane for the parameters $q_y/q_x = 1/10$ and $|v_{0y}|/v_e^* = 0.3$.

As discussed above, trapped wave quantum orbits were predicted to exist for the case of strongly anisotropic turbulence [Eq. (2.53)]. While these solutions have been found numerically for the case of a stationary shear flow, they become more prominent for counter-rotating flows. The degree of anisotropy of the turbulence may be controlled by varying the constant of motion $\delta\omega$. Choosing $\delta\omega$ such that $k_y\rho_s \approx 0.1$ [see Fig. 2.12(b) for a distribution of k_y], and the parameters $q_y/q_x = 1/8$ and $v_{0y}/v_e^* = 0.45$, Fig. 2.12(a) demonstrates the presence of closed KAM orbits for k_x as large as $k_x\rho_s \approx 0.5$. For Figs. 2.10 and 2.11, where there is no signature of this trapping mechanism, $k_y\rho_s$ varied between magnitudes of $0.3 - 1.2$, hence the turbulence was primarily isotropic for the region in which this trapping mechanism is predicted to be active, thus demonstrating that the presence of these orbits depends sensitively on the degree of anisotropy of the turbulence.

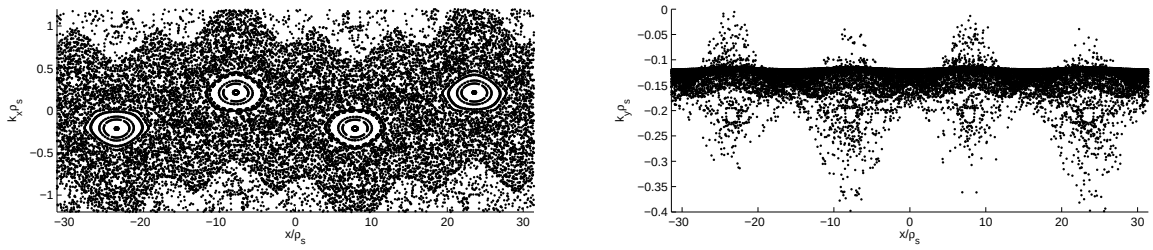

Figure 2.12: Poincaré surface of sections in the k_x-x and $k_y - x$ plane for the parameters $q_y/q_x = 1/8$ and $|v_{0y}|/v_e^* = 0.45$. The value of y chosen was 90 degrees out of phase with previous plots, such that the 3-D nature of the trapping solution is evident.

2.4.2.3 Generalized Hamiltonian: inclusion of axisymmetric component

In the previous sections the special case of a purely non-axisymmetric flow structure was considered. Here we are interested in understanding the more general case in which both a non-axisymmetric flow component as well as an axisymmetric component are present. For the case of $\phi_{NA}/\phi_A = 0.2$, a Poincaré surface of section is plotted in Fig. 2.13. Fig. 2.13 indicates that while there exists a thin stochastic layer near the separatrix, the k_x-x plane is largely integrable. This result is not surprising, since, as discussed above, for a purely non-axisymmetric flow O-points smoothly evolve into X-points providing a robust means of breaking KAM tori regardless of the poloidal harmonic of the flow. This is in contrast to systems which possess a strong axisymmetric component. For these systems, as wave quanta traverse the poloidal circumference, the relative strength of an O-point will be modified by the non-axisymmetric component, effecting a transition to stochasticity for wave quanta near the separatrix, but leaving KAM tori further inside the separatrix intact. Thus, for the limit of $\phi_{NA}/\phi_A \ll 1$, nonlinear wave trapping can be seen to introduce a robust means of impeding the transport of wave quanta to high-$k_\perp$, and thus quenching the transfer of energy to large scales.

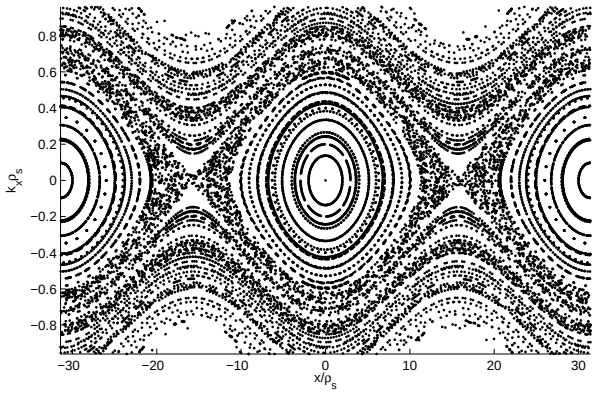

Figure 2.13: Poincaré surface of section in the k_x-x and $k_y - x$ plane for the parameters $q_y/q_x = 1/10$ and $\phi_{NA}/\phi_A = 0.2$.

Considering now the case of $\phi_{NA}/\phi_A = 0.8$, Fig. 2.14 demonstrates the existence of a large region of stochasticity. We have chosen a somewhat narrower view than in previous plots such that the details of the phase space are made evident. From Fig. 2.14 it's clear that the elliptic point located near $x = 0$, $k_x = 0$ has bifurcated into three elliptic points and two hyperbolic points. Also, note that the region immediately surrounding the three elliptic points, while stochastic, is significantly darker than the surrounding stochastic sea, indicating the tendency of particles to spend a disproportionate amount of time in this region. A similar phase space structure was observed in Ref. [41], and was classified as a stochastic layer trap. This stochastic layer trap corresponds to a sticky phase space domain capable of strongly affecting the statistics of the overall system due to wave quanta spending a disproportionate amount of time localized to this region. Thus, for a strong non-axisymmetric component, while KAM tori associated with the unperturbed orbit are largely broken, residual correlations introduce a degree of phase space stickiness, which is capable of strongly impacting the overall transport of the system. Note that this sticky domain is localized around $k_x = 0$, thus wave quanta which enter this quasi-trap are strongly confined in both position as well as wave number space.

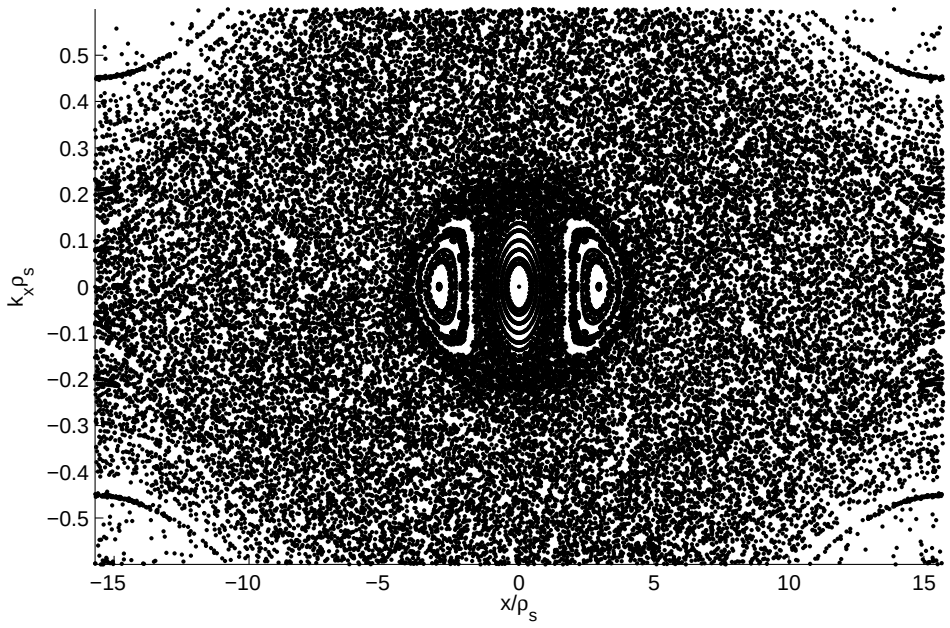

Figure 2.14: Poincaré surface of section in the k_x-x and $k_y - x$ plane for the parameters $q_y/q_x = 1/10$ and $\phi_{NA}/\phi_A = 0.8$.

In summary, the introduction of a weak non-axisymmetric perturbation to the zonal flow shear profile has been shown to break KAM tori associated with nonlinearly trapped wave packets and so produce chaotic orbits. The absence of these KAM tori allows for nonlinear wave trapping to be largely circumvented as a saturation mechanism for the large scale shear flow. Note that while in this analysis we have focused on the convective cell as the symmetry breaking mechanism, the presence of any appreciable non-axisymmetric component to the shear flow profile will likely have a similar effect. Also note that this result has been obtained in the limit of an infinite Kubo number, the ideal region for wave trapping to occur.

2.5 Transport Model

In the above, an excitation threshold as well as key properties of the linear mode structure and nonlinear dynamics of the convective cell were discussed. These investigations utilized idealized models in order to illustrate these fundamental characteristics clearly. Due to the idealized nature of these models however, much of the self-consistent time dependent dynamics of the micro-turbulence and shear flows has been lost. Here, we seek to recover this information and demonstrate the form of different time dependent solutions of the convective cell and drift wave system in various parameter regimes. Emphasis is placed on understanding how these different solutions impact the formation of ITBs, and thus the amount of input power required. In particular, a simple set of zero dimensional amplitude equations are derived and used to phenomenologically model the formation of an ITB. While this simple phenomenological model is incapable of accurately representing the detailed spatial structure of the drift wave-convective cell system, it does allow insight into the interplay between turbulence intensity, Reynolds stress driven zonal flows and convective cells, mean $\mathbf{E} \times \mathbf{B}$ flows, as well as their relation to mechanisms which trigger transport barriers.

2.5.1 Model equations

The system of equations we consider are similar to those utilized in Refs. [42, 43] (also, see Refs. [44, 45]), and are given by

$$\frac{\partial \epsilon}{\partial t} = \gamma P' \epsilon - a_1 v_{cc}^2 \epsilon - a_2 v_{EB}^2 \epsilon - a_3 \epsilon^2, \tag{2.61}$$

$$\frac{\partial v_{cc}}{\partial t} = b_1 \epsilon v_{cc} - b_2 v_{cc}, \tag{2.62}$$

$$\frac{\partial P'}{\partial t} = -c_1 \epsilon P' - c_2 P' + Q, \tag{2.63}$$

$$v_{EB} = d_1 P'^2. \tag{2.64}$$

The terms on the right hand side of Eq. (2.61) have clear analogues to terms contained within Eq. (2.36). Specifically they correspond to linear growth, convective cell shearing, mean flow shear, and local self-saturation of the turbulence intensity. Similarly, by analogy with Eq. (2.38), Eq. (2.62) contains convective cell generation via Reynold's stresses as well as linear damping. Here, the linear damping is understood to represent field line bending, viscosity, friction, and potentially collisionless processes, which in the context of a zero dimension model all have the same functional form. Also, the pressure equation contains both turbulent and neoclassical transport coefficients, as well as heat input. Finally, the mean flows are slaved to the pressure gradient via Eq. (2.64). Note that these equations should be understood to apply near the location of a low-q resonance where the convective cell is most active.

2.5.2 Solution to reduced two field system

Before analyzing the complete system of equations given by Eqs. (2.61)-(2.64), it is convenient to consider the two field system given by Eqs. (2.61) and (2.62) where P' is utilized as the control parameter, and Eq. (2.64) closes the system. This simplified model is instructive, as many of the fixed point states which occur in the full system are present within this reduced model. Thus it provides a means of clearly illustrating much of the complete system's underlying behavior, with significantly less clutter (see Table I for a summary). In this simple limit there exist three fixed points. The first can be trivially seen to occur for $v_{cc}^2 = 0$ and $\epsilon = 0$. Performing a simple linear stability analysis around this point yields purely real eigenvalues with a stability condition given by $\gamma < a_2' P'^3$, where $a_2' \equiv a_2 d_1^2$. For stable solutions, this point possesses the dual properties of low transport (only neoclassical) and high mean field shear, and thus may be understood to correspond to an ITB mode.

Table 2.1: Summary of the values of the fixed points and stability criteria for the two field model.

	Fixed Points	Stability Criteria
ITB	$\epsilon = 0,\, v_{cc}^2 = 0$	$\gamma < a_2' P'^3$
CCR	$\epsilon = (b_2/b_1)\,,\, v_{cc}^2 = (1/a_1)\left[\gamma P' - a_2' P'^4 - a_3\,(b_2/b_1)\right]$	$\gamma P' > a_2' P'^4 + a_3\,(b_2/b_1)$
UR	$\epsilon = (1/a_3)\left(\gamma P' - a_2' P'^4\right),\, v_{cc}^2 = 0$	$\gamma P' < a_2' P'^4 + a_3\,(b_2/b_1)$

The second solution which is pertinent to this analysis is localized around $\epsilon = b_2/b_1$ and $v_{cc}^2 = (1/a_1)\left[\gamma P' - a_2' P'^4 - a_3\,(b_2/b_1)\right]$. The eigenvalues for this mode are generally complex and have a stability condition given by $\gamma P' > a_2' P'^4 + a_3\,(b_2/b_1)$. Thus, eigenmodes centered around this point may be understood to correspond to spiral modes. This eigenmode structure leads to a self regulating system, where the turbulent transport is not completely quenched, but is significantly reduced via convective cell shearing. Thus, it is convenient to refer to this state as a convective cell regulated (CCR) state. Also, for the case of $a_3 \approx 0$ the stability criteria for the ITB state and the CCR state are complementary, i.e. once the CCR fixed point goes unstable, the ITB state becomes an attractor. Thus, it's easy to see that transitions from CCR to ITB mode are readily attainable. Note that for the two field model, P' is utilized as the control parameter. In the next section P' will be replaced by the heat flux Q, as P' will be allowed to vary dynamically.

The last fixed point present within this reduced model corresponds to $\epsilon = (1/a_3)\left(\gamma P' - a_2' P'^4\right)$ and $v_{cc}^2 = 0$. The eigenvalues for this point are real, with a stability condition given by $\gamma P' < a_2' P'^4 + a_3\,(b_2/b_1)$. Thus, this state is relevant for strong cell damping (large b_2) in which the cell is submarginal (also note this solution necessarily appears before the ITB mode). We refer to this state as the unregulated (UR) state of the system. Note that unlike the CCR state, the UR state's stability criterion possesses a large region of coexistence with the ITB state, making bifurcations between these two states difficult. Hence, it's clear that the role of the CCR mode is to provide an efficient means of entering the ITB mode, by avoiding the difficult UR→ITB transition route. Also

note that while this large region of coexistence of the UR and ITB modes makes transitions between these two solutions difficult (a minus for confinement), this region of coexistence also allows for the possibility of hysteresis (a plus).

2.5.3 Three field evolution

Considering the three field model given by Eqs. (2.61)-(2.64), we may identify fixed point solutions in direct analogy with the previous section. Beginning with the ITB state, where the fixed point is now given by $\epsilon = 0$, $v_{cc}^2 = 0$, and $P' = Q/c_2$. Performing a linear stability analysis about this point yields pure real eigenvalues with a stability criterion $\gamma < a_2' \left(Q/c_2\right)^3$, which can be seen to be identical to that found for the two field model in the previous section. This isomorphism is not surprising as the role of P' is essentially replaced by Q in the three field model.

For the CCR state, the fixed point is given by

$$\epsilon = \frac{b_2}{b_1} \equiv N, \quad P' = \frac{Q}{c_1 N + c_2} \equiv q, \quad v_{cc}^2 = \left\{\gamma - a_2' q^3\right\} \frac{q}{a_1} - \frac{a_3}{a_1} N. \tag{2.65}$$

Note that while this fixed point is similar to the two field case, the nontrivial dependence of P' on Q (note the N dependence in the denominator) will introduce somewhat more complex stability criteria. The eigenvalue condition for perturbations around this point is cubic, and in general complex. Here we are primarily interested in the stability criteria near this fixed point, thus it is convenient to apply the Routh-Hurwitz method (which provides a set of criteria for all roots having negative real parts), yielding the nontrivial stability criteria:

$$\gamma q > a_2' q^4 + a_3 N, \tag{2.66}$$

and

$$\left[a_3 N + (c_1 N + c_2)\right]\left[a_3\left(c_1 N + c_2\right) + c_1 q\gamma - 4a_2' c_1 q^4\right] > 2a_3 b_2\left(a_2' q^4 + a_3 N - \gamma q\right), \tag{2.67}$$

where Eq. (2.66) is isomorphic to the two field system, and can be recognized as being merely the reality condition of the fixed point of v_{cc}^2. However, with the addition of Eq. (2.67), a more stringent criterion applies to the stability of the CCR mode. This added constraint will be shown to be crucial to the CCR→ITB bifurcation.

Finally, for the state with $v_{cc}^2 = 0$, but $\epsilon \neq 0$, referred to in the two field model as the UR state, the fixed points are given by $v_{cc}^2 = 0$, $P' = Q/\chi_{st}$, where $\chi_{st} \equiv c_1\epsilon + c_2$ is given by

$$0 = -\frac{a_3}{c_1}\chi_{st}^5 + a_3\frac{c_2}{c_1}\chi_{st}^4 + \gamma Q\chi_{st}^3 - a_2' Q^4. \tag{2.68}$$

Thus, while for the two field model only a single fixed point existed for $v_{cc}^2 = 0$, but $\epsilon \neq 0$, here multiple solutions may exist, depending on the parameter regime. Insight can be gained into the behavior of these solutions via numerical solution of Eqs. (2.61)-(2.64). In order to focus exclusively on the behavior of this set of modes, and their transition to the ITB mode, we choose a parameter regime with strong cell damping, so that Eq. (2.66) is never satisfied. Fig. 2.15(a) shows the evolution of the turbulence intensity, convective cell amplitude, and pressure gradient vs. time. The heat input is initially zero, but is linearly increased with time. For small t only one root of Eq. (2.68) exists, whose value can be seen to increase in time [see Fig. 2.15(b)]. However as time evolves a second root appears. We refer to these roots as the weak UR (WUR) and strong UR (SUR) transport modes. Also note for this parameter regime, the ITB fixed point becomes stable at roughly $t \approx 125$ (in arbitrary units). Thus, while the system is clearly in SUR for $t \lesssim 190$, there is coexistence with both the ITB and WUR states for $t \approx 125$ through $t \approx 190$, thus illustrating the difficulty of (S)UR→ITB transitions. From Fig. 2.15(a), it's clear that the

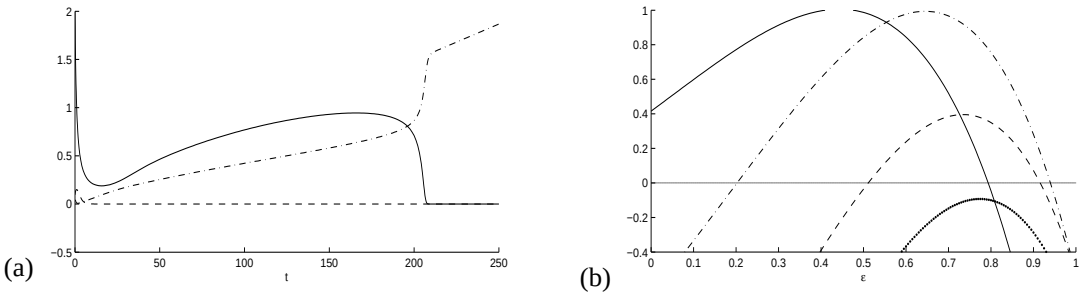

Figure 2.15: (a) The evolution of turbulence intensity, convective cell amplitude, and pressure gradient are denoted respectively by the solid, the broken, and broken-dotted. (b) Roots of Eq. (2.68) for times $t_1 \approx 103$, $t_1 \approx 155$, $t_1 \approx 180$, and $t_1 \approx 192$ denoted by the solid, broken-dotted, broken, and dotted lines respectively. UR fixed point solutions disappear coincident with transition to ITB state.

system transitions into ITB mode at roughly $t \approx 190$. This bifurcation results from the fixed point solutions of the WUR and SUR modes vanishing, as shown in Fig. 2.15(b).

The coexistence of multiple stable fixed points allows for the possibility of hysteresis between the SUR and ITB modes. This hysteresis is demonstrated in Fig. 2.16(a), where we have linearly increased the power input until the system bifurcates into ITB mode, and then ramped down the power linearly at the same rate. As can clearly be seen, a large region of hysteresis is present. Note that the width of this region is exaggerated due to the turbulence intensity going almost exactly to zero before the ITB mode becomes unstable. That is, the ITB mode becomes unstable at $Q = 1$, such that the turbulence intensity begins to grow at this point, however because the amplitude of the turbulence intensity is nearly zero, the amplitude remains negligible until roughly $Q \approx 0.6$. More precisely, the eigenvalue for the ITB mode (there of course exist three, but two are trivially stable) is given by $\lambda = \left[\gamma - a_2' \left(Q/c_2\right)^3\right] \left(Q/c_2\right)$. For large Q, the system decays exponentially with a rate that scales as Q^4, thus rapidly damping the eigenmode for $Q > 1$. In contrast, for small Q, the eigenmode is amplified, but with a far weaker growth rate, thus leading to a wide region of hysteresis. This discrepancy may be easily corrected via the introduction of a weak noise term into Eq. (2.61), whose magnitude is chosen to be three orders of magnitude smaller

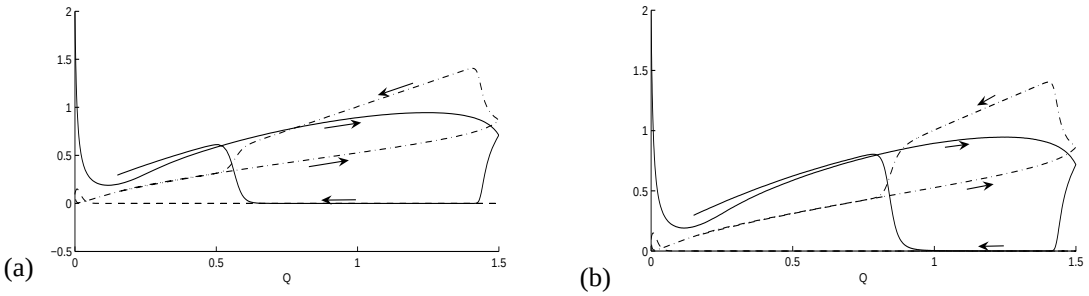

Figure 2.16: (a) The evolution of turbulence intensity, convective cell amplitude, and pressure gradient are denoted respectively by the solid, the broken, and broken-dotted. The arrows delineate whether the power is being increased or decreased. A clear region of hysteresis is observed. (b) Same as (a) but with noise added.

than the linear growth rate such that the underlying dynamics are largely unperturbed. The results of the simulation of the modified system are shown in Fig. 2.16(b), where the width of the hysteresis region can be seen to be significantly reduced.

In order to consider the CCR→ITB transition, the large scale damping may be reduced in comparison to the above simulations, such that the inequalities in Eqs. (2.66) and (2.67) are satisfied, allowing for the cell to be destabilized. As shown in Figs. 2.17(a) and 2.17(b) (with the noise term turned off), after a transient burst by the convective cell, the system begins to approach SUR mode. However, as the input power is increased, the system transitions into CCR mode. As can be seen in Fig. 2.17(b), the eigenmode corresponds to an inward spiral, as anticipated from the two field calculation. Once the input power becomes large enough, the stability criterion given by Eq. (2.67) is violated, resulting in a transition into ITB mode. Note that this transition occurs with significantly less input power than in the SUR→ITB bifurcation. Thus, while entry into ITB mode is possible in the absence of the convective cell, the power threshold for such a transition is substantially higher. This significant reduction in input power for entry into ITB mode may be understood to result from CCR mode pushing the system into the basin of attraction of the ITB attractor. Thus, once the CCR fixed point becomes unstable, ITB mode may be readily accessed.

We now consider the impact of holding the power input fixed after the CCR fixed point

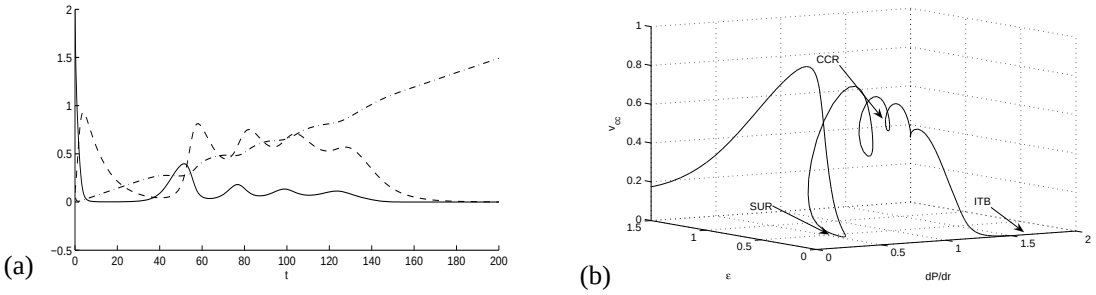

Figure 2.17: (a) The evolution of turbulence intensity, convective cell amplitude, and pressure gradient are denoted respectively by the solid, the broken, and broken-dotted, where the cell damping has been substantially reduced. (b) 3-D phase space of ϵ, v_{cc}, and P'. After transient burst of convective cell, system begins to approach SUR mode, subsequently transitions into CCR mode, and finally transitions into ITB mode once CCR fixed point becomes unstable.

becomes unstable, but before the ITB attractor appears. As is evident from Figs. 2.18(a) and 2.18(b), after the CCR fixed point goes unstable, the system undergoes a Hopf bifurcation into a limit cycle solution. From Fig. 2.18(a), it is clear that this solution results in bursty transport. Transition from this state into the quiescent ITB mode is possible via further increasing the input power.

In summary, four distinct modes of the system are predicted by the simple model:

a.) the ITB mode corresponds to an $\epsilon = v_{cc}^2 = 0$ solution (i.e. zero microturbulence, convective cell) which is accessible for high input power regimes. This mode should be understood to correspond to a somewhat idealized state of an experimental ITB, since for an experimental system, MHD modes (not contained within this simple model), are likely to degrade transport for high β values, and push the system away from this attractor.

b.) (S)UR mode represents a *high* transport state which exists for strong large scale damping. Transition into ITB mode is possible via this mode, however at a cost of high input power. Fairly wide regions of hysteresis were observed however, suggesting that while reaching ITB mode via this mode is costly initially, it may be possible

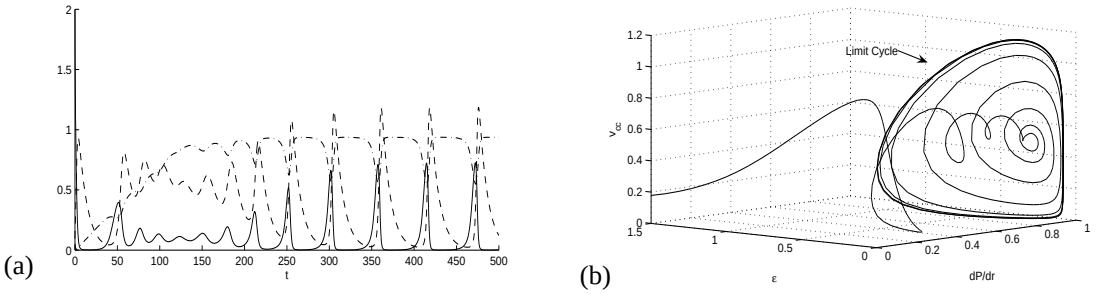

Figure 2.18: (a) The evolution of turbulence intensity, convective cell amplitude, and pressure gradient are denoted respectively by the solid, the broken, and broken-dotted, where rate of power input is held fixed after the CCR fixed point becomes unstable. (b) 3-D phase space of ϵ, v_{cc}, and P'. Same plot as Fig. 2.17(b), however power input is held fixed after instability of CCR fixed point. System fails to reach ITB mode, instead is absorbed into limit cycle solution.

to significantly reduce the input power afterward without back transitioning.

c.) CCR mode corresponds to a regime of cell regulated transport. This mode is active for regimes of weak large scale damping (low collisionality and magnetic shear), and has been shown to provide a means for the system to access ITB mode with a minimum of input power. Hysteresis between CCR and ITB mode plays no role in this transition scenario, as the ITB attractor doesn't appear until *after* the CCR mode becomes unstable, hence there is no regime of coexistence between these two attractors.

d.) limit cycle solutions, characterized by bursty transport, were obtained via a supercritical Hopf bifurcation of the CCR mode for input powers slightly above the CCR stability criteria. Upon subsequently increasing the power input, beyond the threshold of the ITB attractor, the system transitions into ITB mode. Also note that because the limit cycle solution appears via a supercritical Hopf bifurcation, there is no hysteresis between the CCR and limit cycle solutions.

2.6 Conclusion

In the above analysis we have proposed an ITB trigger mechanism which addressed key components of experimental observations of ITB formation, namely:

a.) an electrostatic trigger mechanism

b.) profile flattening or "corrugation" *at* the rational surface

c.) barrier formation *nearby* the rational surface.

The addition of a novel candidate ITB trigger mechanism to an already crowded field is necessary, as existing theories of ITB formation appear to be largely incompatible with the above observations. Also, this mechanism is particularly attractive as it provides a simple and direct means of linking the transport barrier to the region nearby the low-q surface.

Alternatively, the generation of shear flows near low-q surfaces may be linked to the response of micro-turbulence to the appearance of the low-q resonance. In particular, coupling of many co-located high m, n harmonics has been shown to lead to strongly inhomogeneous structures in the vicinity of the low-q surface [46]. Such coupling has been shown to overcome magnetic shear damping and result in localized peaks in the fluctuation intensity profile. Since such localized peaks necessarily imply a sharp slope in the fluctuation intensity profile, their resulting Reynolds stress naturally produces flow shear which is strongest *nearby* the resonant surface, thus triggering the formation of a transport barrier there. This scenario will be explored further in a future publication. Also, we note that these two possibilities are not mutually exclusive, and may in fact work in synergy.

To summarize, the main results of this paper are as follows:

a.) secondary convective cells, while generally subdominant to zonal flows, are likely to be active near regions of weak magnetic shear. This follows as a result of field line bending being substantially reduced in these regions

b.) secondary convective cells satisfy the experimentally observed criteria of strong mixing *at* the low-q surface and strong shear *nearby* the resonant surface

c.) nonlinear wave trapping is unlikely to be effective in saturating the growth of convective cells. This follows as a result of the non-axisymmetric component of the shear flow removing k_y as an integral of motion of the system, and thus breaking the KAM tori associated with the trapped quasi-particle orbits

d.) the power input required to trigger a mean flow bifurcation into an ITB state has been shown to be significantly reduced via the CCR$\rightarrow$ITB mode transition scenario

In conclusion, we remind the reader that this paper has proposed a novel mechanism for the formation of ITBs nearby low order resonant-q surfaces. This mechanism centers on a low-m electrostatic convective cell, excited by modulational instability of ambient drift wave turbulence and damped by friction and field line bending. Thus, such cells are probably significant only in conditions of weak magnetic shear, as often exist near OAMq profiles.

Appendix A: Derivation of Convective Cell Eigenvalue Condition

In this appendix we provide details of the derivation of Eqs. (2.41a) and (2.41b). We begin with Eq. (2.38), which we rewrite here for convenience as

$$0 = \frac{\partial^2 \phi\left(p\right)}{\partial p^2} - \Xi\left(p\right)\phi\left(p\right), \tag{2.A1}$$

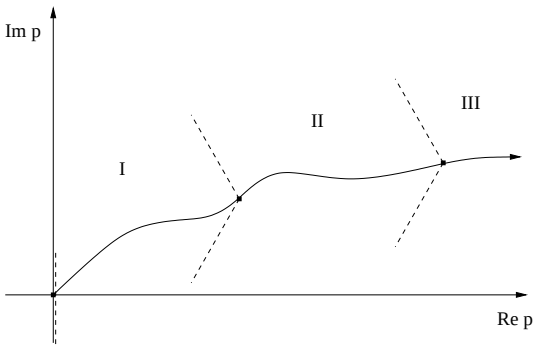

Figure 2.19: Sketch of local Stokes structure in the complex p plane. Dotted lines indicate Stokes lines in the vicinity of turning points. The location of zeros in the potential are denoted by points. Finally, the solid line is an example of a path through the various WKB regions.

where

$$\Xi\left(p\right)\equiv\left(1-\frac{\omega_d^*}{\omega}\right)^{-1}\left[\left(\frac{\nu_c-\left|\nu_T\left(p\right)\right|}{\left|\nu_T\left(0\right)\right|}\right)p^2+\frac{\Delta x^2}{\left|\nu_T\left(0\right)\right|}\left[\gamma_d-i\left(\omega-\omega_d^*\right)\right]\right]p^2, \qquad (2.A2)$$

and $p\equiv\Delta x q_x$. A WKB solution can be readily derived from Eq. (2.A1), yielding:

$$\phi_{WKB}\left(p\right)=\frac{C}{\left(\Xi\left(p\right)\right)^{1/4}}\exp\left(i\int^p dp\sqrt{-\Xi\left(p\right)}\right)+\frac{D}{\left(\Xi\left(p\right)\right)^{1/4}}\exp\left(-i\int^p dp\sqrt{-\Xi\left(p\right)}\right), \qquad (2.A3)$$

where C and D correspond to arbitrary constants. The potential given by Eq. (2.A2) possesses six roots, two of which are zero, and the other four which we will label $\pm p_1$ and $\pm p_2$, are generally complex. As is clear from the form of Eq. (2.A3), each of these roots, correspond to singularities in the WKB solution. Thus, connection formulas will be required in order to match WKB solutions valid in different regions. This asymptotic analysis is complicated due to the necessity of performing the analysis in the complex p plane. This requires an understanding of the location of the Stokes lines [lines for which the real part of the exponents in Eq. (2.A3) vanish], such that the matching can be carried out unambiguously. A sketch of the local Stokes structure in the complex p plane is shown in Fig. 2.19, which will serve as a 'guide' for the asymptotic analysis carried out below.

Considering first the region near $p = 0$, or the limit:

$$|p|^2 < \left| \frac{\Delta x^2}{|\nu_T(0)|} \left[\gamma_d - i(\omega - \omega_d^*) \right] \right|, \tag{2.A4}$$

(where we have ignored the ν_c term for simplicity), Eq. (2.A2) may then be approximated as

$$\Xi(p) \approx \left(1 - \frac{\omega_d^*}{\omega}\right)^{-1} \frac{\Delta x^2}{|\nu_T(0)|} \left[\gamma_d - i(\omega - \omega_d^*) \right] p^2 \equiv V_{p0} p^2, \tag{2.A5}$$

such that the solutions of Eq. (2.A1) have the form

$$\phi(p) = A\sqrt{p} K_{1/4}\left(\sqrt{V_{p0}} p^2/2\right) + B\sqrt{p} I_{1/4}\left(\sqrt{V_{p0}} p^2/2\right). \tag{2.A6}$$

As can be seen by examination of Eq. (2.A2), $\Xi(p)$ is invariant as $p \to -p$, thus it is only necessary to consider positive values of p. Hence, as a boundary condition at $p = 0$ we apply $\phi(0) = 0$ for odd modes and $\partial\phi(p)/\partial p|_{p=0} = 0$ for even modes. For brevity, we will only discuss even modes, although the derivation for odd modes would follow analogously. Applying the boundary condition $\partial\phi(p)/\partial p|_{p=0} = 0$, yields the relation $A = \left(\sqrt{2}/\pi\right) B$. Next it is necessary to match this solution with the WKB solution in the limit $\sqrt{V_{p0}} p^2/2 > 1$. Note that this limit is nontrivial, as Eq. (2.A4) must be simultaneously satisfied. The self-consistency constraint can be easily derived as $V_{p0}(1 - \omega_d^*/\omega) > 2^{2/3}$, which can be rewritten as

$$\left| \left(1 - \frac{\omega_d^*}{\omega}\right)^{-1/3} \frac{\Delta x^2}{|\nu_T(0)|} \left[\gamma_d - i(\omega - \omega_d^*) \right] \right| > 2^{2/3}. \tag{2.A7}$$

Which for the case of weak magnetic shear is well satisfied in nearly all relevant regimes. Assuming the condition given by Eq. (2.A7) is satisfied, Eq. (2.A6) may be expanded as

$$\phi(p) \approx B(p) \left\{ \sqrt{2} \exp\left(-\frac{1}{2}\sqrt{V_{p0}} p^2\right) + \exp\left(\frac{1}{2}\sqrt{V_{p0}} p^2\right) \right\}, \tag{2.A8}$$

where $B(p)$ is an arbitrary p dependent quantity, whose specific form is not required in order to obtain the lowest order eigenvalue condition. Matching to the WKB solution whose potential is approximated by Eq. (2.A5) yields the WKB expression valid in region I of Fig. 2.19

$$\phi_I(p) = B(p)\left\{\sqrt{2}\exp\left(i\int_0^p dp\sqrt{-\Xi(p)}\right) + \exp\left(-i\int_0^p dp\sqrt{-\Xi(p)}\right)\right\}. \quad (2.A9)$$

Similarly, near p_1, $\Xi(p)$ can be expanded to linear order yielding the expression

$$\frac{\partial^2\phi(p)}{\partial p^2} = \left(-\frac{\partial\Xi(p)}{\partial p}\right)|_{p=p_1}(p_1 - p)\,\phi(p), \quad (2.A10)$$

whose general solution is given by $\phi(s) = EAi(s) + FBi(s)$, where Ai and Bi are Airy functions of the first and second kind respectively, E and F are arbitrary constants, and $s \equiv \left(-\partial\Xi/\partial p|_{p=p_1}\right)^{1/3}(p_1 - p)$. Following a similar matching procedure as that outlined above for both $s > 0$ and $s < 0$, yields the WKB expression valid in region II as

$$\phi_{\mathrm{II}A}(p) = B(p)\left\{\frac{b}{2}\sin\left[\int_{p_1}^p dp\sqrt{-\Xi(p)} + \frac{\pi}{4}\right] + \cos\left[\int_{p_1}^p dp\sqrt{-\Xi(p)} + \frac{\pi}{4}\right]\right\}, \quad (2.A11)$$

where

$$b \equiv 2\sqrt{2}\exp\left\{\frac{4}{3}\left(-\frac{\partial\Xi}{\partial p}|_{p=p_1}\right)^{1/2} p_1^{3/2}\right\}.$$

Following an analogous procedure near p_2, and implementing the boundary condition $\phi(\Re p \to \infty) = 0$, yields the WKB expression also valid in region II

$$\phi_{\mathrm{II}B}(p) = B'(p)\sin\left[\int_p^{p_2} dp\sqrt{-\Xi(p)} + \frac{\pi}{4}\right], \quad (2.A12)$$

matching Eqs. (2.A11) and (2.A12) yields the expression for the eigenvalue:

$$\int_{p_1}^{p_2} dp\sqrt{-\Xi\left(p\right)} = \pi\left(l_e - \frac{1}{2}\right) + \delta, \tag{2.A13}$$

where l_e is a positive integer, and δ is defined by Eq. (2.42a).

Appendix B: Derivation of Convective Cell Trapping Criterion

Here we present a derivation of a trapping solution induced by the convective cell. It is convenient to consider the limit of weak shearing such that $\tau_{cc}/\tau_{os} > 1$. This assumption allows the use of a multi-scale perturbative analysis, with an expansion parameter given by $\epsilon \sim k_\perp \rho_s \sim (v_{0y}/v_e^*) \sim (q_y/q_x)$. Note that as shown in the next section via numerical simulation, convective cell induced wave trapping may take place for moderate values of $k_\perp \rho_s$. However, here we assume the weakly dispersive limit, allowing the use of the approximation $\delta\omega \approx v_e^* k_y \left(1 - k_\perp^2 \rho_s^2\right) + \mathbf{v}_0 \cdot \mathbf{k}$, as an analytic expedient. The slow drift of the wave packets will be obtained via separating the solution into fast and slow variables, i.e.

$$\frac{d}{dt} \to \frac{d}{dt} + \epsilon\frac{d}{dT}, \quad k_x\left(t, T\right) = k_x\left(t, T\right) + \epsilon k_x\left(T\right), \tag{2.B1}$$

where t and T are treated as independent variables. It is also convenient to take a simple limit of Eq. (2.56), such that the electrostatic potential can be written as $\bar{\phi} = \phi_0 \sin\left(q_x x\right)\cos\left(q_y y\right)$. In contrast to zonal flow wave trapping, which is centered around maximums or minimums of the shear flow, convective cell wave trapping is localized to the zeros of the poloidal velocity. Thus, it is convenient to shift our spatial coordinate to $\xi = x - \left(\pi/2\right)\left(1/q_x\right)$, and utilize the expansion

$\bar{\phi} \approx \phi_0 \cos(q_y y)\left(1 - (1/2)(q_x\xi)^2 + (1/24)(q_x\xi)^4 - \cdots\right)$. Considering first the evolution of the poloidal coordinate, the lowest order equation is given by

$$\frac{dy^{(0)}(t)}{dt} = v_e^*, \tag{2.B2}$$

$$\Rightarrow y^{(0)}(t) = v_e^* t + y(0) = v_e^* t, \tag{2.B3}$$

where $y(0) = 0$ for simplicity. This lowest order term corresponds to the non-dispersive component of the poloidal phase velocity, which uniformly translates the quasi-particle in the poloidal direction. The next nonzero contribution is given at second order by:

$$\frac{dy^{(2)}(t)}{dt} = -v_e^* \frac{v_{0y}}{v_e^*}\left(q_x\xi^{(1)}(t)\right)\cos(q_y y(t)) - v_e^*\left(k_x^{(1)}(t)^2 + 3k_y^{(1)}(t)^2\right)\rho_s^2, \tag{2.B4}$$

where the zeroth order contribution to the radial coordinate vanishes by assumption. Integrating Eq. (2.B4), yields

$$y^{(2)}(t) = -v_e^* \frac{v_{0y}}{v_e^*}\int^t dt'\left(q_x\xi^{(1)}(t')\right)\cos(q_y y(t')) - v_e^*\int^t dt'\left(k_x^{(1)}(t')^2 + 3k_y^{(1)}(t')^2\right)\rho_s^2. \tag{2.B5}$$

Approximations to $k_x^{(1)}$, $k_y^{(1)}$ and $\xi^{(1)}$ will be obtained perturbatively from Eqs. (1.28) and (1.29). However, here we note that $y^{(2)}(t)$ cannot be solved in a purely perturbative manner, i.e. although $y^{(2)}(t)$ is small in comparison to $y^{(0)}(t)$, expanding in $y^{(2)}(t)$ inside the cosine is of course not justified, as $y^{(2)}(t)$ will in general be large for long t. Hence, it is convenient to separate the contributions from $y^{(2)}(t)$ into two distinct forms

$$y^{(2)}(t) = r v_e^* t + f(t), \tag{2.B6}$$

where r is a constant, corresponding to a frequency shift in the lowest order solution, and $f(t)$ is a bounded function. The self-consistency of this form will be checked at the end of

the derivation.

Considering now the radial component, the lowest order nonzero contribution can be written

$$\frac{dq_x\xi^{(1)}(s)}{ds} = -2\frac{q_x}{q_y}k_y^{(1)}(s)\,k_x^{(1)}(s)\,\rho_s^2 + \frac{v_{0y}}{v_e^*}\sin(s)\,, \tag{2.B7}$$

where the change of variables $s = v_e^*(1+r)\,t$ has been introduced. Integrating Eq. (2.B7) yields:

$$q_x\xi^{(1)}(s) = -2\frac{q_x}{q_y}\int^s ds' k_y^{(1)}(s')\,k_x^{(1)}(s')\,\rho_s^2 - \frac{v_{0y}}{v_e^*}\cos(s)\,, \tag{2.B8}$$

The first term on the R.H.S. of Eq. (2.B8) corresponds to the radial group velocity of the wave packet, whereas the second term in this expression results from the radial flow component of the convective cell.

Similarly, the lowest order nonzero contribution to the poloidal wave number is given by $k_y^{(1)} = k_{0y} = \text{const}$. The next non-vanishing contribution may be obtained by taking the poloidal component of Eq. (4.A2), yielding:

$$\frac{dk_y^{(3)}(s)}{ds} = -\frac{v_{0y}}{v_e^*}\frac{q_y}{q_x}k_x^{(1)}(s)\cos(s) - k_{0y}\frac{v_{0y}}{v_e^*}\left(q_x\xi^{(1)}(s)\right)\sin(s)\,, \tag{2.B9}$$

$$\Rightarrow k_y^{(3)}(s) = -\frac{v_{0y}}{v_e^*}\frac{q_y}{q_x}\int^s ds' k_x^{(1)}(s')\cos(s') - k_{0y}\frac{v_{0y}}{v_e^*}\int^s ds'\left(q_x\xi^{(1)}(s')\right)\sin(s')\,. \tag{2.B10}$$

In order to close the system of Eqs. (2.B5), (2.B8), and (2.B10) it will be necessary to solve for $k_x^{(1)}$. This can most conveniently be done via Eq. (2.51), which to the lowest non-vanishing order can be written as

$$\frac{d^2k_x^{(1)}(s)}{ds^2} = -k_{0y}\frac{v_{0y}}{v_e^*}\frac{q_x}{q_y}\sin(s)\,, \tag{2.B11}$$

which yields the solution

$$k_x^{(1)}(s) = k_{0y}\frac{v_{0y}}{v_e^*}\frac{q_x}{q_y}\sin(s)\,. \tag{2.B12}$$

Utilizing Eq. (2.B12), Eqs. (2.B5), (2.B8), and (2.B10) may be solved, yielding:

$$\begin{aligned} q_y y^{(2)}(t) &= \left\{ \frac{1}{2}\left(\frac{v_{0y}}{v_e^*}\right)^2 - (k_{0y}\rho_s)^2 \left[3 + \left(\frac{q_x}{q_y}\right)^2 \left(\frac{v_{0y}}{v_e^*}\right)^2 \right] \right\} q_y v_e^* t \\ &+ \frac{1}{2}\left(\frac{v_{0y}}{v_e^*}\right)^2 \sin\left(q_y v_e^* (1+r)\, t\right) \cos\left(q_y v_e^* (1+r)\, t\right), \end{aligned} \tag{2.B13}$$

$$q_x \xi^{(1)}(s) = \frac{v_{0y}}{v_e^*} \left\{ \left(\frac{q_x}{q_y}\right)^2 (k_{0y}\rho_s)^2 - 1 \right\} \cos\left(q_y v_e^* (1+r)\, t\right), \tag{2.B14}$$

$$k_y^{(3)}(s) = -\frac{1}{2} k_{0y} \left(\frac{q_x}{q_y}\right)^2 \left(\frac{v_{0y}}{v_e^*}\right)^2 (k_{0y}\rho_s)^2 \sin^2\left(q_y v_e^* (1+r)\, t\right). \tag{2.B15}$$

From Eq. (2.B13), r and $f(t)$ may be recognized to be

$$r = \left\{ \frac{1}{2}\left(\frac{v_{0y}}{v_e^*}\right)^2 - (k_{0y}\rho_s)^2 \left[3 + \left(\frac{q_x}{q_y}\right)^2 \left(\frac{v_{0y}}{v_e^*}\right)^2 \right] \right\}, \tag{2.B16}$$

$$f(t) = \frac{1}{2}\left(\frac{v_{0y}}{v_e^*}\right)^2 \sin\left(q_y v_e^* (1+r)\, t\right) \cos\left(q_y v_e^* (1+r)\, t\right), \tag{2.B17}$$

which both have the assumed form. Using Eqs. (2.B12-2.B15) and Eq. (2.51), the slow drift of the quasi-particle may be obtained after time averaging over a single period of the rapid temporal oscillations. The lowest non-vanishing equation enters at the fourth order, and is given by

$$\begin{aligned} \frac{d^2 k_x(S)}{dS^2} &= -2\left(\frac{v_{0y}}{v_e^*}\right)^2 \left(\frac{q_x}{q_y}\right)^2 (k_{0y}\rho_s)^2 \left[1 - \left(\frac{q_x}{q_y}\right)^2 (k_{0y}\rho_s)^2 \right] \left\langle \cos^2(s) \right\rangle_s k_x(S) \\ &- 2\left(\frac{v_{0y}}{v_e^*}\right)^2 \left(\frac{q_x}{q_y}\right)^2 (k_{0y}\rho_s)^2 \left\langle \cos^2(s) \right\rangle_s k_x(S) \\ &+ \left(\frac{v_{0y}}{v_e^*}\right)^2 \left\{ \left\langle \sin^2(s) \right\rangle_s - \left\langle \cos^2(s) \right\rangle_s \right\} k_x(S), \end{aligned} \tag{2.B18}$$

where $\langle \cdots \rangle_s \equiv \int_0^1 ds\,(\cdots)$. Performing the averages, Eq. (2.B18) can be reduced to

$$\frac{d^2 k_x(S)}{dS^2} = -\left(\frac{v_{0y}}{v_e^*}\right)^2 \left(\frac{q_x}{q_y}\right)^2 (k_{0y}\rho_s)^2 \left[2 - \left(\frac{q_x}{q_y}\right)^2 (k_{0y}\rho_s)^2\right] k_x(S), \tag{2.B19}$$

which for

$$\frac{1}{2}\left(\frac{q_x}{q_y}\right)^2 (k_{0y}\rho_s)^2 < 1, \tag{2.B20}$$

corresponds to a simple harmonic oscillator with a bounce frequency in dimensional units given by

$$\omega_{cc} = v'_{0y}(k_{0y}\rho_s)\sqrt{2 - \left(\frac{q_x}{q_y}\right)^2 (k_{0y}\rho_s)^2}, \tag{2.B21}$$

which completes the derivation of the bounce frequency and trapping criterion.

Part of this chapter has been published in Physics of Plasmas, C. J. McDevitt and P. H. Diamond, **14**, 112306 (2007). C. J. McDevitt was the primary investigator and author of this paper.

Chapter 3

Multi-Scale Interaction of a Tearing Mode with Drift Wave Turbulence: A Minimal Self-Consistent Model

3.1 Introduction

MHD stability continues to be a critical consideration in the design of magnetic confinement devices, especially tokamaks. It has long been known that MHD instabilities can and do limit discharge performance. For example, the low-β, current gradient driven disruption is usually explained in terms of interaction between magnetic islands developing from tearing instabilities. The β-limit and the associated high-β disruption are usually associated with pressure gradient driven ballooning or kink modes. In recent years, appreciation of the importance of neoclassical tearing modes (NTMs) has risen considerably. NTMs are driven by the bootstrap current (i.e. produced by the pressure gradient and toroidicity), and result from the interaction of seed currents with parallel and cross-field transport and the resulting feedback loop between the island, the local currents and the pressure gradient. In

simple terms, island induced flattening of the pressure gradient drives further island growth. The details of NTM theory are numerous and a review is far beyond the scope of this paper. The interested reader is referred to ([47, 48, 49, 50, 51, 52]). However, it is instructive to note that polarization currents and cross-field turbulent transport are *both* thought to be critical to NTM evolution. Since the cross-field transport is driven by ambient micro turbulence, and the turbulent advection of vorticity which drives the nonlinear polarization drift also is responsible for generating zonal flows, the statement that *NTM evolution is strongly coupled to the ambient turbulence dynamics* appears irrefutable. Therefore, a successful theory of NTM evolution must treat the low-m island and the high m, n and k_r turbulence consistently, and on an equal footing.

Tokamaks are not the only confinement devices where the interaction of turbulence with large scale MHD is important. The Reversed Field Pinch (RFP) has long been characterized by disappointing confinement, which is a consequence of the nonlinear interaction and overlap of the same $m = 1$ tearing modes which drive the poloidal currents (i.e. the "dynamo") to sustain the magnetic configuration. Recently, however, a spontaneous transition to a quasi-single helicity (QSH) state of good confinement was predicted on the basis of numerical simulations and subsequently observed in experiment [53, 54, 55, 56]. The QSH state is predicted to appear for Hartmann numbers below a critical value, i.e. for $H = 1/\sqrt{\nu\eta} < H_{crit}$ [57], where H has been normalized to the Alfven time and the minor radius of the plasma. While the collisional resistivity η in RFP plasmas may be sufficient to be compatible with the $H < H_{crit}$ condition [58], the viscosity ν is *certainly not*, since neoclassical corrections to the classical ion viscosity are negligible for RFP geometry. Thus, ν must be interpreted as a *turbulent viscosity*, which can be due to ambient turbulence driven by resistive interchanges, drift-ITG modes, or other tearing modes (residual in the QSH state). Thus, we once again arrive at a problem which requires the simultaneous, self-consistent treatment of low-m MHD and high-k turbulence.

The problems of NTM evolution in tokamaks and evolution of the QSH state in a RFP are both *multi-scale problems*, in that *they require treatment over a broad range of disparate space and time scales*. Interestingly, another such problem is drift wave-zonal flow interaction, in which high-$\mathbf{k}$ drift waves drive an $n = 0$, $m = 0$ zonal flow and, in turn, are regulated by its shear. Either an analytical or computational approach to such multi-scale problems requires what is, in effect, a *dynamic subgrid scale model*, which allows feedback of the resolved scales on the unresolved (small) scales. In the case of the NTM, or tearing modes in RFPs, the feedback will be due to:

a.) large scale flow shears, which strain high-$\mathbf{k}$ modes

b.) large scale mixing (i.e. radial) flows, which modify the turbulence profile

c.) modification of the density, temperature, etc, profiles by the large scale mode, which in turn, alters the excitation of turbulence.

Note that b.) and c.) have no counterpart in the zonal flow problem, since flows there are azimuthally symmetric. However, it is again interesting to mention that the 'inverse cascade' which drives zonal flow formation is a good example of a process which lies outside the standard ansatz of enhanced turbulent dissipation, which forms the underpinning of most subgrid models. Indeed, since *inverse energy transfer is generic to drift wave turbulence*, it is readily apparent that a multi-scale model requires more physics content then enhanced dissipation, alone.

It is an understatement to say that the multi-scale problem is hideously complicated. Thus, we have sought to further the cause of simplicity by defining the *absolutely minimal working model*, namely that of low-m resistive (current gradient driven) tearing evolution in the presence of electrostatic drift wave turbulence in a cylinder. The tearing mode dynamics are described by reduced MHD (RMHD) and the small scale, large-m mode dynamics

are described by an *electrostatic fluid model*, such as the Hasegawa-Mima, Hasegawa-Wakatani, or fluid ITG equations. This minimal model avoids the geometrical complexity of toroidal effects, facilitates analytical progress and physical insight, and permits easy visualization. Moreover, *even further simplification* is made possible by exploiting the disparity in space-time scales between the tearing mode and the background drift waves. In particular, for a tearing mode with wave-vector $\mathbf{q}$ [here $\mathbf{q} = (q_x,\ q_\theta,\ \text{and}\ q_z)$, where q_x is comparable to the inverse layer width and q_θ, q_z are standard notations], and for drift waves with wave vector $\mathbf{k}$, it is the case that $\gamma_q \ll \omega_k$, $q_\theta \ll k_\theta$, and $q_x < k_x$. It is thus apparent that the tearing mode adiabatically modulates the background drift wave population, and the interaction may be treated using a wave-kinetic equation for the evolution of an adiabatic invariant of the drift wave population. Thus, the minimal model ultimately reduces to:

a.) RMHD for the tearing mode, including the effects of stresses and fluxes driven by the drift waves

b.) a wave kinetic equation for $N\left(\mathbf{k}, x, t\right)$, the drift wave population density proportional to the spectral density. Here N is strained and advected by the tearing mode flows.

Note that albeit simple, the 'minimal model' defines a closed self-consistent feedback loop for the interaction of low-m MHD and high-$\mathbf{k}$ drift waves. This feedback loop is shown schematically in Fig. (3.1). Since the drift wave stresses and transport fluxes (directly related to N) evolve in response to straining and mixing by the tearing mode, our minimal model does indeed qualify as a 'dynamic subgrid-scale model'.

To orient the reader, we think it worthwhile at the outset to survey the physics of multi-scale interaction in the minimal model. As noted above, a critical element of the multi-scale problem is the effect of stresses and transport of small scales on large scales. These effects

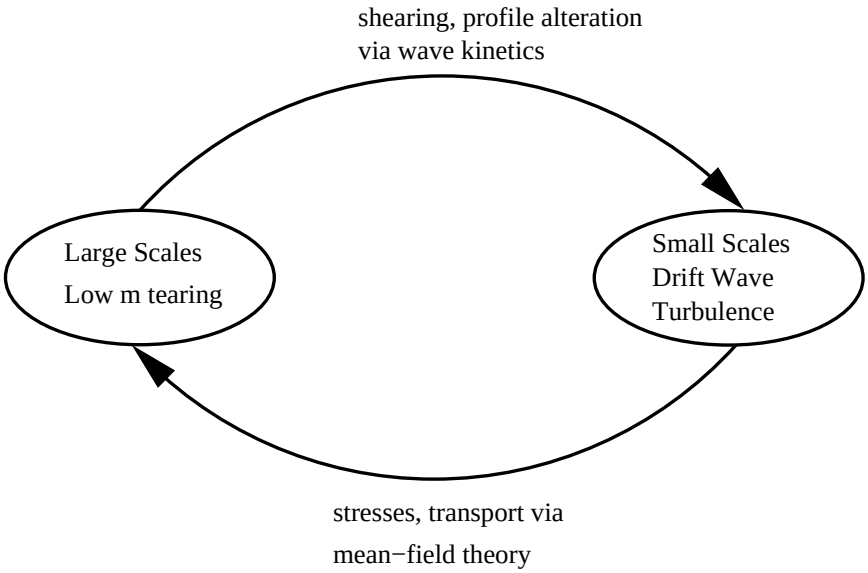

Figure 3.1: Minimal Multi-scale Model.

are nearly always the result of quadratic nonlinear interaction, so that schematically:

$$\frac{\partial}{\partial t} L_q \sim \text{Linear Terms } + \sum_{\mathbf{k}} C_{k,q} A_{k+q} B_{-k} \ ,$$

where A and B are amplitudes of small scale modes and $C_{k,q}$ is a coupling coefficient. Here, L_q is the amplitude of the large scale mode. As $|\mathbf{q}| \ll |\mathbf{k}|$, it is natural then to express this interaction in terms of the population density of the small scales. Thus, the equation for L_q may be re-expressed as:

$$\frac{\partial}{\partial t} L_q \sim \text{Linear Terms } + \sum_{\mathbf{k}} C_{k,q} f\left(-\mathbf{k}\right) \delta N_q \left(\mathbf{k}, t\right) \ ,$$

where $\delta N_q \sim |A_k|^2$ and $B_k = f\left(\mathbf{k}\right) A_k$. The output of this procedure is a set of 'mean field' equations for the low-m perturbation in the presence of the high $\mathbf{k}$, ω_k background. Indeed, *the high→low coupling* enters *via the modulation of the high-*$\mathbf{k}$ *background population by the low-*m *perturbation*. This modulation induces a stress or 'pondermotive force' (related to that familiar from Langmuir turbulence) on the low-$\mathbf{k}$ mode. In RMHD, three

nonlinearities are present, namely $\mathbf{v} \cdot \nabla\psi$ in Ohm's law, $\mathbf{v} \cdot \nabla\nabla_\perp^2\phi$ and $\mathbf{B} \cdot \nabla\nabla_\perp^2\psi$ in the vorticity equation. For purely electrostatic background turbulence, the first and third of these vanish, leaving the polarization nonlinearity as the only channel for high→low interaction. Interestingly, this is *precisely* the same nonlinearity which is responsible for the coupling of high-$\mathbf{k}$ drift wave beat interactions into zonal flows and convective cells. It is no surprise then, that the end-product of this mean field calculation is a *negative turbulent viscosity*. The sign is, or course, a consequence of the fact that energy flows from small to large scales, as it does in the case of zonal flow formation. That phenomenon in turn may be understood as a simple incarnation of the more general concept of an inverse cascade. Throughout this paper, we use the term "inverse cascade" as a general catch-all phrase for transfer of energy to large scales. Thus, our use of "inverse cascade" includes modulational instability generation of zonal flows, Reynolds stress driven large scale flows, etc., as well as strictly *local* transfer of energy to large scales. Note that this mechanism can drive low-m vortical flows at resonant surfaces even when the tearing mode is linearly stable (i.e. $\Delta' < 0$). Hence, one broader implication of the multi-scale problem is that high-$\mathbf{k}$ energy fluctuation is channeled to low m, n resonant surfaces, as well as to scale-independent friction drag. Energy deposited at such low order rational q surfaces is dissipated both by resistivity (via field line bending) and by frictional drag. This intriguing question of the ultimate fate of energy coupled to large scales via inverse cascade will be discussed further in the conclusions.

The second critical element of the multi-scale problem is the feedback of large scales on small. This closing of the loop allows the feedback of large→small, which makes the model self-consistent. Use of a wave kinetic equation for N, i.e.

$$\frac{\partial}{\partial t}N_k + \frac{\partial}{\partial \mathbf{k}}\left(\omega_k + \mathbf{k}\cdot\mathbf{V}\right)\cdot\frac{\partial}{\partial \mathbf{x}}N_k - \frac{\partial}{\partial \mathbf{x}}\left(\omega_k + \mathbf{k}\cdot\mathbf{V}\right)\cdot\frac{\partial}{\partial \mathbf{k}}N_k = \gamma_k N_k + C\left(N_k\right) \ ,$$

where $\mathbf{V}$ is the velocity of the mean field, ω_k is the linear frequency of the drift waves, and

$C\left(N_k\right)$ is the collisional operator, provides a useful framework for understanding the various feedback loops. Since $q_x \gg q_y$, tearing mode flows are primarily poloidal. Hence, the radially sheared poloidal flows generated by the low-m mode will shear and regulate the high-**k** turbulence in a manner similar to the way zonal flows regulate drift waves (see Fig. (3.2)). This effect is accounted for by the $\partial/\partial x\left(k_y V_y\right)\partial N_k/\partial k_x$ term in the wave kinetic equation, which results in amplification of k_x. Note that strong shears can trap background drift waves [40, 21], producing a strongly nonlinear multi-scale interaction. Another interesting feedback loop operates via $V_x \partial N_k/\partial x$. This corresponds to tearing-mode induced modification of the turbulence profile. The $V_x \partial N_k/\partial x$ term also accounts for turbulence spreading [59, 60, 61], a process which is potentially important in NTM evolution. Finally, the modifications in ∇P, ∇T , ∇n induced by the tearing mode can feed-back on γ_k, the local growth or excitation rate for the high-**k** turbulence. It is interesting to note that low→high feedback occurs in both **k** space (via shearing) and position space (via radial mixing). These two processes can act synergistically, as well.

We note here that the problem of how a tearing mode interacts with background turbulence is one with a long, albeit intermittent, history in magnetic fusion theory. Most of the previous attempts have focused on a search for anomalous dissipation in the Ohm's Law, such as a turbulent electron viscosity [62, 63, 64] or resistivity [65]. The hope here was to find a dissipation mechanism which was robust in the limit of small collisional resistivity. These models all focused on nonlinearities in Ohm's Law, did not consider feedback on the ambient micro turbulence, and so were not self-consistent. Other studies have considered the effect of incoherent emission from high-**k** modes as a 'trigger' for [66] or a means of 'accelerating' [67] the linear growth of low-m. Neither of these studies treated feedback self-consistently. However, we wish to emphasize that incoherent emission effects are potentially important and merit further study. Ongoing research strongly suggests that incoherent emission from higher harmonics can substantially accelerate the growth of low-m

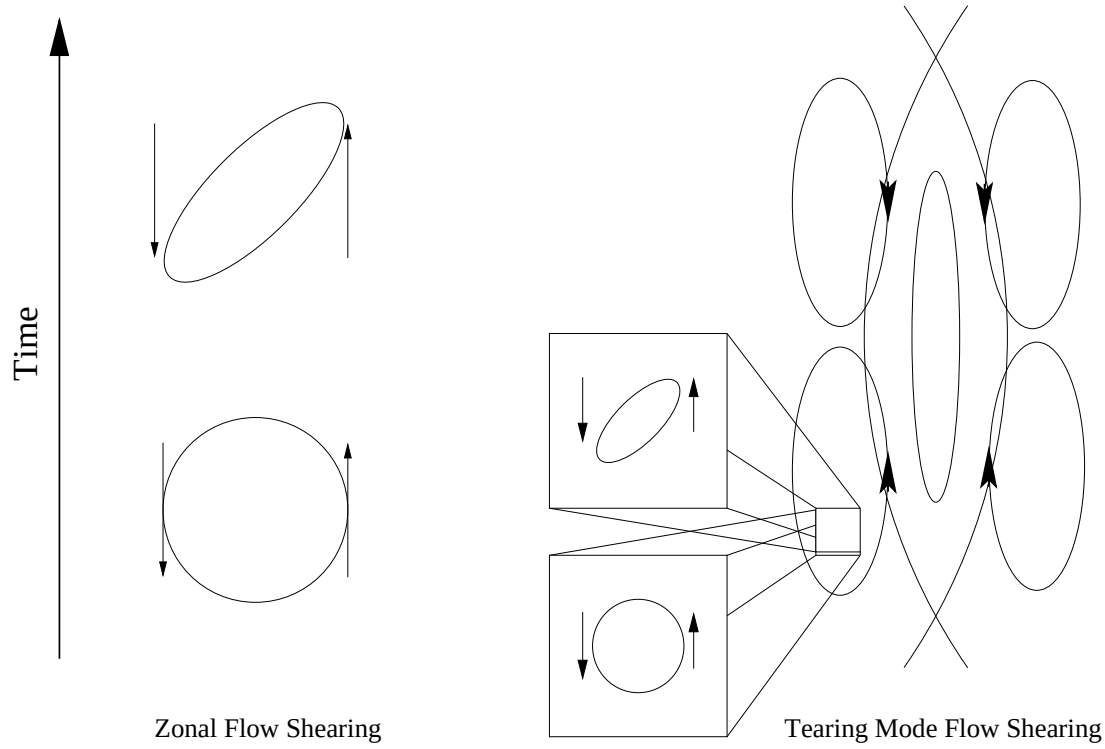

Figure 3.2: Zonal shear flows are similar to the shear flows of thin, low-m magnetic islands.

NTM's.

In this paper, then, we present a minimal model of multi-scale interaction between high-$\mathbf{k}$ drift waves and a low-m tearing mode in a cylinder. The basic model is set forth and mean field equations for the low-m dynamics are derived. The wave-kinetic equation for the drift wave population density is presented and discussed, and the key physics of the high-$\mathbf{k}\rightleftharpoons$low-$m$ feedback loops is elucidated. We study the stability, scales and growth rates of both a low-m, electrostatic vortex mode and a low-m tearing mode, with $\Delta' > 0$. The key small scale$\rightarrow$large scale effect (for the case of electrostatic turbulence) is a negative turbulent viscosity. For realistic parameters, this effect dominates inertia, and thus (along with field line bending) sets the scale of the tearing layer. Outgoing wave boundary conditions are imposed in order to control the rapid oscillations induced by the negative viscosity. In contrast to most cases in MHD, a real frequency is also induced. We also sketch an outline of the 'Rutherford' calculation for the case of a finite size island. The

meaning and interpretation of the Rutherford theory in the presence of self-consistently evolving background turbulence are discussed.

The remainder of this paper is organized as flows: In Sec. 2 we discuss the general multi-scale formulation of the problem. In Sec. 3 we present a linear theory of the tearing instability in the presence of a negative viscosity. In Sec. 4 we provide a discussion of the coupled evolution of a magnetic island in a background of ambient micro turbulence. Finally, Sec. 5 contains the conclusions and a discussion of broader issues and future work.

3.2 Formulation

3.2.1 Wave Kinetic for Small Scale Drift Waves

As shown in [68, 5] for the case of drift wave-zonal flow systems, wave kinetics is a useful formalism for studying modulational instabilities. Zonal flows induce a nonlinear frequency shift in the wave kinetic equation via a Doppler shift, and modulation of the diamagnetic drift velocity. The modulation of the drift wave turbulence *by* the zonal flow reacts back *on* the zonal flow through the polarization nonlinearity. This can be shown to lead to a nonlocal transfer of energy *from* the drift waves *to* the zonal flow, thus amplifying the initial shear perturbation. A schematic flow chart of the drift wave-zonal flow system is given in Fig. (3.3).

In this work we will be focusing on low $m \neq 0$ modes, for which the above picture is somewhat modified. For the case of a low-m tearing mode, both the inverse cascade and the current gradient (via the tearing mechanism) can drive large scale flow. Also, the back-reaction on the drift wave turbulence is more complex. Aside from shearing the drift wave turbulence as in the case of zonal flows, a low-m tearing mode will react back on the turbulence both by modifying the pressure profile (flattening the pressure gradient inside the island and potentially steepening it outside), and perturbing the magnetic field topology,

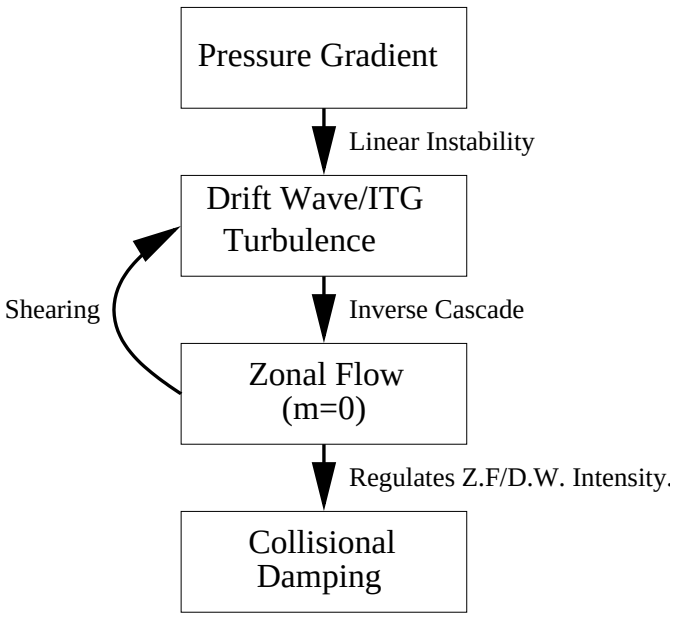

Figure 3.3: Schematic of drift wave-zonal flow phenomenon.

thus modifying the effective local magnetic shear. The structure of the high-$\mathbf{k}$ turbulence should be calculated in the evolving magnetic geometry which incorporates the island. A schematic flow chart of the low-m tearing mode interaction with drift wave turbulence is given in Fig. (3.4).

In order to derive a wave kinetic equation for the small scales, it is useful to first identify a quantity which varies adiabatically. One might expect an adiabatic invariant such as wave action, of the form $N_k = E_k/\omega_k$. However, as was shown in [13, 11], the *actual* adiabatic invariant for a drift wave system in the presence of mean flows is $N_k = \left(1+\rho_s^2 k_\perp^2\right)^2 \left|\phi_k^>\right|^2$. This quantity can be recognized as the drift wave potential enstrophy, which is a measure of the vorticity density associated with the drift waves. Note however, for zonal flows, with $k_\theta = 0$, the wave action and potential enstrophy are identical. We note in passing that, similar to the 2D Euler equation, the Hasegawa-Mima equation corresponds to a law of conservation of potential vorticity along fluid trajectories. Thus, it is not surprising that the 'adiabatic invariant' is the potential enstrophy. However, in contrast to the Hasegawa-Mima equation, the 2D Euler equation possesses no 'waves'. This observation could lead

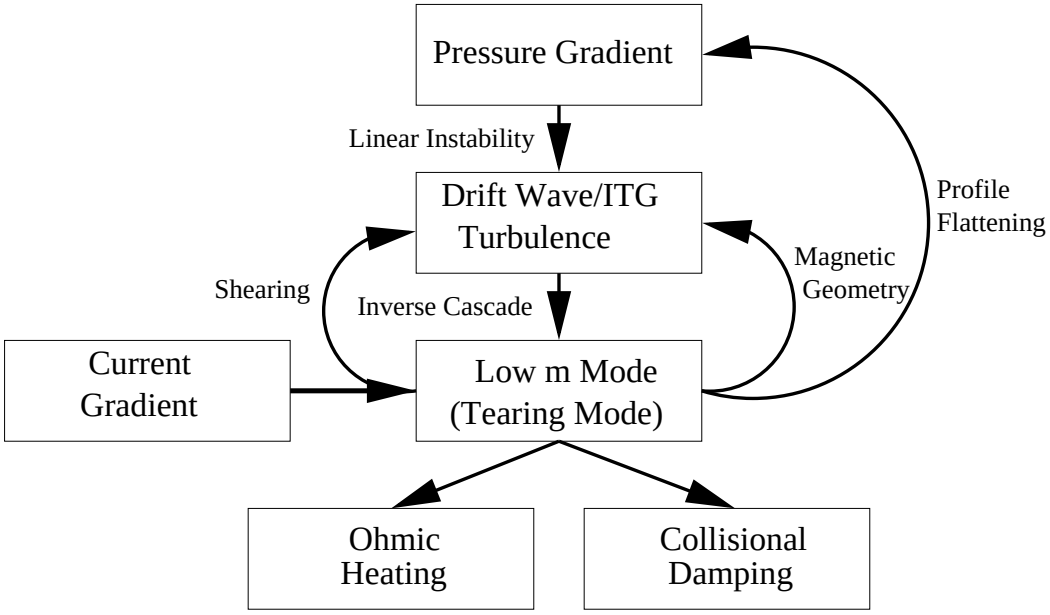

Figure 3.4: Schematic of Low-m mode interaction with drift wave turbulence.

one to conclude that a description of incompressible 2D hydrodynamic turbulence via a wave kinetic equation is impossible, since their are no "wave quanta". However, as shown by [11], a wave kinetic equation can be derived from the 2D Euler equation, where in this limit, the adiabatic invariant is the enstrophy density which can be interpreted as the "roton" number density.

Proceeding with the derivation of the wave kinetic equation, it is convenient to separate the fields into a large scale, mean field piece plus a small scale fluctuation defined by:

$$f^{<}(\mathbf{x}) = \sum_{|\mathbf{k}|<|\mathbf{k}_c|} f_k^{<} exp\left(i\mathbf{k}\cdot\mathbf{x}\right) \ , \tag{3.1}$$

$$f^{>}(\mathbf{x}) = \sum_{|\mathbf{k}|>|\mathbf{k}_c|} f_k^{>} exp\left(i\mathbf{k}\cdot\mathbf{x}\right) \ , \tag{3.2}$$

where $|\mathbf{k}_c|$ defines the cutoff scale between the small scale and large scale systems. Applying this scale separation procedure, an equation for the micro turbulence, which is similar to the Hasegawa-Mima equation [19], but retains the mean field contribution, can be written

as

$$0 = \left(\frac{\partial}{\partial t} + \frac{c}{B_0}\left(\hat{\mathbf{z}} \times \nabla\phi^{<}\right)\cdot\nabla\right)\frac{e\phi^{>}}{T_e} + v_e^*\frac{\partial}{\partial y}\frac{e\phi^{>}}{T_e} - \rho_s^2\left(\frac{\partial}{\partial t} + \frac{c}{B_0}\left(\hat{\mathbf{z}} \times \nabla\phi^{<}\right)\cdot\nabla\right)\nabla_\perp^2\frac{e\phi^{>}}{T_e}\,. \tag{3.3}$$

Here, $\rho_s = c_s/\omega_{ci}$, $c_s = \sqrt{T_e/m_i}$, $v_e^* = cT_e/\left(eB_0L_n\right)$ is the electron diamagnetic drift velocity, and $\hat{z}$ is in the direction of the mean magnetic field. We are primarily interested in investigating the nonlocal interaction of drift waves with large scale, low-m modes. Hence, local interactions between drift waves, i.e. the quadratic nonlinearities in $\phi^{>}$, have been dropped. Local interactions will be introduced later via the insertion of a phenomenological collisional operator in the Boltzmann equation for the wave number density. Also, note the addition of an advective term representing the large scale mean flow.

Exploiting the scale separation and averaging over the fast scales, a wave kinetic equation for the evolution of the drift wave potential enstrophy density in the presence of a weakly varying background can be written (see [13] for details)

$$\frac{\partial}{\partial t}N_k + \frac{\partial}{\partial \mathbf{k}}\left(\omega_k + \mathbf{k}\cdot\mathbf{V}_0\right)\cdot\frac{\partial}{\partial \mathbf{x}}N_k - \frac{\partial}{\partial \mathbf{x}}\left(\omega_k + \mathbf{k}\cdot\mathbf{V}_0\right)\cdot\frac{\partial}{\partial \mathbf{k}}N_k = S\,, \tag{3.4}$$

$$\omega_k = \frac{v_e^* k_y}{1+\rho_s^2k_\perp^2}, \quad \mathbf{V}_0 = \frac{c}{B_0}\left(\hat{\mathbf{z}} \times \nabla\phi^{<}\right), \quad N_k = \left(1+\rho_s^2k_\perp^2\right)^2 I_k\,.$$

Here N_k is the enstrophy density, I_k is a Wigner function defined as $I_k = \int d\mathbf{q}e^{i\mathbf{q}\cdot\mathbf{x}}\left\langle\phi^{>}_{k+q}\phi^{>}_{-k}\right\rangle$, and the brackets represent an average over the small, rapidly varying scales. The second term on the left in Eq. (3.4) corresponds to the advection term with a doppler shift due to the mean flow. Here the "mean flow" is the flow associated with the MHD mode. The third term describes the refraction of the drift waves as a result of any spatial dependence of the real frequency (i.e. spatial variations of the density gradient), and through the weak spatial variation of the mean field. Notice that in the absence of

the source term S, this amounts to the conservation of wave quanta number N_k along ray trajectories. The source term S can be symbolically written as $S = \gamma_k N_k - \Delta\omega_k N_k^2$. The first term corresponds to the linear drive of the drift waves, which should be computed *in the presence of the tearing mode*. This is necessary since the island will modify both the local profiles and the drift wave mode structure. The second term corresponds to the nonlinear like-scale interaction. In the absence of the nonconservative source term, Eq. (3.4) is isomorphic to the Vlasov equation, and thus provides a particularly convenient description of the intensity field of the drift wave turbulence.

3.2.2 Mean Field Equations for Large Scale Tearing Mode

In the previous section we introduced a wave kinetic formulation which allowed us to describe the development of the drift wave turbulence in terms of an adiabatically varying wave population density N_k. This approach enables us to develop a *dynamic subgrid scale* model for drift wave-MHD interaction. This model is 'dynamic' since there is feedback, via shearing and modulation, by the large scale flows on the small scale turbulence, which exerts a stress on it. We are now interested in a description of the mean field (i.e. tearing mode) equations in the presence of the background micro turbulence. We describe the MHD fields at low m via RMHD. This description ignores a number of effects that become important in the low collisionality, high temperature regime. However, it constitutes the absolute minimal description of unstable tearing mode dynamics. Furthermore, as has been observed in drift wave-zonal flow systems, the background turbulence behaves as a source of energy for the large scales, and drives mean flows via the stress term. Thus, we seek to understand how the inclusion of this external drive affects the evolution of the tearing mode. For this reason, it will be convenient to begin with as simple a description as

possible. The RMHD equations are given by

$$0 = \frac{\partial}{\partial t}\psi + \frac{c}{B_0}(\hat{\mathbf{z}} \times \nabla\phi) \cdot \nabla\psi - v_A \frac{\partial}{\partial z}\phi - \eta_c \nabla_\perp^2 \psi \,, \tag{3.5}$$

$$0 = \frac{\partial}{\partial t}\nabla_\perp^2\phi + \frac{c}{B_o}(\hat{\mathbf{z}} \times \nabla\phi) \cdot \nabla\nabla_\perp^2\phi - v_A \frac{\partial}{\partial z}\nabla_\perp^2\psi - \frac{c}{B_0}(\hat{\mathbf{z}} \times \nabla\psi) \cdot \nabla\nabla_\perp^2\psi - \nu_c \nabla_\perp^2 \nabla_\perp^2 \phi \,. \tag{3.6}$$

Here $\hat{z}$ points in the direction of the equilibrium magnetic field, ψ has been normalized to v_A/c, and the Alfven velocity is defined as $v_A = B_0/\sqrt{4\pi}$, where ρ_0 has been set equal to one. Since the small scales are described by an electrostatic model, small scale magnetic perturbations are neglected. Thus, the stream function and flux function can be written as $\phi = \phi^< + \phi^>$, $\psi = \psi^<$. Substituting these definitions into Eqs. (3.5) and (3.6) and averaging, gives the large scale equations:

$$0 = \frac{\partial}{\partial t}\psi^< + \frac{c}{B_0}(\hat{\mathbf{z}} \times \nabla\phi^<) \cdot \nabla\psi^< - v_A \frac{\partial}{\partial z}\phi^< - \eta_c \nabla_\perp^2 \psi^< \,, \tag{3.7}$$

$$0 = \frac{\partial}{\partial t}\nabla_\perp^2\phi^< + \frac{c}{B_o}(\hat{\mathbf{z}} \times \nabla\phi^<) \cdot \nabla\nabla_\perp^2\phi^< - v_A \frac{\partial}{\partial z}\nabla_\perp^2\psi^< - \frac{c}{B_0}(\hat{\mathbf{z}} \times \nabla\psi^<) \cdot \nabla\nabla_\perp^2\psi^< - \nu_c \nabla_\perp^2 \nabla_\perp^2 \phi^< + \frac{c}{B_0}\left\langle (\hat{\mathbf{z}} \times \nabla\phi^>) \cdot \nabla\nabla_\perp^2\phi^> \right\rangle \,. \tag{3.8}$$

Note the absence of a stress term within the induction equation. This precludes the appearance of a turbulent resistivity. As considered in [69, 5], electrostatic fluctuations can generate an anomalous resistivity through the $\left\langle \tilde{n}\tilde{E}_\parallel \right\rangle$ term. This anomalous resistivity can be calculated by modulating the parallel acceleration term with respect to $\psi^<$, which can be written symbolically as $\delta\left\langle \tilde{n}\tilde{E}_\parallel \right\rangle \sim \sum_k C_k \left(\delta N_k/\delta\psi^<\right)\psi^<$. However, in this simple model for electrostatic drift waves (as can be seen from Eq. (3.4)), N_k is unaffected by

perturbations in $\psi^<$ ($\delta N_k/\delta\psi^< = 0$). This is a consequence of assuming that drift waves and Alfven waves decouple, which is valid only in a low beta plasma. In the finite beta regime, perturbations of $\psi^<$ would enter into the wave kinetic equation by bending the mean magnetic field lines, and then modulating the frequency of the drift-Alfven modes as discussed in [70]. Just as the negative viscosity excites low-m flows which are similar to zonal flows, this effect could drive a low-m magnetic field similar to a zonal field. Also, note that for a large magnetic island, the effective magnetic shear at the X point differs substantially from that of the O point. Thus, for large magnetic perturbations, $\psi^<$ would modulate N_k through modifications of the local magnetic shear leading to $\delta N_k/\delta\psi^< \neq 0$, and so produce a turbulent resistivity. However, for the present 'minimalist' study we will not consider this possibility.

The simple averaging procedure employed above, reduces the system into a set of resolved equations for the large scales, and a population density equation for the unresolved small scales. However, while the phase information of small scale fluctuations is averaged out, the evolution of the intensity $N_k \sim \left\langle \phi_k^> \phi_{-k}^> \right\rangle$ evolves dynamically via modulations by the large scale mean field. Thus, Eqs. (3.4, 3.7, 3.8) provide a minimal self-consistent description of the drift wave-tearing mode system.

3.2.3 Closure of Drift Wave-Tearing Mode System

In order to close the drift wave-tearing mode system, it is necessary to explicitly write the Reynolds stress term within the RMHD equations in terms of the drift wave enstrophy.

After integrating by parts twice, the Reynolds stress $\left\langle (\hat{\mathbf{z}} \times \nabla \phi^{>}) \cdot \nabla \nabla_{\perp}^{2} \phi^{>} \right\rangle$ can be written

$$\left\langle (\hat{\mathbf{z}} \times \nabla \phi^{>}) \cdot \nabla \nabla_{\perp}^{2} \phi^{>} \right\rangle (\mathbf{x}, t) = -\left(\frac{\partial^2}{\partial x^2} - \frac{\partial^2}{\partial y^2} \right) \left\langle \frac{\partial \phi^{>}}{\partial x} \frac{\partial \phi^{>}}{\partial y} \right\rangle (\mathbf{x}, t) + \frac{\partial^2}{\partial x \partial y} \left[\left\langle \left(\frac{\partial \phi^{>}}{\partial x} \right)^2 \right\rangle (\mathbf{x}, t) - \left\langle \left(\frac{\partial \phi^{>}}{\partial y} \right)^2 \right\rangle (\mathbf{x}, t) \right] , \tag{3.9}$$

where we have written the brackets in the form $\langle ... \rangle (\mathbf{x}, t)$, to emphasize that the averages are over the fast spatial and temporal scales, such that a slow spatial and temporal dependence remains. After Fourier transforming, the stress terms can be rewritten in terms of the drift wave enstrophy density:

$$\left\langle (\hat{\mathbf{z}} \times \nabla \phi^{>}) \cdot \nabla \nabla_{\perp}^{2} \phi^{>} \right\rangle (\mathbf{x}, t) = -\left(\frac{\partial^2}{\partial x^2} - \frac{\partial^2}{\partial y^2} \right) \int d\mathbf{k} \frac{k_x k_y}{\left(1 + \rho_s^2 k_{\perp}^2\right)^2} N_k (\mathbf{x}, t) + \frac{\partial^2}{\partial x \partial y} \int d\mathbf{k} \frac{\left(k_x^2 - k_y^2\right)}{\left(1 + \rho_s^2 k_{\perp}^2\right)^2} N_k (\mathbf{x}, t) \ . \tag{3.10}$$

From this expression it is clear that for isotropic turbulence, both integrals vanish. Thus, a necessary condition for a finite contribution to the mean field vorticity equation from the background drift wave turbulence is either anisotropy of the equilibrium drift wave spectrum, or a 'seed' asymmetry, which arises from the large scale mean fields which modulate the drift wave spectrum. The latter is the subject of the present discussion, as we are concerned with tearing interaction with the ambient drift wave turbulence.

Considering small deviations from the equilibrium drift wave spectrum N_k^0 (i.e. seed asymmetries), Eq. (3.4) can be linearized for small perturbations of the form $(\delta N_k, \ \phi^{<}) \sim e^{i\mathbf{q}\cdot\mathbf{x} - i\omega_q t + \gamma_q t}$, yielding an expression for the response of the drift waves to the tearing mode field:

$$\delta N_k = \frac{c}{B_0} \frac{-1}{(\omega_q - \mathbf{q} \cdot \mathbf{v}_{gr}) + i (\gamma_q + \gamma_k)} \left\{ q_y \frac{\partial N_k^0}{\partial x} - i \left(\mathbf{k} \times \mathbf{q} \right)_z \mathbf{q} \cdot \frac{\partial N_k^0}{\partial \mathbf{k}} \right\} \phi^{<} \ . \tag{3.11}$$

Here, ω_q and γ_q correspond to the real frequency and growth rate of the MHD mode respectively, and are assumed slow in comparison to the ambient drift wave turbulence, γ_k is the linear growth rate of the drift wave turbulence, and $\mathbf{v}_{gr} = \partial\omega_q/\partial\mathbf{k}$. The first term in brackets corresponds to the spatial modification of the turbulence profile due to modulations of the large scale mean field. For purposes of simplicity, in this analysis we will consider a spatially uniform turbulence profile, and thus focus purely on the k space dynamics (the second term in brackets). We note that $\partial N_k^0/\partial x$ - driven contributions to δN_k will enter with a phase $\pi/2$ different from $\partial N_k^0/\partial\mathbf{k}$ - driven contributions. These may be especially important to the finite-sized island evolution problem. Also, notice that the linearization above is purely for convenience. Though the W.K.E. (naively) appears to be nonlinear, it is actually bilinear (ignoring the collision operator), so that even for strong modulation fields, the response of N_k may be calculated by the method of characteristics. Physically, such strong modulations can cause trapping of drift waves in the island flows. Substituting Eq. (3.11) into the polarization drift term of the vorticity equation [Eq. (3.10)] gives to lowest order

$$\begin{aligned}
\left\langle (\hat{\mathbf{z}} \times \nabla\phi^{>}) \cdot \nabla\nabla_\perp^2\phi^{>} \right\rangle = & -c_s^2 \int d\mathbf{k} \frac{\rho_s^2 k_y^2}{\left(1+\rho_s^2 k_\perp^2\right)^2} \frac{\gamma_k}{\left(\gamma_k^2 + \left(\mathbf{q}\cdot\mathbf{v}_{gr}\right)^2\right)} k_x \frac{\partial N_k^0}{\partial k_x} \frac{\partial^4\phi^{<}}{\partial x^4} \\
& - c_s^2 \int d\mathbf{k} \frac{\rho_s^2 k_x^2}{\left(1+\rho_s^2 k_\perp^2\right)^2} \frac{\gamma_k}{\left(\gamma_k^2 + \left(\mathbf{q}\cdot\mathbf{v}_{gr}\right)^2\right)} k_y \frac{\partial N_k^0}{\partial k_y} \frac{\partial^4\phi^{<}}{\partial y^4} \\
& + c_s^2 \int d\mathbf{k} \frac{\rho_s^2}{\left(1+\rho_s^2 k_\perp^2\right)^2} \frac{\gamma_k}{\left(\gamma_k^2 + \left(\mathbf{q}\cdot\mathbf{v}_{gr}\right)^2\right)} \\
& \cdot \left(k_x^3 \frac{\partial N_k^0}{\partial k_x} + k_y^3 \frac{\partial N_k^0}{\partial k_y} \right) \frac{\partial^2}{\partial x^2} \frac{\partial^2\phi^{<}}{\partial y^2} \, , \\
= & -\nu_{xx} \frac{\partial^4\phi^{<}}{\partial x^4} - \nu_{yy} \frac{\partial^4\phi^{<}}{\partial y^4} + \nu_{xy} \frac{\partial^2}{\partial x^2} \frac{\partial^2\phi^{<}}{\partial y^2} \, ,
\end{aligned} \tag{3.12}$$

where

$$\nu_{xx} = c_s^2 \int d\mathbf{k} \frac{\rho_s^2 k_y^2}{\left(1+\rho_s^2 k_\perp^2\right)^2} \frac{\gamma_k}{\left(\gamma_k^2 + \left(\mathbf{q}\cdot\mathbf{v}_{gr}\right)^2\right)} k_x \frac{\partial N_k^0}{\partial k_x} \ , \tag{3.13}$$

$$\nu_{yy} = c_s^2 \int d\mathbf{k} \frac{\rho_s^2 k_x^2}{\left(1+\rho_s^2 k_\perp^2\right)^2} \frac{\gamma_k}{\left(\gamma_k^2 + \left(\mathbf{q}\cdot\mathbf{v}_{gr}\right)^2\right)} k_y \frac{\partial N_k^0}{\partial k_y} \ , \tag{3.14}$$

$$\nu_{xy} = c_s^2 \int d\mathbf{k} \frac{\rho_s^2}{\left(1+\rho_s^2 k_\perp^2\right)^2} \frac{\gamma_k}{\left(\gamma_k^2 + \left(\mathbf{q}\cdot\mathbf{v}_{gr}\right)^2\right)} \left(k_x^3 \frac{\partial N_k^0}{\partial k_x} + k_y^3 \frac{\partial N_k^0}{\partial k_y} \right) \ . \tag{3.15}$$

Inserting these expressions into the large scale vorticity equation yields

$$\begin{aligned} 0 = & \frac{\partial}{\partial t}\nabla_\perp^2 \phi^< + \frac{c}{B_0}(\hat{\mathbf{z}}\times\nabla\phi^<)\cdot\nabla\nabla_\perp^2\phi^< - v_A \frac{\partial}{\partial z}\nabla_\perp^2\psi^< - \frac{c}{B_0}(\hat{\mathbf{z}}\times\nabla\psi^<)\cdot\nabla\nabla_\perp^2\psi^< \\ & - \nu_{xx}\frac{\partial^4}{\partial x^4}\phi^< - \nu_{yy}\frac{\partial^4}{\partial y^4}\phi^< + \nu_{xy}\frac{\partial^2}{\partial x^2}\frac{\partial^2}{\partial y^2}\phi^< \ . \end{aligned} \tag{3.16}$$

Here the collisional viscosity has been dropped, since it is, in general, negligible compared to the turbulent viscosity. The stress terms (i.e. the last three terms on the right of the vorticity equation) have the form of an "anomalous" or "turbulent" viscosity. Note that for $k_x \frac{\partial N_k^0}{\partial k_x} < 0$ (i.e. $N_k^0 \sim |k|^{-\alpha}$, which is observed in all studies and predicted by all models of drift wave turbulence), the value of ν_{xx} (the dominant term for the tearing mode ordering $\partial/\partial x \gg \partial/\partial y$, which applies on large scales), will be *negative*. The presence of a negative viscosity on large scales due to nonlocal interactions with the background micro turbulence is a result familiar from considerations of drift wave-zonal flow systems. In simple terms, it is a consequence of the fact that in 2D (here the strong B_0 enforces quasi-two-dimensionality), fluid kinetic energy tends to inverse cascade (producing large scale growth), rather than forward cascade which, produces dissipation at large scales. However, our purpose in emphasizing the result here is that with one exception [66], there has been very little effort put into investigating the impact of a turbulent source on tearing mode physics. Also, ref. [66] did not self-consistently treat the back-reaction of large scales on small scales.

We estimate the magnitude of the anomalous viscosity, using a mixing length argument. For drift waves, we can approximate $e\phi^{>}/T_e \sim 1/\left(k_\perp L_n\right)$, where L_n is the perpendicular length scale over which the density varies. The magnitude of the turbulent viscosity can then be estimated to be $|\nu_{xx}| \approx \frac{c_s^2}{\gamma_k}\frac{1}{k_\perp^2 L_n^2} \approx \frac{c_s^2}{\gamma_k}\frac{\rho_s^2}{L_n^2}$. Finally, estimating the linear drift wave growth rate to be of the order of the drift wave linear frequency, $\gamma_k \approx v_e^* k_y \approx c_s/L_n$, yields an estimate of the turbulent viscosity as $|\nu_{xx}| \approx \frac{\rho_s}{L_n}\omega_{ci}\rho_s^2 \sim D_{GB}$. Here D_{GB} denotes the gyro-Bohm diffusivity, which is far in excess of the ion-ion collisional viscosity ρ_i^2/τ_{ii}, or the neoclassical viscosity. To estimate the relative sizes of the turbulence driven flux and linear inertia, we compare $\nu_{xx} \sim D_{GB}$ with $\gamma_T w_T^2$, where γ_T and w_T are the usual tearing mode growth rate and linear layer width, respectively. A simple calculation yields the conclusion that turbulent stresses will exceed inertia for $D_{GB} > \left(\Delta' a\right)^{7/5}\left(1/S\right)^{2/5}\left(L_s/am\right)^2$

$$D_{GB} > \left(\Delta' a\right)^{7/5}\left(1/S\right)^{2/5}\left(L_s/am\right)^2 \ . \tag{3.17}$$

Here $S = \tau_R/\tau_A$. Thus, in practical terms, the turbulent stresses *always* exceed inertia. Hence, the turbulent Reynolds stress is seen to be the *dominant microscopic* effect on the large scales.

Note that the above analysis has been done for the case of homogeneous turbulence. As discussed in Appendix C, this analysis needs to be extended to include the affect of magnetic shear on the mode structure of the micro turbulence. Also, as seen in Appendix C, the radial length scales of the micro turbulence depend strongly on their linear frequency. Thus, a linear fluid theory of ITG turbulence is briefly summarized in Appendix B.

As explained in Appendix C a strong nonlocal transfer of energy from the small scale micro turbulence to the large scale MHD modes is found for modes with q_y significantly smaller than q_x. This result is in qualitative agreement with Eq. (3.16) for modes with $\partial/\partial x \gg \partial/\partial y$, which is the relevant tearing mode ordering. However, due to the added complexity of the wave kinetic equation when magnetic shear is included, we will use

the simple expression given by Eq. (3.16), for the remainder of this analysis. However, inclusion of magnetic shear on the ambient micro turbulence would not qualitatively change our analysis.

3.3 linear theory of the tearing instability in the presence of a negative turbulent viscosity

The negative turbulent viscosity derived above has a magnitude far in excess of the collisional viscosity present within typical plasmas. Furthermore, for the universally observed case where $k_x \frac{\partial N_k^0}{\partial k_x} < 0$, the turbulent viscosity will be *negative*, such that energy is fed to the large scales. In considering the effect of a negative viscosity on tearing modes and magnetic islands, it is instructive to first consider the form of the RMHD equations near the resonant surface. Considering perturbations of the form $f(\vec{x},t) = f(x)\, e^{iq_y y + \gamma_q t}$, Eqs. (3.16) and (3.5) can be linearized to give

$$\gamma_q \frac{\partial^2 \phi^<}{\partial x^2} = i q_y v_A \frac{x}{L_s} J + \nu_{xx} \frac{\partial^4 \phi^<}{\partial x^4} \,, \tag{3.18}$$

$$\eta_c J = \gamma_q \psi^< - i q_y v_A \frac{x}{L_s} \phi^< \,, \tag{3.19}$$

where J is the parallel current, and L_s is the shear length, $x = r - r_{m,n}$, and $r_{m,n}$ is the m,n rational surface. Also, since we are considering modes strongly localized around the resonant surface, we have applied the ordering $\partial/\partial x \gg \partial/\partial y$. In the limit in which the inverse growth rate of the tearing mode is long in comparison to the skin time of the resistive layer ($\tau \sim \delta^2/\eta_c$ where δ is the width of the resistive layer), ψ can be assumed to be constant. Making use of this approximation and substituting Eq. (3.19) into Eq. (3.18) yields:

$$-\nu_{xx} \frac{\partial^4 \phi^<}{\partial x^4} + \gamma_q \frac{\partial^2 \phi^<}{\partial x^2} = \frac{q_y^2 v_A^2}{\eta_c} \frac{x^2}{L_s^2} \phi^< - \frac{q_y v_A}{\eta_c} \frac{x}{L_s} \psi_0 \,. \tag{3.20}$$

From Eq. (3.20) three regimes can be distinguished: First, in the limit of weak viscosity $|\nu_{xx}| \ll \gamma_T \delta^2$, the viscous term can be dropped and the system reduces to that treated by ref. [14]. In the opposite limit, for which $|\nu_{xx}| \gg \gamma_T \delta^2$, Eq. (3.20) reduces to the viscosity dominated limit, which was analyzed for the positive viscosity case by refs. [71, 72]. Finally, an electrostatic limit can also be distinguished ($\psi_0 = 0$). This regime describes an electrostatic vortex driven by an inverse cascade of energy to low but finite m, where resistive field line bending ultimately limits the width of the cellular flow. This regime can be easily seen to correspond to the purely MHD limit of the convective cell treated in the previous chapter.

Turning to the second regime (i.e. viscosity dominated), it is clear that a strong negative viscosity will have a strong impact on the linear dynamics of the reconnecting mode, i.e. the counterpart, for this study, of the traditional tearing mode. Integrating Eq. (3.19) across the resistive layer, and writing Eq. (3.20) in dimensionless units gives

$$0 = sgn\left(\nu_{xx}\right) \frac{\partial^4 \Phi}{\partial \sigma^4} + \frac{1}{\alpha} \frac{\partial^2 \Phi}{\partial \sigma^2} + \sigma \left(1 + \sigma \Phi\right) \ , \tag{3.21}$$

$$\Delta' = -\frac{i\omega_q}{\eta_c} x_\nu \int d\sigma \left(1 + \sigma \Phi\right) \ , \tag{3.22}$$

where $\Delta' = \left(\psi'\left(0^+\right) - \psi'\left(0^-\right)\right)/\psi_0$, $\alpha = i\left|\nu_{xx}\right|/\omega_q x_\nu^2$, $\sigma = x/x_\nu$, $\Phi = \frac{q_y v_A}{\omega_q} \frac{x_\nu}{L_s} \frac{\phi^<}{\psi_0^<}$, $x_\nu = \left(\eta_c \left|\nu_{xx}\right|\right)^{1/6} \left(\frac{L_s}{q_y v_A}\right)^{1/3}$. In the limit $\xi^2/\alpha \sim \left|\frac{x_\nu^2}{\nu_{xx}} \omega_q\right| < 1$ (i.e. the viscous dominated regime), the inertial term (second term on the right) is negligible, and Eq. (3.21) reduces to

$$0 = sgn\left(\nu_{xx}\right) \frac{\partial^4 \Phi}{\partial \sigma^4} + \sigma \left(1 + \sigma \Phi\right) \ . \tag{3.23}$$

In order to lower the order of the above equations, it will be convenient to introduce the

Fourier transform defined by

$$\Phi(\sigma) = \int_{-\infty}^{\infty} dq_x e^{-iq_x\sigma} \Phi(q_x) \ . \tag{3.24}$$

Here the integration is over the solutions within the singular layer. Eqs. (3.22) and (3.23) then become

$$\frac{d^2\Phi(q_x)}{dq_x^2} - sgn(\nu_{xx}) q_x^4 \Phi(q_x) = 2\pi i \frac{d}{dq_x}\delta(q_x) \ , \tag{3.25}$$

$$\Delta' = -\frac{i\omega_q}{\eta_c} x_\nu \left(2\pi\delta(q_x) + i\frac{d\Phi(q_x)}{dq_x} \mid_{q_x=0} \right) \ . \tag{3.26}$$

The solution of Eq. (3.25) is given by

$$\Phi(q_x) = i\pi sgn(q_x) \frac{\Phi_{hom}(|q_x|)}{\Phi_{hom}(0)} \ . \tag{3.27}$$

Substituting Eq. (3.27) into Eq. (3.26) gives the eigenvalue relation in terms of the homogeneous solution

$$\Delta' = -i\pi \frac{\omega_q}{\eta_c} x_\nu \frac{1}{\Phi_{hom}(0)} \frac{d\Phi_{hom}}{dq_x} \mid_{q_x=0} \ . \tag{3.28}$$

Before discussing the effect of a negative viscosity on the reconnecting mode, it is useful to briefly review the *positive viscosity* case $\left(k_x \frac{\partial N_k^0}{\partial k_x} > 0\right)$. Following [71] closely, the homogeneous solution of Eq. (3.25) is given by

$$\Phi_{hom}(q_x) = A\sqrt{q_x} I_{\frac{1}{6}}\left(\frac{q_x^3}{3}\right) + B\sqrt{q_x} K_{\frac{1}{6}}\left(\frac{q_x^3}{3}\right) \ , \tag{3.29}$$

where A and B are arbitrary constants, and I and K represent modified Bessel functions. Since the I solution diverges exponentially for large q_x, we retain only the K piece. Expanding Eq. (3.29) (with A set to zero), yields to first order

$$\Phi(q_x) \approx B\left(\pi \frac{6^{1/6}}{\Gamma\left(\frac{5}{6}\right)} - \frac{1}{6^{1/6}} \frac{\pi}{\Gamma\left(\frac{7}{6}\right)} q_x \right) \ . \tag{3.30}$$

After inserting Eq. (3.30) into Eq. (3.28), the dispersion relation obtained is

$$\begin{aligned}\gamma_q &= \frac{6^{1/3}}{\pi}\frac{\Gamma\left(\frac{7}{6}\right)}{\Gamma\left(\frac{5}{6}\right)}\frac{\eta_c^{5/6}}{\nu_{xx}^{1/6}}\left(\frac{q_y v_A}{L_s}\right)^{1/3}\Delta' \,, \\ &\approx .48\frac{\Gamma\left(\frac{7}{6}\right)}{\Gamma\left(\frac{5}{6}\right)}\frac{\eta_c^{5/6}}{\nu_{xx}^{1/6}}\left(\frac{q_y v_A}{L_s}\right)^{1/3}\Delta' \sim P^{-1/6}\tau_\eta^{-2/3}\tau_A^{-1/3} \,, \end{aligned} \tag{3.31}$$

which is identical to the expressions derived by [71, 72]. Note that the limit $\nu_{xx} \rightarrow 0$ is unimportant, since the result of Eq. (3.31) is valid only for the viscosity dominated regime. Furthermore, the growth rate can be seen to be (weakly) inversely proportional to ν_{xx}. Physically this can be understood as viscous damping reducing the strength of the fluid eddies driven by the linear $\mathbf{J} \times \mathbf{B}$ force.

Now, we consider the more subtle case of a negative viscosity $\left(k_x \frac{\partial N_k^0}{\partial k_x} < 0\right)$. It is useful to first consider the form of Eq. (3.23) in real space, i.e.

$$0 = -\frac{\partial^4 \Phi}{\partial \sigma^4} + \sigma\left(1 + \sigma\Phi\right) \,. \tag{3.32}$$

Note that the effect of changing the sign of the fourth order derivative is to introduce solutions that oscillate rapidly, which we are unable to match to the second order exterior solution. It is useful at this point to construct an eikonal formulation of the solution of Eq. (3.32), for large σ. We proceed by considering solutions of the form $\Phi\left(\sigma\right) = f\left(\sigma\right)e^{i\psi(\sigma)} - 1/\sigma$, where $f\left(\sigma\right)$ corresponds to a slowly varying amplitude, and $\psi\left(\sigma\right)$ corresponds to a rapidly varying phase. Eq. (3.32) then becomes:

$$0 = -\frac{d^4}{d\sigma^4}\left(fe^{i\psi} - \frac{1}{\sigma}\right) + \sigma\left(1 + \sigma\left(fe^{i\psi} - \frac{1}{\sigma}\right)\right) \,. \tag{3.33}$$

Only solutions which die off slower than $1/\sigma$ are relevant for large σ. This allows us to drop the fourth derivative of $1/\sigma$. Taking derivatives, and separating the real and imaginary

parts, gives to lowest order:

$$0 = -f\left(\psi'\right)^4 + \sigma^2 f \ , \tag{3.34}$$

$$0 = 4f'\left(\psi'\right)^3 + 6f\left(\psi'\right)^2\psi'' \ , \tag{3.35}$$

where f' and ψ' denote derivatives with respect to σ. Eqs. (3.34) and (3.35) can then easily be solved, yielding:

$$\begin{aligned}\Phi\left(\sigma\right) &= sgn\left(\sigma\right)\frac{D}{\left|\sigma\right|^{3/4}}exp\left(i\frac{2}{3}\left|\sigma\right|^{3/2} + i\phi_D\right) \\ &+ sgn\left(\sigma\right)\frac{E}{\left|\sigma\right|^{3/4}}exp\left(-i\frac{2}{3}\left|\sigma\right|^{3/2} + i\phi_E\right) - \frac{1}{\sigma} \ .\end{aligned} \tag{3.36}$$

The oscillatory terms in this expression result from balancing the fourth order viscous term, against $\sigma^2\Phi$, the linear $\mathbf{J}\times\mathbf{B}$ force. It follows that the $\gamma_q\psi^<$ term plays no role in determining the structure of the oscillations. Thus, the general form of this solution can be understood as a consequence of coupling the *electrostatic vortex mode to the low-m tearing mode, which connects to the ideal MHD exterior*. From this expression we note that the oscillations die off more slowly than the residual tearing mode term. Hence, *unless some other mechanism damps the oscillations, it is not possible to match the oscillatory solutions to the exterior solution*. In Fourier space, this can be understood by considering the homogeneous solution of Eq. (3.25), which is

$$\Phi_{hom}\left(q_x\right) = A\sqrt{q_x}J_{\frac{1}{6}}\left(\frac{q_x^3}{3}\right) + B\sqrt{q_x}Y_{\frac{1}{6}}\left(\frac{q_x^3}{3}\right) \ . \tag{3.37}$$

Two observations concerning this equation are possible. First, upon Fourier transforming Eq. (3.37), the solutions in real space can be seen to undergo oscillations which are ninety degrees out of phase with one another. Thus, fixing the ratio of the amplitudes A/B is equivalent to setting the phase of the oscillations. Second, since both of these solutions converge for $q_x \to \infty$, neither solution can be dropped. These considerations leave us with

an undetermined constant A/B in the eigenvalue relation, which can be written as

$$\Delta' = -i\frac{\pi}{2}\frac{1}{6^{1/6}}\frac{\Gamma\left(\frac{5}{6}\right)}{\Gamma\left(\frac{7}{6}\right)}\frac{\omega_q}{\eta_c}x_\nu\left(\frac{3^{1/3}}{2^{1/6}}+\frac{1}{6^{1/6}}\frac{A}{B}\right) . \tag{3.38}$$

From this expression it is clear that another boundary condition is needed in order to specify A/B in the dispersion relation, Eq. (3.38). This extra boundary condition corresponds to setting the phase of the oscillations of the solution. Thus, the boundary condition *cannot* be determined from the solution in the exterior region alone. It is plausible from physical considerations then to impose outgoing wave energy boundary conditions [73]. Thus, we see that the effect of the negative viscosity is to set up normal mode solutions which carry energy from the layer, near the $\mathbf{k}\cdot\mathbf{B}_0 = 0$ surface, toward the exterior region where the the propagating waves are absorbed by ion Landau damping or some other dissipative mechanism. Like other familiar cases of outgoing wave boundary conditions, the damping does not appear *explicitly* in the theory, as outgoing wave boundary conditions *tacitly presume a sink* for the outgoing wave.

As shown in Appendix A, this outgoing wave energy condition implies that A/B is pure imaginary, so the dispersion relation takes the form

$$\gamma_q \sim \frac{\eta_c}{x_\nu}\Delta' \sim \frac{\eta_c^{5/6}}{|\nu_{xx}|^{1/6}}\left(\frac{q_y v_A}{L_s}\right)^{1/3}\Delta' , \tag{3.39}$$

$$Re\left(\omega_q\right) \sim \frac{\eta_c^{5/6}}{|\nu_{xx}|^{1/6}}\left(\frac{q_y v_A}{L_s}\right)^{1/3}\Delta' , \tag{3.40}$$

where Δ' is purely real. Note that here the growth rate and frequency have the same scaling. This is primarily a consequence of neglecting the electron pressure gradient and other "two fluid" and kinetic effects. Including the electron and ion diamagnetic drift into the mean field equations yields a dispersion relation of the form $\gamma_\nu^6/\left(1+ic_1\right)^6 \sim -\left(\omega_q-\omega_e^*\right)^5\left(\omega_q-\omega_i^*\right)$, where c_1 is a number of order unity set by matching to the eikonal

solution. In the limit $\gamma_\nu \ll \omega_e^*$, which is relevant for drift tearing modes, the real frequency is given approximately by $Re\,(\omega_q) \approx \omega_e^*$.

3.4 Outlook for nonlinear island evolution

The classical Rutherford regime [15] corresponds to a filamented 'near equilibrium' state, which evolves slowly and self-similarly in time. Consistent with self-similarity, the magnetic island width grows with a power of time (i.e. proportional to t), as opposed to exponentially in time, as in the linear phase. It is interesting to note that in the presence of turbulence at the 'typical', Gyro-Bohm level, the negative viscosity term dominates inertia, *even in the linear phase*. However, it is by no means clear that the negative viscosity is a-priori negligible in the Rutherford phase. Furthermore, since the Rutherford phase is one of slow evolution, keeping finite flow excitation by negative viscosity compels us to also retain *damping* of the low m flows.

While a complete discussion of the nonlinear island evolution is beyond the scope of this paper, we can, however, sketch elements of the calculation here. First, as mentioned in the proceeding paragraph, it is important to take note of the conceptual distinction between the classical Rutherford state and the nonlinear evolution of the reconnecting mode discussed here. In the classic Rutherford calculation, the balance is first plus third order $\mathbf{J} \times \mathbf{B}$ force vs. inertia, so

$$(\mathbf{B} \cdot \nabla J)^{(1)} + (\mathbf{B} \cdot \nabla J)^{(3)} = \frac{d}{dt} \nabla_\perp^2 \phi \,. \tag{3.41}$$

For island width exceeding tearing layer width (i.e. $w_I > x_T$), $(\mathbf{B} \cdot \nabla J)^{(3)} > \frac{d}{dt} \nabla_\perp^2 \phi$, so the balance simplifies to

$$(\mathbf{B} \cdot \nabla J)^{(1)} + (\mathbf{B} \cdot \nabla J)^{(3)} \approx 0 \,, \tag{3.42}$$

or

$$\mathbf{B}\cdot\nabla J = 0\,, \tag{3.43}$$

so $J = J(\psi)$ can be inserted into Ohms Law, yielding a differential equation for the evolution of the island width. Here, for finite island size, the balance becomes

$$(\mathbf{B}\cdot\nabla J)^{(1)} + (\mathbf{B}\cdot\nabla J)^{(3)} = \left(\frac{d}{dt}\nabla_\perp^2\phi\right)_R - \frac{\partial^2}{\partial x^2}\left(\int d\vec{k}\frac{k_x k_y}{\left(1+\rho_s^2 k_\perp^2\right)^2}\delta N_k(x,t)\right) + \gamma\left[\nabla^2\phi\right]\,. \tag{3.44}$$

Here $\left(\frac{d}{dt}\nabla_\perp^2\phi\right)_R$ refers to the inertia of the reconnecting mode, the second term on the RHS refers to the modulation of the turbulent vorticity transport (i.e. Reynolds stress) by the island and $\gamma\left[\nabla^2\phi\right]$ refers to the neoclassical flow damping [74, 75], which may need to account for island-induced toroidal symmetry breaking. For typical background turbulence levels, reconnecting mode inertia is already subdominant, so

$$\mathbf{B}\cdot\nabla J = -\frac{\partial^2}{\partial x^2}\left(\int d\vec{k}\frac{k_x k_y}{\left(1+\rho_s^2 k_\perp^2\right)^2}\delta N_k(x,t)\right) + \gamma\left[\nabla^2\phi\right]\,. \tag{3.45}$$

Thus, the $\mathbf{J}\times\mathbf{B}$ force equals the imbalance between the flow drive induced by modulation of the Reynolds stress and the flow damping. Both of the latter two depend upon island size. Note that in the *complete absence of an island*, Eq. (3.45) reduces to the marginality condition for the modulation stability of a low-m vortex or zonal flow (for $m = 0$). Similarly, neglecting *both* turbulence modulation and flow damping recovers "classical Rutherford", namely $\mathbf{B}\cdot\nabla J = 0$. Thus, the structure outlined in Eq. (3.45) recovers both of the requisite limiting cases. It follows that

$$J = J(\psi) + (\mathbf{B}\cdot\nabla)^{-1}\left\{-\frac{\partial^2}{\partial x^2}\left(\int d\mathbf{k}\frac{k_x k_y}{\left(1+\rho_s^2 k_\perp^2\right)^2}\delta N_k(\mathbf{x},t)\right) + \gamma\left[\nabla^2\phi\right]\right\}\,. \tag{3.46}$$

so that the island current is the sum of a Δ'-driven contribution (associated with the homogeneous solution $J(\psi)$) and a contribution due to the *competition* between flow generation and damping. Note that both $\delta N(\mathbf{k}, x, t)$ and γ in Eq. (3.46) must be computed as a function of the island width w_I, and will depend nonlinearly upon it. Note also that, as mentioned after Eq. (3.46), retaining both $\partial N_k^0/\partial x$ and $\partial N_k^0/\partial \mathbf{k}$ contributions to δN_k guarantees turbulence driven contributions to the current J that are *both* real and imaginary. Further discussion of the finite island calculation is beyond the scope of this paper, and will be addressed in a future publication.

We emphasize that a self-consistent description of the drift wave turbulence with the magnetic island is essential. That is, as the magnetic island evolves, the large heat conductivity along magnetic field lines will flatten the temperature profile, killing the free energy source of the turbulence. Thus, the external source may be turned off for sufficiently large islands. However, turbulence driven by the temperature gradient outside the island, presumably steepened, may diffuse inward due to local interactions (i.e. collisions between quasi particles). This "spreading" of the turbulence may allow for the micro turbulence to be present in linearly stable regions.

3.5 Conclusions and Discussion

In this paper, we have explored a minimal self-consistent model of the multi-scale interaction of a tearing mode with ambient, electrostatic drift wave turbulence. The principal results of this paper are:

a.) its self-consistent formulation in terms of Reynolds stress effects of small scales (drift waves) upon large scales (tearing mode), along with the back-reaction of large scale straining and shearing flows on small scale turbulence. Here, the multi-scale interaction is described by nonlinear modulation of the drift wave intensity field by

the tearing mode flows.

b.) the identification of the *negative* turbulent viscosity as the principal effect of electrostatic drift wave turbulence on a simple, low-m tearing mode.

c.) the calculation of the growth rate of a 'reconnecting mode' (with $\Delta' > 0$), which couples to an ideal MHD exterior. This is the analogue of the familiar tearing mode, but with negative viscosity providing the coupling to background turbulence. Moreover, for typical "mixing length level" turbulence amplitudes, inertia is negligible, even in the *linear growth phase*. The reconnecting mode has growth rate $\gamma_q \sim \frac{\eta_c^{5/6}}{|\nu_{xx}|^{1/6}} \left(\frac{q_y v_A}{L_s}\right)^{1/3} \Delta'$ and layer width $\Delta_q = \left(\eta_c |\nu_{xx}|\right)^{1/6} \left(\frac{L_s}{q_y v_A}\right)^{1/3}$. Outgoing wave boundary conditions must be imposed to match the inner layer to the MHD exterior.

In addition to presenting the specific results enumerated above, we take this opportunity to discuss two broader implications of this work. First (as discussed in Sec. 4), the theory of finite size magnetic islands must be extended to encompass excitation of island flows by turbulence modulation and the damping of flows due to breaking of axisymmetry. Any imbalance between these two effects will produce a current which in turn affects island size. Second, in reference to the finite size island case, the reader should keep in mind that the turbulence intensity profile ($\sim N\left(\mathbf{k}, x, t\right)$) is *not static*. In particular, flattening of $\nabla_{\mathbf{x}} N$ within an island will likely steepen $\nabla_x N$ in adjacent regions, which results in either a 'back-wash' of turbulence spreading or the possible formation of a transport barrier, since steep $\nabla_x N$ in turn implies enhanced flow and flow shear drive via Reynolds stress [76, 24]. Clearly, some sort of bifurcation condition delimits the boundary between these two very different 'basin's of attraction' for the system state. Significant further work is required to elucidate this transition.

We also again emphasize here that this model is indeed a 'minimalist' 'toy' model, which omits many detailed effects relevant to NTM evolution in tokamaks. These include, but certainly are not limited to the effects of toroidicity and bootstrap current drive, the effects of turbulent heat transport on island evolution, neoclassical modifications of the polarization drift, island-induced modifications of the density, temperature and turbulence intensity profiles, incoherent emission from turbulence, spreading of turbulence from adjacent regimes into the island, etc, etc. Indeed, the list is endless! Many years of interesting research will be necessary to resolve these and the other interesting questions pertinent to the theory of multi-scale interaction of turbulence with MHD.

Appendix A: Outgoing Wave Energy Boundary Conditions

In order to calculate the ratio A/B in Eq. (3.38), it is necessary to match our exact solution Eq. (3.37) to the outgoing piece of the eikonal solution. The fluctuating piece of Eq. (3.36) can be rewritten

$$\tilde{\Phi}\left(\sigma\right) = sgn\left(\sigma\right)\frac{D}{\left|\sigma\right|^{3/4}}e^{ik_x|x|+i\phi_D} + sgn\left(\sigma\right)\frac{E}{\left|\sigma\right|^{3/4}}e^{-ik_x|x|+i\phi_E}\ , \tag{3.A1}$$

where k_x is defined as $k_x = (2/3)\sqrt{|x|}/x_\nu^{3/2}$. k_x can be related to the frequency through the dispersion relation $Re\left(\omega_q\right) \sim \left(\eta_c\Delta'\right)/x_\nu$, which yields $k_x = (2/3)\sqrt{|x|}\omega_q^{3/2}/\left(\eta_c\Delta'\right)^{3/2}$. Thus, the sign of v_{gr} can be determined from $v_{gr}^{-1} = \partial k_x/\partial\omega_q$. Applying the outgoing wave energy boundary condition then gives (for large values of x i.e. $x \gg x_\nu$)

$$\tilde{\Phi}\left(x\right) = sgn\left(x\right)\frac{D}{\left|\sigma\right|^{3/4}}e^{ik_x|x|+i\phi_D}\ . \tag{3.A2}$$

We are now interested in matching the exact solution to the eikonal solution, in order to

determine the ratio A/B. The exact solution in Fourier space can be written as

$$\Phi\left(q_x\right) = -i\frac{\pi^2}{\Gamma\left(1/6\right)}\frac{1}{6^{1/6}}\text{sgn}\left(q_x\right)\left\{\frac{A}{B}\sqrt{|q_x|}J_{\frac{1}{6}}\left(\frac{|q_x|^3}{3}\right) + \sqrt{|q_x|}Y_{\frac{1}{6}}\left(\frac{|q_x|^3}{3}\right)\right\} \ . \quad \text{(3.A3)}$$

This solution can be rewritten in real space as

$$\begin{aligned}\frac{A}{B}\frac{1}{2\pi}\int dq_x e^{iq_x\sigma}\text{sgn}\left(q_x\right)\sqrt{|q_x|}J_{\frac{1}{6}}\left(\frac{|q_x|^3}{3}\right) &= \frac{A}{B}\frac{3^{1/6}}{4}\frac{\Gamma\left(2/3\right)}{\Gamma\left(1/6\right)\Gamma\left(7/6\right)}\sigma\ {}_0F_3\left(\frac{2}{3},\frac{5}{6},\frac{7}{6};\frac{\sigma^6}{1296}\right) \\ &- \frac{A}{B}\frac{1}{9}\frac{\pi}{3^{5/6}}\left(\frac{2}{3}\right)^{1/3}\frac{\Gamma\left(-4/3\right)}{\Gamma\left(1/6\right)\Gamma\left(7/6\right)}\sigma^3 \\ &\cdot\ {}_0F_3\left(\frac{7}{6},\frac{4}{3},\frac{3}{2};\frac{\sigma^6}{1296}\right) \ , \end{aligned} \quad \text{(3.A4)}$$

and:

$$\begin{aligned}\frac{1}{2\pi}\int dq_x e^{iq_x\sigma}\text{sgn}\left(q_x\right)\sqrt{|q_x|}Y_{\frac{1}{6}}\left(\frac{|q_x|^3}{3}\right) &= -i\frac{3^{2/3}}{12}\sigma\Gamma\left(2/3\right)\ {}_0F_3\left(\frac{2}{3},\frac{5}{6},\frac{7}{6};\frac{\sigma^6}{1296}\right) \\ &+ \frac{6^{1/3}}{180}\frac{\Gamma\left(-1/3\right)\Gamma\left(11/6\right)}{\Gamma\left(7/6\right)}\sigma^3\ {}_0F_3\left(\frac{7}{6},\frac{4}{3},\frac{3}{2};\frac{\sigma^6}{1296}\right) \\ &+ i\frac{\sigma^5}{120}\ {}_1F_4\left(1;\frac{4}{3},\frac{3}{2},\frac{5}{3},\frac{11}{6};\frac{\sigma^6}{1296}\right) \ , \end{aligned} \quad \text{(3.A5)}$$

where ${}_pF_q$ is a generalized hypergeometric function. Matching Eq. (3.A3) to Eq. (3.A2), with the use of Eqs. (3.A4) and (3.A5), leads to $A/B = i$. A plot comparing the eikonal solutions to the exact solutions is given in Fig. (3.5).

Appendix B: Linear Theory of ITG Turbulence for a Cylindrical RFP

In the above analysis we considered an absolutely minimal model of the background micro turbulence in order to illuminate a number of the salient features of the tearing mode-

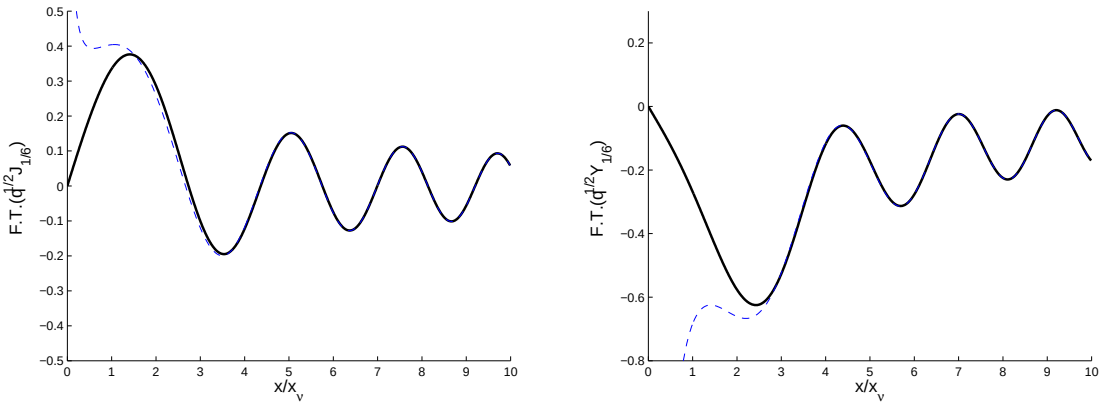

Figure 3.5: Plots of eikonal solutions versus exact solution. The solid lines correspond to the exact solutions, whereas the broken lines correspond to the eikonal solutions.

drift wave interaction. Here, we are also interested in introducing a somewhat more sophisticated model of the ambient micro turbulence by including the impact of magnetic shear on the linear mode structure. As will be seen below, when magnetic shear is added to the system, the extent of the radial localization, and thus the degree of anisotropy, all affect the linear dynamics. Consider a set of fluid equations similar to those given in Lee-Diamond [77], except with the addition of a curvature term, which is important for the RFP. Thus:

$$\begin{aligned} 0 &= \frac{\partial}{\partial t}\left(1-\nabla_\perp^2\right)\phi + v_e^*\left(1-2\frac{L_n}{R}+\kappa\nabla_\perp^2\right)\frac{\partial}{\partial y}\phi - \frac{2}{R}\frac{\partial}{\partial y}P + \nabla_\parallel v_\parallel \\ &- (\hat{\mathbf{z}}\times\nabla\phi)\cdot\nabla\nabla_\perp^2\phi \end{aligned} \tag{3.B1}$$

$$0 = \frac{\partial}{\partial t}v_\parallel + \nabla_\parallel(\phi+P) + (\hat{\mathbf{z}}\times\nabla\phi)\cdot\nabla v_\parallel \tag{3.B2}$$

$$0 = \frac{\partial}{\partial t}P + (\hat{\mathbf{z}}\times\nabla\phi)\cdot\nabla P + v^*\kappa\frac{\partial}{\partial y}\phi + \frac{\Gamma}{\tau}\nabla_\parallel v_\parallel \tag{3.B3}$$

$$v_e^* \equiv -\frac{cT_e}{eB}\frac{d(\ln n_0)}{dx}, \quad \tau \equiv \frac{T_e}{T_i}, \quad \eta_i \equiv \frac{d(\ln T_i)/dx}{d(\ln n_0)/dx}, \quad \kappa \equiv \left(\frac{1+\eta_i}{\tau}\right)$$

$$\phi \equiv \frac{e\Phi}{T_e}, \quad v_z \equiv \frac{v_{zi}}{c_s}, \quad P \equiv \frac{P_i}{\langle P_{i0} \rangle}\frac{T_i}{T_e}$$

The space and time scales are in units of ρ_s and ω_{ci}^{-1} respectively, R is the curvature of the mean magnetic field, L_n is the the density gradient, and Γ is the ratio of specific heats. Note that the nonlinearity within the equation for the electrostatic potential is the same as in the Hasegawa-Mima equation. However, unlike the previous model, the parallel dynamics are included, and the vorticity equation is coupled to the pressure via a curvature term. Both the inclusion of parallel dynamics as well as magnetic curvature provide linear drives.

Assuming a radially inhomogeneous sheared slab geometry, the radial eigenmode equation is given by:

$$\begin{aligned} 0 = \partial_{xx}\phi_k(x) + \left(1 - \frac{2}{R}\frac{k_y}{\omega_{k_y}}\frac{\Gamma}{\tau}\right)\left(\frac{k_y}{\omega_{k_y}}\right)^2\left(\frac{x}{L_s}\right)^2\phi_k(x) - k_y^2\phi_k(x) \\ + \left(\frac{\omega_{k_y}}{v_e^* k_y} + \kappa\right)^{-1}\left(1 - 2\frac{L_n}{R} - \frac{\omega_{k_y}}{v_e^* k_y}\right)\phi_k(x) - \left(\frac{\omega_{k_y}}{v_e^* k_y} + \kappa\right)^{-1}\frac{2}{R}\frac{k_y}{\omega_{k_y}}\kappa\phi_k(x) \end{aligned} \quad \text{(3.B4)}$$

where x is the radial distance from the resonant surface defined by $\mathbf{k} \cdot \mathbf{B} = 0$. Choosing boundary conditions such that the growing mode is localized, gives solutions of the form

$$\phi_k(x) \sim e^{-\frac{i}{2}\mu_k x^2}, \quad \mu_k = -\frac{1}{L_s}\frac{|k_y|}{|\omega_{k_y}|^2}\left(\omega_{k_y} - i\gamma_{k_y}\right)\left(1 - \frac{2}{R}\frac{k_y}{\omega_{k_y}}\frac{\Gamma}{\tau}\right)^{\frac{1}{2}} \quad \text{(3.B5)}$$

where, for the RFP, the shear is negative. The parameter μ_k introduces two length scales:

a.) $\mathrm{Re}\,(\mu_k) = 1/x_t^2$ which sets the length scale over which the mode varies in the radial direction.

b.) $\mathrm{Im}\,(\mu_k) = 1/x_i^2$ which gives the envelop width of the mode.

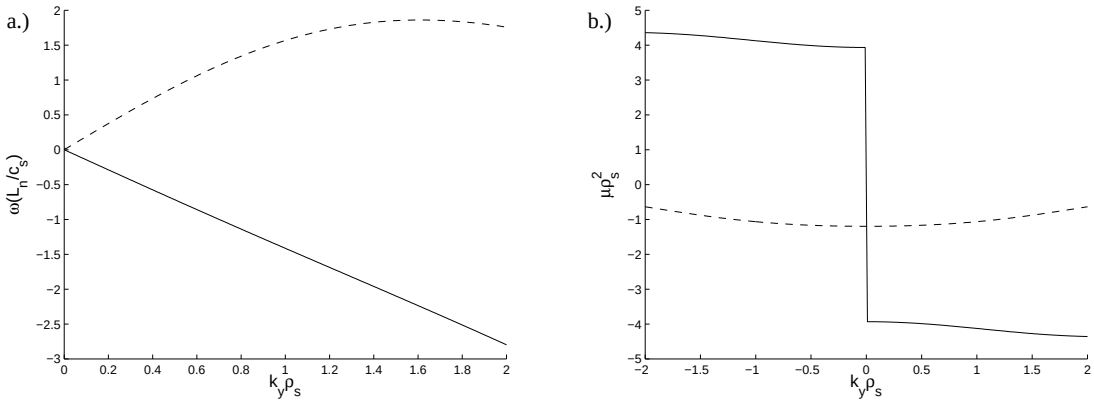

Figure 3.6: Figure (a.) shows a plot of the linear growth rate and frequency. The solid line denotes the real part of $\omega_q(L_n/c_s)/5$ and the broken line denotes and growth rate $\gamma_q(L_n/c_s)$. Figure (b.) displays a plot of the real and imaginary part of μ_k. The solid line denotes the real part of μ and broken line corresponds to the imaginary part of μ plotted as a function of k_y

Substituting Eq. (3.B5) into Eq. (3.B4), gives the linear dispersion relation

$$0 = \left(1+k_y^2\right)\omega_{k_y}^2 + v_e^* k_y \left[\frac{i}{|L_s|}\frac{1}{v_e^*} sign\left(k_y\right)\left(1-\frac{2}{R}\frac{k_y}{\omega_{k_y}}\frac{\Gamma}{\tau}\right)^{\frac{1}{2}} + k_y^2\kappa + 2\frac{L_n}{R} - 1\right]\omega_{k_y}$$
$$+ \frac{2}{R}\kappa k_y^2 v_e^* + \frac{i}{|L_s|}\kappa sign\left(k_y\right)k_y^2 v_e^*\left(1-\frac{2}{R}\frac{k_y}{\omega_{k_y}}\frac{\Gamma}{\tau}\right)^{\frac{1}{2}} \quad \text{(3.B6)}$$

From the dispersion relation Eq. (3.B6), μ_k can be computed . For typical RFX parameters $\frac{T_e}{T_i} = 2$, $\eta_i = 15$, $\frac{a}{L_s} = q'/\epsilon = -1/8$, $\frac{R}{a} = 1.6$, $\Gamma = 5/3$, $\epsilon = a/R_m$, where a and R_m are the minor and major radius' respectively, plots of the linear frequency and growth rate are shown in Fig. (3.6).

Appendix C: Wave Kinetic Equation for ITG Turbulence in Sheared Magnetic Field

For a self-consistent description of the drift wave-tearing mode system, it is necessary to consider the effect of magnetic shear on the micro-turbulence. Indeed, for finite island

size, one should even compute the linear stability of high-n turbulence taking the magnetic geometry of the island into account. Radial magnetic shear will ultimately lead to modes being localized near resonant surfaces. Thus a radial length scale, which is in general different from that of the poloidal length scale, will emerge.

We begin by considering a set of fluid equations, given in Appendix B, which model ITG turbulence in the presence of a sheared magnetic field. For the following analysis it will be necessary to approximate the radial structure of ITG modes for the system. As a lowest order approximation, we will use the linear eigenmodes (derived in Appendix B). While this approximation is crude, it will provide some insight into the effect of anisotropic radially localized turbulence on the anomalous viscosity.

The large scale RMHD equations are coupled to the micro turbulence only through $N_k \sim \langle \phi^> \phi^> \rangle$. Thus, it is sufficient to derive a single WKE describing the evolution of $\langle \phi^> \phi^> \rangle$. However, considering Eqs. (3.B1-3.B3), it's clear that $\langle \phi^> \phi^> \rangle$ will be coupled to the cross terms $\langle \phi^> P^> \rangle$ and $\langle \phi^> V_z^> \rangle$, which will, in turn, couple to $\langle P^> P^> \rangle$, $\langle V_z^> V_z^> \rangle$, and $\langle P^> V_z^> \rangle$, thus defining a set of six coupled nonlinear WKE's. For simplicity, we will drop the cross terms appearing in the equation for $\langle \phi^> \phi^> \rangle$, leaving us with only a single WKE. Note that while this approximation is crude, the qualitative structure of the anomalous viscosity introduced into the RMHD equations will be insensitive to the details of the WKE, but vary sensitively with the various length scales characteristic of the turbulence.

The derivation of the WKE for ITG turbulence follows ref. [78] closely, and is outlined below. The primary difference is that the linear dynamics are determined via ITG equations, and that the result is generalized for the case of strong magnetic shear (relevant for a RFP). We begin by considering solutions of the form

$$\left(\phi^> \left(\vec{x},t\right), P^> \left(\vec{x},t\right), V^> \left(\vec{x},t\right)\right) = \int d^2k \left(\phi_k^> \left(x,t\right), P_k^> \left(x,t\right), V_k^> \left(x,t\right)\right) e^{iky+ik_z z} \,, \tag{3.C1}$$

where k_y has been written as k. Thus Eq. (3.B1) will now take the form

$$0 = \partial_t \left(1 - \partial_{xx} + k^2\right) \phi_k^> (x,t) + iV_e^* k \left(1 - 2\frac{L_n}{R} + \kappa \left(\partial_{xx} - k^2\right)\right) \phi_k^> (x,t)$$
$$- \frac{2i}{R} k P_k^> (x,t) + ik_z V_k^> (x,t) - i \sum_{k=k_1+k_2} k_1 \phi_{k_1}^< (x,t) \left(1 - \partial_{xx} + k_2^2\right) \partial_x \phi_{k_2}^> (x,t)$$
$$+ i \sum_{k=k_1+k_2} k_2 \partial_x \phi_{k_1}^< (x,t) \left(1 - \partial_{xx} + k_2^2\right) \phi_{k_2}^> (x,t) \ . \tag{3.C2}$$

Here the summations are short hand notation for integrations, i.e. $\sum_{k=p+q} \rightarrow \int dpdq\delta\left(-k+p+q\right)$. It is now useful to separate the time dependence of the small scale fields into a slowly varying amplitude (resulting from the modulations of the large scale mean fields), and a rapidly varying piece, so that:

$$\left(\phi_k^> (x,t), P_k^> (x,t), V_k^> (x,t)\right)$$
$$\rightarrow \left(a_k (t) e^{-i\omega_k t} \phi_k^> (x), b_k (t) e^{-i\omega_k t} P_k^> (x), c_k (t) e^{-i\omega_k t} V_k^> (x)\right) \ , \tag{3.C3}$$

where $\phi_k^> (x)$ is the linear eigenmode, and x is defined as the distance from the $r_{m,n}$ resonant surface ($k_1 = m_1/r$ and $k_{1z} = n_1/R$). We can now define a Wigner function as $I_k (y,t) = \int dp e^{ipy} \langle a_{k+p} (t) e^{-i\omega_{k+p} t} a_{-k} (t) e^{-i\omega_{-k} t} \rangle$. We choose the normalization $\int dx \phi_k^> (x) \phi_{-k}^> (x) = 1$ for the radial eigenmodes, where $\mu_{-k}^{(r)} = -\mu_k^{(r)}$ and $\mu_{-k}^{(i)} = \mu_k^{(i)}$. An equation describing the evolution of the intensity of the drift wave turbulence can be derived by multiplying Eq. (3.C2) (with $k \rightarrow -k$) by $\phi_{k'}^> (x,t)$, and adding the same equation with -$k \leftrightarrow k'$. Setting $k' = k+p$, where p corresponds to the wave number of the large

scales, and dropping the cross terms gives:

$$\begin{aligned}
&\phi^{>}_{-k}(x)\,\phi^{>}_{k+p}(x)\left(\frac{\partial}{\partial t}+i\left(\omega_{-k}+\omega_{k+p}\right)\right)\left(a_{-k}(t)\,e^{-i\omega_{-k}t}a_{k+p}(t)\,e^{-i\omega_{k+p}t}\right)\\
&=i\sum_{-k=k_1+k_2}a_{k+p}e^{-i\omega_{k+p}t}a_{k_2}e^{-i\omega_{k_2}t}k_1\phi^{>}_{k+p}(x)\left(1-\partial_{xx}+k_2^2\right)\partial_x\phi^{>}_{k_2}(x)\,\phi^{<}_{k_1}(x,t)\\
&-i\sum_{-k=k_1+k_2}a_{k+p}e^{-i\omega_{k+p}t}a_{k_2}e^{-i\omega_{k_2}t}k_2\phi^{>}_{k+p}(x)\left(1-\partial_{xx}+k_2^2\right)\phi^{>}_{k_2}(x)\,\partial_x\phi^{<}_{k_1}(x,t)\\
&-i\sum_{k+p=k_1+k_2}a_{-k}e^{-i\omega_{-k}t}a_{k_2}e^{-i\omega_{k_2}t}k_1\phi^{>}_{-k}(x)\left(1-\partial_{xx}+k_2^2\right)\partial_x\phi^{>}_{k_2}(x)\,\phi^{<}_{k_1}(x,t)\\
&+i\sum_{k+p=k_1+k_2}a_{-k}e^{-i\omega_{-k}t}a_{k_2}e^{-i\omega_{k_2}t}k_2\phi^{>}_{-k}(x)\left(1-\partial_{xx}+k_2^2\right)\phi^{>}_{k_2}(x)\,\partial_x\phi^{<}_{k_1}(x,t)\ .
\end{aligned}$$

Here ω_k includes the real frequency and growth rate of the linear mode. In order to simplify the notation we define $\tilde{a}_k(t)=a_k(t)\,e^{-i\omega_k t}$. Expanding the linear piece in the ratio $p/k\ll 1$, averaging over the fast scales, integrating across the distribution of resonant surfaces, applying the operator $\int dpe^{ipy}$, and using the normalization condition gives the evolution equation for I_k which is:

$$\left(\frac{\partial}{\partial t}+v_{gr}\frac{\partial}{\partial y}+\gamma_k\right)I_k=S_1+S_2+S_3+S_4 \tag{3.C4}$$

$$S_1=i\int dpe^{ipy}\int dx\sum_{-k=k_1+k_2}\langle\tilde{a}_{k+p}\tilde{a}_{k_2}\rangle\,k_1\phi^{>}_{k+p}(x)\left(1-\partial_{xx}+k_2^2\right)\partial_x\phi^{>}_{k_2}(x)\,\phi^{<}_{k_1}(x)$$

$$S_2=-i\int dpe^{ipy}\int dx\sum_{-k=k_1+k_2}\langle\tilde{a}_{k+p}\tilde{a}_{k_2}\rangle\,k_2\phi^{>}_{k+p}(x)\left(1-\partial_{xx}+k_2^2\right)\phi^{>}_{k_2}(x)\,\partial_x\phi^{<}_{k_1}(x)$$

$$S_3=-i\int dpe^{ipy}\int dx\sum_{k+p=k_1+k_2}\langle\tilde{a}_{-k}\tilde{a}_{k_2}\rangle\,k_1\phi^{>}_{-k}(x)\left(1-\partial_{xx}+k_2^2\right)\partial_x\phi^{>}_{k_2}(x)\,\phi^{<}_{k_1}(x)$$

$$S_4=i\int dpe^{ipy}\int dx\sum_{k+p=k_1+k_2}\langle\tilde{a}_{-k}\tilde{a}_{k_2}\rangle\,k_2\phi^{>}_{-k}(x)\left(1-\partial_{xx}+k_2^2\right)\phi^{>}_{k_2}(x)\,\partial_x\phi^{<}_{k_1}(x)$$

where γ_k includes both the linear growth rate of the ITG mode, as well as the shear damping piece. In order to evaluate the nonlinear terms it is useful to inverse Fourier transform the

ensemble averaged terms [13] i.e. for S_1

$$\begin{aligned}\left\langle \tilde{a}_{k+p}\left(t\right)\tilde{a}_{-k+k_1}\left(t\right)\right\rangle &= \left\langle \tilde{a}_{(-k+k_1)+(p-k_1)}\left(t\right)\tilde{a}_{-k+k_1}\left(t\right)\right\rangle \\ &= \int dy' e^{-i(p-k_1)y'} I_{-k+k_1}\left(y',t\right)\end{aligned} \tag{3.C5}$$

Inserting this expression into S_1 gives

$$\begin{aligned}S_1 = i\int dk_1 dy' dp k_1 e^{i(y-y')p} e^{ik_1 y'} I_{-k+k_1}\left(y',t\right) \\ \cdot \int dx \phi^{>}_{k+p}\left(x\right)\left(1-\partial_{xx}+k_2^2\right)\partial_x \phi^{>}_{k_2}\left(x\right)\phi^{<}_{k_1}\left(x\right)\end{aligned}$$

The other nonlinear terms can be treated similarly. It is now necessary to evaluate the spatial integrals. To lowest order, $\phi^{<}_{k_1}\left(x\right)$ may be treated as a constant and pulled out of the integral. However, since we are anticipating that the large scale mean fields vary strongly in the radial direction, we instead expand $\phi^{<}_{k_1}\left(x\right)$ about the r_{m_1,n_1} resonant surface. Keeping up to second order in the power series expansion for $\phi^{<}_{k_1}\left(x\right)$, and performing the spatial integrals gives

$$\frac{\partial}{\partial t}N_k + \frac{\partial}{\partial k}\left(\omega_k + \delta\omega_k\right)\frac{\partial}{\partial y}N_k - \frac{\partial}{\partial y}\delta\omega_k\frac{\partial}{\partial k}N_k = \gamma_k N_k - F\left[\phi^{<}\right]N_k - \Delta\omega_k N_k^2\ , \tag{3.C6}$$

$$\delta\omega_k = \frac{k\left[\left(1+k^2-\frac{1}{2}\mu_{ik}\right)\left(k^2-\frac{1}{2}\mu_{ik}\right)+\left(\frac{1}{4}\mu_{rk}\right)^2\right]}{\left(1+k^2-\frac{1}{2}\mu_{ik}\right)^2+\frac{1}{4}\left(\mu_{rk}\right)^2}\frac{\partial\phi^{<}}{\partial x}\ ,$$

$$N_k = \left[\left(1+k^2-\frac{1}{2}\mu_{ik}\right)\left(k^2-\frac{1}{2}\mu_{ik}\right)+\frac{1}{4}\mu_{rk}^2\right]I_k\ .$$

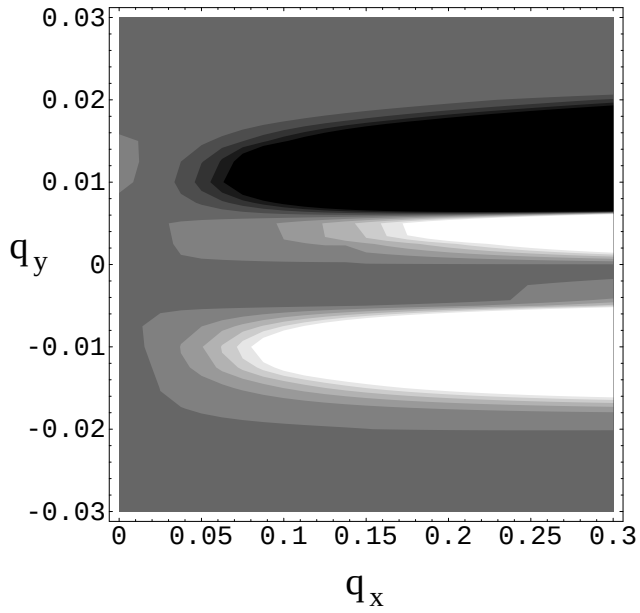

Figure 3.7: Plot of $C(\mathbf{q})$ as a function of q_y and q_x.

$$
\begin{aligned}
F[\phi^<] = & -\frac{\mu_{rk}\partial_x\phi^<}{\left(1+k^2-\frac{1}{2}\mu_{ik}\right)^2+\frac{1}{4}\mu_{rk}^2} \\
& + \left[\left(1+k^2\right)\left(k^2-3\mu_{ik}\right)+\frac{3}{4}\left|\mu_k\right|^2\right]\frac{\mu_{rk}\partial_k r_k\partial_{yy}\phi^<}{\left(1+k^2-\frac{1}{2}\mu_{ik}\right)^2+\frac{1}{4}\mu_{rk}^2} \\
& + \frac{1}{2}\frac{k}{\left|\mu_k\right|^2}\left[k^2\left(1+k^2-\frac{1}{2}\mu_{ik}\right)-\frac{1}{4}\left|\mu_k\right|^2\right]\frac{\mu_{rk}\partial_{xxx}\phi^<}{\left(1+k^2-\frac{1}{2}\mu_{ik}\right)^2+\frac{1}{4}\left(\mu_{rk}\right)^2} \\
& - \left[\frac{1}{2}\mu_{rk}^2+\left(1+k^2-\frac{1}{2}\mu_{ik}\right)\left(\mu_{ik}+\frac{1}{2}k\partial_k\mu_{ik}\right)-\frac{1}{4}k\mu_{rk}\partial_k\mu_{rk}\right] \\
& \cdot \frac{\partial_{xy}\phi^<}{\left(1+k^2-\frac{1}{2}\mu_{ik}\right)^2+\frac{1}{4}\mu_{rk}^2} \\
& + \frac{1}{2}\left(1+k^2-\frac{1}{2}\mu_{ik}\right)\frac{k\mu_{rk}\partial_k\mu_{rk}\partial_{xy}\phi^<}{\left[\left(1+k^2-\frac{1}{2}\mu_{ik}\right)^2+\frac{1}{4}\mu_{rk}^2\right]^2},
\end{aligned}
$$

Following a similar procedure as in the homogeneous case shown above (explained in detail in [78]), Eq. (3.C6) can be linearized and inserted into Eq. (3.8). This allows the polarization nonlinearity in the vorticity equation for the large scales to be written as:

$$
\left\langle\left(\hat{\mathbf{z}}\times\nabla\phi^>\right)\cdot\nabla\nabla_\perp^2\phi^>\right\rangle(\mathbf{x},t) = C(\mathbf{q})\,\phi^<. \tag{3.C7}
$$

The structure of $C(\mathbf{q})$ is plotted in Fig. 3.7as a function of q_y and q_x for the parameters given in Appendix B, and with $\alpha = -3$, which is the exponent of the equilibrium wave action spectrum.

Here q_x and q_y should be interpreted as inverse radial length scales associated with the large scale mode. The dark portions of the graph correspond to negative values of $C(\mathbf{q})$. It's apparent that the above structures die off rapidly for large poloidal wave numbers (small poloidal scales), however the magnitude of $C(\mathbf{q})$ remains much more pronounced for large radial wave numbers (small radial scales). This leads one to expect strong excitation of poloidally extended, narrow radial structures, as is the case with a tearing mode or zonal flow.

This chapter has been published in Physics of Plasmas, C. J. McDevitt and P. H. Diamond, **13**, 032302 (2006). C. J. McDevitt was the primary investigator and author of this paper.

Chapter 4

Transport of Parallel Momentum by Collisionless Drift Wave Turbulence

4.1 Introduction

Interest in toroidal momentum transport has been recently stimulated by the discovery of 'spontaneous' or 'intrinsic' rotation [79] and the realization that such intrinsic rotation may be required to suppress resistive wall modes in ITER [80], where neutral beam injection (NBI) is of limited utility and high cost. Spontaneous rotation refers to the observation that tokamak plasmas appear to rotate toroidally, at quite healthy velocities, in the absence of any apparent toroidal momentum input.

Theoretical approaches to the problem of turbulent transport of toroidal momentum and intrinsic rotation have focused on attempts to calculate the various elements of the momentum flux [81]. Various works include calculations of the momentum diffusivity χ_ϕ [82], calculations of the momentum convection velocity V in various models [83, 84, 85, 86], and calculations of the residual stress driven by fluctuations and ∇P, which can act as a *local* anomalous momentum source [87]. Most of the calculations of off-diagonal flux elements involve some assumption of a mechanism for broken $k_\parallel$ spectral symmetry, since

$\left\langle \tilde{v}_r \tilde{v}_\parallel \right\rangle \sim \left\langle \nabla_y \tilde{\phi} \nabla_\parallel \tilde{\phi} \right\rangle$ requires $\left\langle k_\parallel \right\rangle_{eff} \neq 0$ for a significant non-diffusive component. In one case, such symmetry breaking occurred via an interesting interplay of curvature coupling and ballooning structure [85]. In scenarios involving the electric field shear, progress was facilitated by drawing upon previous results for the effect of shear on turbulence and transport [88, 89, 90, 91]. Other approaches have invoked the effects of blobs or other coherent structures [92]. Most of the calculations implemented so far have been extremely simple and based on fluid models. Even the few kinetic calculations have not treated the response of both resonant and non-resonant particles and have not addressed parallel acceleration effects. However, the general structure of a kinetic model has been discussed, to some extent, in Ref. [93].

In this chapter, we focus primarily on the structure of the resonant component of the radial flux of parallel momentum. While our emphasis is on resonant particle contributions to the radial momentum flux, a momentum conservation theorem is derived such both wave fluxes and the exchange of momentum between resonant particles and waves can be readily accounted for. Similarly, the momentum conservation theorem provides a generalized expression for the total momentum flux The detailed structure of the resonant particle momentum flux is explicitly derived, accounting for diffusive, convective, and residual stress terms. It is found that the magnitude and sign of the off-diagonal terms depend sensitively on the linear mode properties of the underlying turbulence, as well as the strength of the radial electric field shear. Thus, making possible strong transitions in the direction and magnitude of the momentum flux induced by off-diagonal components as the plasma undergoes transport bifurcations, or the properties of the linear modes are varied.

The remainder of this chapter is organized as follows. In section II a momentum conservation theorem is proved emphasizing the dual role of waves and resonant particles in transporting momentum. Section III contains a derivation of the structure of the resonant particle momentum flux, with a discussion of its relation to experiment and to previous

work. Finally, in section IV we conclude.

4.2 Momentum Conservation Theorem

In this section we discuss the conservation of momentum and the structure of the momentum budget relation in the mean field theory of drift wave turbulence. We assume a simple geometry $r,\ \theta,\ \phi$ and leave extensions to toroidal geometry to a future paper. A momentum conservation theorem is proven, with special emphasis placed on delineating the roles of resonant particles and waves in momentum balance and transport. Starting from the gyrokinetic equation in collisionless electrostatic turbulence:

$$0 = \frac{\partial F^{(s)}}{\partial t} + \frac{\partial}{\partial \mathbf{x}} \cdot \left(\dot{\mathbf{X}} F^{(s)} \right) + \frac{\partial}{\partial v_\parallel} \left(\dot{V}_\parallel F^{(s)} \right), \tag{4.1a}$$

where

$$\dot{\mathbf{X}} = v_\parallel \hat{\mathbf{b}} + \frac{c}{B} \hat{\mathbf{b}} \times \nabla \left\langle \widetilde{\Phi} \right\rangle_\alpha, \quad \dot{V}_\parallel = -\frac{q_s}{m_s} \hat{\mathbf{b}} \cdot \nabla \left\langle \widetilde{\Phi} \right\rangle_\alpha, \tag{4.1b}$$

and, $\langle \cdots \rangle_\alpha \equiv (2\pi)^{-1} \int_0^{2\pi} d\alpha \, (\cdots)$. The mean field equation follows as

$$\frac{\partial \left\langle F^{(s)} \right\rangle}{\partial t} + \frac{\partial}{\partial \mathbf{x}} \cdot \left\langle \dot{\mathbf{X}} F^{(s)} \right\rangle + \frac{\partial}{\partial v_\parallel} \left\langle \dot{V}_\parallel F^{(s)} \right\rangle = 0. \tag{4.2}$$

Here it is convenient to rewrite Eq. (4.2) in the form of a parallel momentum equation. Defining the parallel plasma momentum as $\left\langle P_\parallel \right\rangle = \sum_s m_s \int d^3\bar{v} v_\parallel \left\langle F^{(s)} \right\rangle$, where the velocity moment is defined as $\int d^3\bar{v} \equiv 2\pi \int d\mu dv_\parallel \, (\omega_{cs}/m_s)$, and μ is proportional to the magnetic moment $\mu \equiv m_s v_\perp^2 / (2\omega_{cs})$. Taking the velocity moment of Eq. (4.2), multiplying by the mass of the plasma species, and summing over species, yields:

$$\frac{\partial \left\langle P_\parallel \right\rangle}{\partial t} + \frac{\partial}{\partial \mathbf{x}} \cdot \sum_s \int d^3\bar{v} \left\langle \dot{X} m_s v_\parallel F^{(s)} \right\rangle = \sum_s \int d^3\bar{v} \left\langle \dot{V}_\parallel m_s F^{(s)} \right\rangle. \tag{4.3}$$

Thus, the overall plasma momentum may be understood to evolve due to spatial fluxes induced by fluctuating $\mathbf{E} \times \mathbf{B}$ flows, and a sink/source term introduced by parallel forcing by the fluctuating electrostatic field. In order to understand the nature of this sink/source of parallel momentum, it is useful to briefly review the form of the familiar quasi-linear energy conservation theorems of the 1D Vlasov equation. For that familiar system, energy balance may be stated in either of two equivalent ways: as the conservation of the sum of resonant particle ($\varepsilon_{_{RP}}$) and wave ($\varepsilon_{_W}$) energy densities, i.e.

$$\frac{d}{dt}\left(\varepsilon_{_{RP}} + \varepsilon_{_W}\right) = 0, \tag{4.4a}$$

or as the conservation of the sum of particle and field energy density, i.e.

$$\frac{d}{dt}\left(\varepsilon_{_P} + \varepsilon_{_F}\right) = 0. \tag{4.4b}$$

The equivalence of these two results follows from the fact that $\varepsilon_{_W} = \varepsilon_{_F} + \varepsilon_{_{NRP}}$, i.e. waves (collective modes) are supported both by non-resonant particles (whose energy density is denoted by $\varepsilon_{_{NRP}}$, where $\varepsilon_{_P} = \varepsilon_{_{RP}} + \varepsilon_{_{NRP}}$) and fields. We observe that Eq. (4.4a) can be alternatively re-cast in terms of the quasi-particle density N (wave quanta density – usually action density) by noting that $\varepsilon_{_W} = N\left(\mathbf{k}, \mathbf{x}, t\right)\omega_{\mathbf{k}}$, so that the sum of resonant particle energy and quasi-particle energy is conserved [94].

Similarly, for momentum we can write:

$$\frac{d}{dt}\left(P_{RP} + P_W\right) = 0, \tag{4.5a}$$

and

$$\frac{d}{dt}\left(P_P + P_F\right) = 0. \tag{4.5b}$$

Here P_{RP} is the resonant particle momentum density, P_W is the wave momentum density

(sometimes referred to as the pseudo-momentum density), and $P_P = P_{RP} + P_{NRP}$ is the total particle momentum density. For electrostatic turbulence, the field momentum P_F is necessarily zero ($\widetilde{E} \times \widetilde{B}/4\pi c^2 = 0$, since $\widetilde{B} = 0$). This simple observation can be immediately seen to have two important consequences. First, Eq. (4.5b) reduces to the trivial relationship $dP_P/dt = 0$, indicating that the total mechanical momentum of the system is conserved. In the electrostatic limit, Eq. (4.3) may be easily seen to reduce in an analogous way, i.e.

$$\begin{aligned} \sum_s \int d^3\bar{v} \left\langle \dot{V}_\parallel m_s F^{(s)} \right\rangle &= \frac{\epsilon_\perp}{4\pi} \sum_s \left\langle \hat{b} \cdot \nabla \widetilde{\Phi} \nabla_\perp^2 \widetilde{\Phi} \right\rangle, \\ &= -\frac{\epsilon_\perp}{8\pi} \left\langle \hat{b} \cdot \nabla \left| \nabla_\perp \widetilde{\Phi} \right|^2 \right\rangle = 0, \end{aligned}$$

where we have used the the gyrokinetic Poisson equation [Eq. (4.A3)], assumed periodic boundary conditions in the parallel direction, and used an approximate form of $\epsilon_\perp(k)$ for simplicity (see Appendix A).

The second consequence of the field momentum vanishing is that P_W, which in general accounts for both field as well as non-resonant particle momentum, can be seen to be directly linked to fluctuations in the non-resonant particle momentum, i.e.

$$P_W = \delta P_{NR}, \tag{4.6}$$

where $\delta P_{NR} \equiv P_{NR} - P_{NR}^{(0)}$ is the momentum associated with the fluctuation driven non-resonant particle flow, and $P_{NR}^{(0)}$ is the zeroth order non-resonant particle momentum density, associated with the background (mean) flow. Equation (4.6) is a simple, albeit important, identity which is applicable to any system of electrostatic turbulence, including electrostatic drift waves.

Similarly, the gyrokinetic analog of Eq. (4.5a) can be constructed by considering the

quasi-linear expression for the resonant particle parallel momentum, i.e.

$$\frac{\partial \left\langle P_{\parallel}^{R} \right\rangle}{\partial t} + \frac{\partial}{\partial r}\left(\Pi_{rr}^{R} + \Pi_{rv}^{R}\right) = S_{vx}^{R} + S_{vv}^{R}, \tag{4.7}$$

where

$$\Pi_{rr}^{R} = -\pi \left(\frac{c}{B}\right)^{2} \sum_{s,k,\bar{\omega}} m_s k_\theta^2 \int d^3\bar{v} v_\parallel \delta\left(\bar{\omega} - k_\parallel v_\parallel\right) J_0^2\left(k_\perp \rho_\perp\right) \frac{\partial \left\langle F^{(s)} \right\rangle}{\partial r} \left|\widetilde{\Phi}_{k,\bar{\omega}}\right|^2, \tag{4.8}$$

$$\Pi_{rv}^{R} = -\pi \frac{c}{B} \sum_{s,k,\bar{\omega}} q_s k_\parallel k_\theta \int d^3\bar{v} v_\parallel \delta\left(\bar{\omega} - k_\parallel v_\parallel\right) J_0^2\left(k_\perp \rho_\perp\right) \frac{\partial \left\langle F^{(s)} \right\rangle}{\partial v_\parallel} \left|\widetilde{\Phi}_{k,\bar{\omega}}\right|^2, \tag{4.9}$$

$$S_{vx}^{R} = -\pi \frac{c}{B} \sum_{s,k,\bar{\omega}} q_s k_\parallel k_\theta \int d^3\bar{v} \delta\left(\bar{\omega} - k_\parallel v_\parallel\right) J_0^2\left(k_\perp \rho_\perp\right) \frac{\partial \left\langle F^{(s)} \right\rangle}{\partial r} \left|\widetilde{\Phi}_{k,\bar{\omega}}\right|^2, \tag{4.10}$$

$$S_{vv}^{R} = -\pi \sum_{s,k,\bar{\omega}} \frac{q_s^2}{m_s} k_\parallel^2 \int d^3\bar{v} \delta\left(\bar{\omega} - k_\parallel v_\parallel\right) J_0^2\left(k_\perp \rho_\perp\right) \frac{\partial \left\langle F^{(s)} \right\rangle}{\partial v_\parallel} \left|\widetilde{\Phi}_{k,\bar{\omega}}\right|^2. \tag{4.11}$$

Here we have inserted the quasi-linear plasma response to electrostatic perturbations [i.e. Eq. (4.25) given below] in order to obtain explicit expressions for the flux and source terms, $\left\langle P_{\parallel}^{R} \right\rangle$ indicates that only resonant particles are included in the integration and $\omega - \omega_{EB} \equiv \bar{\omega} + k_\parallel \left\langle v_\parallel \right\rangle$. Similar to the equation for the total plasma momentum [Eq. (4.3)], a source term (here given by $S_{\parallel}^{R} \equiv S_{vx}^{R} + S_{vv}^{R}$) is again present. However, unlike the previous case, this term can be easily seen to be non-zero in the electrostatic limit. In order to understand in more detail the origins of this sink/source of resonant particle parallel momentum it is convenient to rewrite the source term $S_{\parallel}^{R}$ in terms of the gyrokinetc susceptibility (see Appendix A), yielding:

$$S^{R} = \frac{1}{4\pi} \sum_{k} k_\parallel \mathrm{Im}\chi_{k,\omega_k} \epsilon_\perp\left(k\right) k_\perp^2 \left|\widetilde{\Phi}_k\right|^2, \tag{4.12}$$

where ω_k is defined by $\mathrm{Re}D_{k,\omega} = 0$. Equation (4.12) may be rewritten in the simplified

form as

$$S^R = -2\sum_k k_\parallel \gamma_k N_k. \tag{4.13}$$

Here N_k is the wave action density, and is defined by

$$N_k \equiv \frac{1}{8\pi}\left.\frac{\partial D_{k,\omega}}{\partial \omega}\right|_{\omega=\omega_k} \epsilon_\perp(k)\, k_\perp^2 \left|\widetilde{\Phi}_k\right|^2. \tag{4.14}$$

Thus, the expression for resonant particle momentum [Eq. (4.7)] can be written as

$$\frac{\partial \left\langle P_\parallel^R \right\rangle}{\partial t} + \frac{\partial}{\partial r}\left(\Pi_{rr}^R + \Pi_{rv}^R\right) = -2\sum_s k_\parallel \gamma_k N_k. \tag{4.15}$$

As discussed further below, N_k may be understood to correspond to a population of wave quanta. Thus, as is clear from the form of Eq. (4.15), resonant particle momentum is conserved up to wave-particle interaction with the ambient wave population.

From Eq. (4.15) it is clear that a description of wave evolution is required in order to account for the sink/source introduced by wave-particle interaction. This can be accomplished by recalling the quasi-linear wave-energy ("Poynting") theorem for drift waves:

$$\frac{\partial}{\partial t}\varepsilon_{\omega_{\mathbf{k}}} + \nabla\cdot\mathbf{S}_{\mathbf{k}} + Q_{\mathbf{k}} = 0, \tag{4.16}$$

i.e. that wave energy density $\varepsilon_{\omega_{\mathbf{k}}}$ evolves via divergence of the wave energy density flux $\mathbf{S}_{\mathbf{k}}$ and local dissipation $Q_{\mathbf{k}}$. Here, $\varepsilon_{\omega_{\mathbf{k}}}$, $\mathbf{S}_{\mathbf{k}}$ and $Q_{\mathbf{k}}$ are given, respectively, by:

$$\varepsilon_{\omega_{\mathbf{k}}} = \frac{1}{8\pi}\omega_{\mathbf{k}}\left.\frac{\partial D_{k,\omega}}{\partial \omega}\right|_{\omega_{\mathbf{k}}} \epsilon_\perp(k)\left|\widetilde{\mathbf{E}}_\perp\right|^2, \tag{4.17a}$$

$$\mathbf{S}_{\mathbf{k}} = -\frac{1}{8\pi}\omega_{\mathbf{k}}\left.\frac{\partial D_{k,\omega}}{\partial \mathbf{k}}\right|_{\omega_{\mathbf{k}}} \epsilon_\perp(k)\left|\widetilde{\mathbf{E}}_\perp\right|^2, \tag{4.17b}$$

$$Q_{\mathbf{k}} = \frac{1}{4\pi}\omega_{\mathbf{k}}\mathrm{Im}D_{k,\omega_{\mathbf{k}}}\epsilon_\perp(k)\left|\widetilde{\mathbf{E}}_\perp\right|^2. \tag{4.17c}$$

Equation (4.16) is a straightforward adaptation of a more general result for waves in a dielectric medium to the special case of drift waves, which we consider here. The drift-kinetic equivalent of Eqs. (4.16,4.17) are proven in Refs. [95, 96]. In order to relate the spatial momentum flux to the wave energy ε_k, it is convenient to rewrite $\mathbf{S_k}$ utilizing

$$\begin{aligned} 0 &= d\omega \left(\frac{\partial D_{k,\omega}}{\partial \omega} \right) + d\mathbf{k} \cdot \left(\frac{\partial D_{k,\omega}}{\partial \mathbf{k}} \right), \\ \Rightarrow & \left(\frac{\partial D_{k,\omega}}{\partial \mathbf{k}} \right) = -\mathbf{v_{gr}} \frac{\partial D_{k,\omega}}{\partial \omega}, \end{aligned}$$

thus,

$$\mathbf{S_k} = \mathbf{v_{gr}} \varepsilon_{\mathbf{k}}. \tag{4.18}$$

Equation (4.16) can now be rewritten as a parallel wave momentum equation using the definition $\left\langle P_{\parallel}^{w} \right\rangle \equiv \sum_{\mathbf{k}} k_{\parallel} N_k = \sum_{\mathbf{k}} \left(k_{\parallel} / \omega_k \right) \varepsilon_k$

$$\frac{\partial \left\langle P_{\parallel}^{w} \right\rangle}{\partial t} + \nabla \cdot \mathbf{\Pi}_{\parallel}^{w} = -S_{\parallel}^{w}, \tag{4.19}$$

where

$$\mathbf{\Pi}_{\parallel}^{w} \equiv \sum_{k} k_{\parallel} \mathbf{v}_{gr} N_k, \tag{4.20}$$

$$\begin{aligned} S_{\parallel}^{w} \equiv \frac{1}{4\pi} \sum_{k} k_{\parallel} \mathrm{Im} D_{k,\omega_{\mathbf{k}}} \epsilon_{\perp}(k) \, k_{\perp}^{2} \left| \widetilde{\Phi}_{\mathbf{k}} \right|^{2} &= \frac{-1}{4\pi} \sum_{k} k_{\parallel} \gamma_k \left. \frac{\partial D_{k,\omega}}{\partial \omega} \right|_{\omega=\omega_k} \epsilon_{\perp}(k) \, k_{\perp}^{2} \left| \widetilde{\Phi}_{k} \right|^{2}, \\ &= -2 \sum_{k} k_{\parallel} \gamma_k N_k, \end{aligned} \tag{4.21}$$

and $\mathbf{v}_{gr}$ is the group velocity of the underlying waves. Summing Eqs. (4.15) and (4.19) yields the momentum equation

$$\frac{\partial}{\partial t} \left(\left\langle P_{\parallel}^{R} \right\rangle + \left\langle P_{\parallel}^{w} \right\rangle \right) + \nabla \cdot \left(\Pi_{r,\parallel}^{R} + \Pi_{r,\parallel}^{w} \right) = 0. \tag{4.22}$$

Finally, we note that from Eq. (4.6) the total momentum fluctuation can be written as $\delta P_\parallel = \left\langle P_\parallel^R \right\rangle + \left\langle P_\parallel^w \right\rangle$, since wave momentum and non-resonant particle momentum are identical in the frame of the background plasma. Thus, Eq. (4.22) can be written as

$$\frac{\partial \delta P_\parallel}{\partial t} + \nabla \cdot \left(\Pi_{r,\parallel}^R + \Pi_{r,\parallel}^w \right) = 0. \tag{4.23}$$

Note that Eq. (4.23) eliminates the local force in (4.15), in favor of the mean radial flux of parallel wave momentum $\Pi_{r,\parallel}^w$. More generally, Eq. (4.23) relates the total fluctuation-induced parallel force on the plasma to the sum of the fluxes of resonant particle and wave momentum. In the next section, an explicit expression for the resonant particle flux is derived, however before proceeding further, it is useful to comment on some basic properties of the wave momentum flux. First, we note that for a "balanced" spectrum of drift wave turbulence (i.e. $\left\langle k_\parallel \right\rangle \equiv \sum_k k_\parallel N_k / \sum_k N_k = 0$), $\Pi_{r,\parallel}^w$ can be easily seen to vanish identically for $v_{gr}\left(-k_\parallel\right) = v_{gr}\left(k_\parallel\right)$. Thus, parallel symmetry breaking, i.e. an imbalance in the parallel propagation of the drift wave population, is required in order to induce a finite radial flux of parallel momentum. As further discussed below, $k_\parallel$ symmetry breaking also plays an important role in determining the sign and magnitude of the off-diagonal contribution to the resonant particle flux, thus identifying $\left\langle k_\parallel \right\rangle$ as a critical quantity in the description of parallel momentum transport. While a comprehensive description of $k_\parallel$ symmetry breaking is beyond the scope of this chapter, we remark that as is well known, the presence of $\mathbf{E} \times \mathbf{B}$ shear is capable of inducing a finite $\left\langle k_\parallel \right\rangle$ [88, 89, 90, 91], and thus introduce a potentially large contribution to the overall parallel momentum transport due to wave fluxes. We note that although this mechanism is not unique (another obvious example would be growth asymmetry), for regions of strong $\mathbf{E} \times \mathbf{B}$ shear, such as the H-mode pedestal, it is likely dominant.

4.3 Calculation of Resonant Particle Flux

In this section, we present the calculation of the parallel momentum flux carried by resonant particles. The quasi-linear gyrokinetic equation for the evolution of the resonant particle (i.e. ion) momentum is given by

$$\frac{\partial}{\partial t}\left\langle P_{\parallel}^{R}\right\rangle + \frac{\partial}{\partial r}\left\langle \Pi_{r,\parallel}^{R}\right\rangle = m_i \int d^3\bar{v}\dot{V}_{\parallel}\widetilde{F}_i^R, \tag{4.24a}$$

where the resonant particle momentum flux is

$$\Pi_{r,\parallel}^{R} = \left\langle \widetilde{v}_{Er}\widetilde{P}_{\parallel i}\right\rangle = m_i n_0 \int d^3\bar{v}v_{\parallel}\frac{dR}{dt}\widetilde{F}_i^R, \tag{4.24b}$$

and $\widetilde{F}_i^R$ is the resonant, linear ion response. As shown in Section II, the rhs corresponds to momentum exchange between waves and particles and cancels identically with its counterpart in the $k_{\parallel}$ moment of the wave kinetic equation. Hence, the rhs is hereafter neglected, and we need only focus on $\left\langle \Pi_{r,\parallel}^{R}\right\rangle$. Also, we note that since $m_e \ll m_i$, electrons carry a negligible fraction of the total momentum, such that only the ion component of the momentum flux need be calculated. As usual in quasi-linear theory, we simply plug the resonant linear response $\widetilde{F}_i^R$ into $\left\langle \Pi_{r,\parallel}^{R}\right\rangle$ to calculate the flux. The linear response $\widetilde{F}_{i,\mathbf{k}}^R$ is:

$$\widetilde{F}_{i,\mathbf{k}}^R = \frac{-J_0\left(\lambda\right)}{\omega_k - \omega_{EB} - k_{\parallel}v_{\parallel}}c_s^2\left\{\frac{k_\theta}{\omega_{ci}}\frac{\partial\left\langle F_i\right\rangle}{\partial x} + k_{\parallel}\frac{\partial\left\langle F_i\right\rangle}{\partial v_{\parallel}}\right\}\frac{e\widetilde{\Phi}_{\mathbf{k}}}{T_e}, \tag{4.25}$$

where $\lambda \equiv k_\perp\rho_\perp$ and $\omega_{EB} \equiv k_\theta\left\langle v_E\right\rangle$. After some straightforward algebra [evaluation of Eqs. (4.8-4.11)], we obtain the resonant ion momentum flux

$$\left\langle \Pi_{r,\parallel}^{R}\right\rangle = n_0 m_i\left[-\chi_\phi\frac{\partial}{\partial r}\left\langle v_{\parallel}\right\rangle + V_r\left\langle v_{\parallel}\right\rangle + S\right], \tag{4.26a}$$

where for a shifted Maxwellian $\langle F_i \rangle$,

$$\chi_\phi = \sqrt{2\pi} \sum_{\mathbf{k}} \left(k_\theta \rho_i\right)^2 \frac{v_{ti}}{\left|k_\parallel\right|} \Omega^2 \Gamma_0 \left(b\right) e^{-\Omega^2} \left| \frac{e\widetilde{\Phi}_{\mathbf{k}}}{T_i} \right|^2 , \tag{4.26b}$$

$$V_r = \sqrt{\frac{\pi}{2}} \sum_{\mathbf{k}} \left(k_\theta \rho_i\right)^2 \frac{v_{ti}}{\left|k_\parallel\right|} \frac{1}{L_n} \Gamma_0 \left(b\right) \left| \frac{e\widetilde{\Phi}_{\mathbf{k}}}{T_i} \right|^2 e^{-\Omega^2} \left\{ 1 - \frac{\eta_i}{\eta_i^{crit}} - \frac{\bar{\omega}_{\mathbf{k}}}{\omega_{*i}} - \eta_i \Omega^2 \right\}, \tag{4.26c}$$

and

$$S = \sqrt{\pi} \sum_{\mathbf{k}} \left(k_\theta \rho_i\right)^2 \frac{v_{ti}^2}{L_n} \frac{1}{\left|k_\parallel\right|} \Omega \Gamma_0 \left(b\right) \left| \frac{e\widetilde{\Phi}_{\mathbf{k}}}{T_i} \right|^2 e^{-\Omega^2} \left\{ 1 - \frac{\eta_i}{\eta_i^{crit}} - \frac{\bar{\omega}_{\mathbf{k}}}{\omega_{*i}} - \eta_i \Omega^2 \right\} . \tag{4.26d}$$

Here the notation is standard, so $\eta_i^{crit} = 2\left[1 + 2b\left(1 - I_1/I_0\right)\right]^{-1}$, $\Omega = \bar{\omega}_{\mathbf{k}}/\sqrt{2} k_\parallel v_{ti}$, $b = k_\perp^2 \rho_i^2$, I_0 and I_1 are the modified Bessel functions, $v_{*e,i}$ are the electron and ion diamagnetic velocities, $\bar{\omega}_k$ is the Doppler shifted wave frequency defined by $\omega_{\mathbf{k}} - \omega_{EB} \equiv \bar{\omega}_{\mathbf{k}} + k_\parallel \left\langle v_\parallel \right\rangle$, and $\omega_{*e,i} = k_\theta v_{*e,i}$, $\tau = T_e/T_i$, $\Gamma_0 = I_0 e^{-b}$ etc.

Some discussion of the transport coefficients χ_ϕ, V_r and S is appropriate at this point. Predictably, $\chi_\phi \sim \chi_i$ but $\chi_\phi \neq \chi_i$, on account of the structure of resonant coupling to the spectrum of wave phase velocities. χ_ϕ (and obviously, the entire resonant particle flux) decays rapidly [$\sim exp\left(-\Omega^2\right)$] for non-resonant particles, and may be written as $\chi_\phi \sim \langle \widetilde{v}_E^2 \rangle \, \tau_{ac}$ where τ_{ac} is set by the dispersion in the distribution of the ion transit rate. Of course, $\chi_\phi \sim D_{GB}$ for "mixing length estimate" fluctuation levels. The convection velocity V_r is rather sensitive and model dependent. V_r is inward (corresponding to a pinch) for ITG modes in the resonant regime near threshold ($|\Omega| \lesssim 1$). For regimes far from threshold ($\Omega \gg 1$) V_r is necessarily outward, however as noted above, the magnitude of this term is then negligible. Near marginality, but for electron drift waves, the sign of the convective term depends sensitively on η_i, and requires a quantitative description of the microturbulence spectrum. Note that the convective term scales as $V_r/\chi_\phi \sim 1/\left(\Omega^2 L_\perp\right)$, a profile scale length. Thus, the resonant particle pinch complements the non-resonant turbulent

convection (TurCo) pinch [85], derived for toroidal geometry. The latter is non-resonant (and so must represent wave transport), is inward for electron drift waves, can attain either sign (depending on plasma parameters) for ITG modes and has $V_r/\chi_\phi \sim 1/R$ [i.e. $O(\epsilon)$ smaller], but is insensitive to the resonance function. In other words, if the percentage weighting of resonant particles is lower than ϵ, TurCo provides the main convection effect. On the other hand, near marginal stability, where the percentage of resonant particles is high, the resonant particle pinch is the primary cause of convection. Furthermore, near marginality $|\bar{\omega}_{\mathbf{k}} \ll \omega_{*i}|$ and $|\Omega^2| \lesssim 1$, so that

$$\frac{V_r}{\chi_\phi} \approx \frac{1}{\Omega^2}\frac{1}{L_n}\left\{1 - \frac{\eta_i}{\eta_i^{crit}}\right\} ,$$

so that for unstable ITG, the ∇T_i driven pinch is *inward* in rough agreement with Ref. [83], but the ∇n driven pinch is *outward*, opposite to the non-resonant pinch predicted in Ref. [84]. Considering now the third term in the resonant momentum flux given by Eq. (4.26a), since $S/V_r \approx \Omega v_{ti}$, S must vanish in the absence of symmetry breaking (i.e. $S \to 0$ as $\langle k_\parallel \rangle \to 0$). As is also clear, for regimes of finite symmetry breaking, the sign of the residual stress follows identical rules to that of the resonant particle convection term, but multiplied by sgn $\left(\langle k_\parallel \rangle\right)$. Finally, it should be noted that this analysis has not addressed the nature of particle transport or the non-adiabatic electron response. Considering these will surely introduce additional momentum transport effects related to the interplay of particle and momentum transport. Such cross coupling is discussed further in Refs. [87, 86].

4.4 Conclusion

The principle results from the above analysis can be listed as follows:

a.) a derivation of a momentum conservation theorem accounting for the exchange between, as well as momentum fluxes induced by, waves and resonant particles

b.) an explicit evaluation of the structure of the radial flux of resonant particle momentum.

Considering item (ii) first, strong off-diagonal components to the resonant component of the parallel momentum flux have been derived. This flux consists of a diffusive flux (with $\chi_\phi \sim \chi_i$ but not $\chi_\phi \neq \chi_i$), a convective flux which may be inward in certain regimes, and a residual stress piece, explicitly dependent upon the symmetry breaking mechanism (i.e. the origin of $\langle k_\| \rangle \neq 0$). With regard to (i), the extension of well known energy and momentum conservation theorems, familiar from the 1D Vlasov equation, to gyrokinetic modes, corresponds to a straightforward, but practically important step in describing the transport of parallel momentum in a strongly magnetized plasma. In particular, unlike previous studies, which typically focus on either the resonant or non-resonant components of the total momentum flux, and neglect momentum exchanges between these two components, this approach provides a systematic, and conceptually intuitive, framework for a comprehensive treatment of parallel momentum transport.

Appendix A: Derivation of Gyrokinetic Susceptibility

In this appendix we derive an explicit expression for the wave action density from the gyrokinetic equation, and relate it to momentum exchange between resonant particles and waves. The induced plasma response to an external electrostatic perturbation may be written as

$$\delta F^{\text{ind}}_{k,\omega} = \frac{J_0(\lambda)}{\omega - \omega_{EB} - k_\| v_\|} \left\{ \frac{c}{B} \left(\hat{\mathbf{b}} \times \mathbf{k} \right) \cdot \frac{\partial \langle F_s \rangle}{\partial \mathbf{x}} - \frac{q_s}{m_s} k_\| \frac{\partial \langle F_s \rangle}{\partial v_\|} \right\} \widetilde{\Phi}^{\text{tot}}_{k,\omega} \equiv L_{k,\omega} \widetilde{\Phi}^{\text{tot}}_{k,\omega}, \tag{4.A1}$$

where $\widetilde{\Phi}^{\text{tot}} = \widetilde{\Phi}^{\text{ind}} + \widetilde{\Phi}^{\text{ext}}$. Considering the gyrokinetic Poisson equation, an equation for the induced response may be written as

$$k_{\perp}^{2}\widetilde{\Phi}_{k,\omega}^{\text{ind}} = 4\pi\sum_{s} q_{s}\int d^{3}\bar{v}\left\{J_{0}\left(\lambda\right)\delta F_{k,\omega}^{\text{ind}} + \left[J_{0}^{2}\left(\lambda\right)-1\right]\frac{q_{s}\widetilde{\Phi}_{k,\omega}^{\text{ind}}}{T_{s}}\left\langle F_{s}\right\rangle\right\}, \tag{4.A2}$$

where it's understood that $\delta F_{k,\omega}^{\text{ind}}$ is species dependent. Eq. (4.A2) may be simplified via the following notation

$$\epsilon_{\perp}\left(k\right)k_{\perp}^{2}\widetilde{\Phi}_{k,\omega}^{\text{ind}} = 4\pi\sum_{s} q_{s}\int d^{3}v' J_{0}\left(\lambda\right)\delta F_{k,\omega}^{\text{ind}}, \tag{4.A3}$$

where $\epsilon_{\perp}\left(k\right) \equiv 1 + \sum_{s}\left(k_{Ds}^{2}/k_{\perp}^{2}\right)\left[1 - I_{0}\left(b_{s}\right)\exp\left(-b_{s}\right)\right]$. This permittivity may be profitably understood to correspond to a "gyrokinetic vacuum" [97]. While this operator may be defined exactly in Fourier space, it is convenient to expand in b_{s}. To lowest non-trivial order:

$$\epsilon_{\perp}\left(k\right) \approx 1 + k_{Di}^{2}\rho_{i}^{2} \approx k_{Di}^{2}\rho_{i}^{2}.$$

Thus, to lowest order, this operator may be understood to reduce to a constant, which we shall denote by $\epsilon_{\perp} \equiv k_{Di}^{2}\rho_{i}^{2}$. This observation is useful as it makes real space generalizations trivial.

After substitution of Eq. (4.A1) into Eq. (4.A3), the induced response of the electrostatic field can be written in terms of the external perturbations, yielding:

$$\left(1+\chi_{k,\omega}\right)\epsilon_{\perp}\left(k\right)k_{\perp}^{2}\widetilde{\Phi}_{k,\omega}^{\text{ind}} = 4\pi\sum_{s} q_{s}\int d^{3}v' J_{0}\left(\lambda\right)L_{k,\omega}\widetilde{\Phi}_{k,\omega}^{\text{ext}}, \tag{4.A4}$$

where the susceptibility has been defined by

$$\chi_{k,\omega} = -4\pi \sum_s \frac{q_s}{\epsilon_\perp (k)\, k_\perp^2} \int d^3\bar{v} \frac{J_0^2(\lambda)}{\omega - \omega_{EB} - k_\parallel v_\parallel} \left\{ \frac{c}{B} \left(\hat{\mathbf{b}} \times \mathbf{k} \right) \cdot \nabla \langle F_s \rangle - \frac{q_s}{m_s} k_\parallel \frac{\partial \langle F_s \rangle}{\partial v_\parallel} \right\}. \tag{4.A5}$$

The dispersion relationship is defined as

$$0 = D_{k,\omega} \equiv 1 + \chi_{k,\omega}, \tag{4.A6}$$

with a growth rate approximately given by

$$\gamma_k = \left. \frac{-\mathrm{Im} D_{k,\omega}}{\partial D_{k,\omega}/\partial \omega} \right|_{\omega=\omega_k}. \tag{4.A7}$$

Part of this chapter appears in Physics of Plasmas, P. H. Diamond, C. J. McDevitt, O. D. Gurcan, T. S. Hahm and V. Naulin, **15**, 012303 (2008). C. J. McDevitt was a contributing author to this paper.

Chapter 5

Summary and Conclusions

In the above, multi-scale methods have been utilized to describe the interaction of small scale micro-turbulence with large scale flow structures. Reduced, but self-consistent models have been derived to describe transport barrier formation, magnetic reconnection in the presence of drift wave turbulence, as well as plasma rotation. These models, while highly simplified, allow for non-trivial feedback loops between the large scale mean fields and the small scale fluctuations to be readily incorporated. In particular, the inclusion of secondary flow structures resulting from modulational instability of the ambient drift wave turbulence have been seen to play a conspicuous role in both transport barrier formation and magnetic island evolution.

Considering the former, secondary flow structures driven by the background turbulence have been shown to facilitate the formation of transport barriers. While it is generally appreciated that zonal flows, in regimes of low collisionality, may impact the power threshold for barrier formation, in this thesis we have shown that for regimes of weak magnetic shear, poloidally extended finite-m cellular flows are likely to become prevalent. The importance in distinguishing finite-m flows and the special case of poloidally symmetric $m = 0$ flows, can be readily understood by considering that poloidally symmetric flows are incapable of radial mixing. Similarly, while zonal flow drive is strongly dependent on the intensity

and spatial profile of the background turbulence, they possess no direct dependence on the q-profile. This is in contrast to finite-m flows which are strongly coupled to low-q resonant surfaces by resistive field line bending. Hence, we anticipate finite-m cellular flows to play a significant role in determining the transport properties near low-q resonant surfaces.

Similarly, the nonlinear evolution of drift wave turbulence in the presence of finite-m cellular flows has been investigated. It is found that the phase space of the micro-turbulence is largely stochastic, thus justifying the use of quasi-linear theory even in the extreme limit of a stationary coherent mode. This is in contrast to axisymmetric flows, in which the auto-correlation time of the flow pattern must be comparable or shorter than the bounce time of a wave quantum, in order to effect a stochastization of ray orbits. As a corollary, nonlinear wave trapping has been found to be circumvented for purely non-axisymmetric modes, as trapped quasi-particle orbits are destroyed for arbitrarily small q_y values.

Aside from the MHD stable regime discussed above, we have also investigated the evolution of linearly unstable tearing modes in the presence of drift wave turbulence. The dominant interaction is found to occur via the modulation of the drift wave turbulence by the tearing mode flows. This interaction may be straightforwardly incorporated into the mean field equations via a simple closure procedure, yielding a negative viscosity as the dominant effect of the drift waves on the tearing mode evolution. A linear eigenmode analysis was carried out, identifying the modified reconnection rate and resistive layer width.

The multi-scale methods employed above, aside from providing a useful framework for understanding non-local energy transport and thus secondary instabilities, are capable of providing a powerful and intuitive means of describing spatial fluxes of quantities such as energy and momentum. This follows, since the wave kinetic equation can be easily transformed into an equation describing the evolution of wave energy or momentum via multiplication by the energy or momentum per wave quantum, i.e. ω_k and $k_\parallel$ respectively. Any description of energy or momentum transport based purely on wave kinetics is, however,

incomplete as it ignores transport induced via resonant particles. In this thesis, a simplified version of the wave kinetic formalism utilized in Chapters 2 and 3 has been extended to include the exchange of momentum with resonant particles. The extended formalism has been employed in the description of parallel momentum transport in strongly magnetized plasmas. Expressions for parallel momentum flux induced either by waves or resonant particle have been derived, providing a comprehensive description of parallel momentum transport.

Bibliography

[1] W. Horton. Drift waves and transport. *Rev. Mod. Phys.*, 71(3):735 – 778, 1999.

[2] F. Wagner et al. *Phys. Rev. Lett.*, 49(19):1408, 1982.

[3] A. N. Kolmogorov. *C. R. Acad Sci. USSR*, 30:301, 1941. reprinted in *Proc. R. Soc. Lond.* A 434, 9-13 (1991).

[4] U. Frisch. *Turbulence*. Cambridge University Press, Cambridge, 1995.

[5] P. H. Diamond, S.-I. Itoh, K. Itoh, and T. S. Hahm. *Plasma Phys. Control. Fusion*, 47:R35, 2005.

[6] H. Biglari, P. H. Diamond, and P. W. Terry. The influence of sheared poloidal rotation on edge turbulence. *Phys. Fluids B*, 2(1):1–4, 1990.

[7] H. K. Moffatt. *Magnetic Field Generation in Electrically Conducting Fluids*. Cambridge University Press, Cambridge, 1978.

[8] S. Chandrasekhar. *Hydrodynamic and Hydromagnetic Stability*. Dover, New York, 1981.

[9] R. H. Kraichnan and D. Montgomery. Two-dimensional turbulence. *Rep. Prog. Phys.*, 43:547, 1980.

[10] R. H. Kraichnan. Statistical dynamics of two-dimensional flow. *J. Fluid Mech.*, 67:155, 1975.

[11] B. Dubrulle and S. Nazarenko. *Physica D*, 110:123, 1997.

[12] A. M. Balk, S. V. Nazarenko, and V. E. Zakharov. On the nonlocal turbulence of drift type waves. *Phys. Lett. A.*, 146(4):217, 1990.

[13] A. I. Smolyakov and P. H. Diamond. *Phys. Plasmas*, 6(12):4410, 1999.

[14] H. P. Furth, J. Killeen, and M. N. Rosenbluth. *Phys. Fluids*, 6(4):459, 1963.

[15] P. H. Rutherford. *Phys. Fluids*, 16(11):1903, 1973.

[16] R. Fitzpatrick. *Phys. Plasmas*, 2:825, 1995.

[17] A. J. Brizard and T. S. Hahm. *Rev. Mod. Phys.*, 79(2):421, 2007.

[18] A. Brizard. *Phys. Fluids B*, 4(5):1213, 1992.

[19] A. Hasegawa and K. Mima. *Phys. Fluids*, 21(1):87, 1978.

[20] W. Horton, R. D. Estes, and D. Biskamp. *Physma Physics*, 22:663, 1979.

[21] P. Kaw, R. Singh, and P. H. Diamond. *Plasma Phys. Control. Fusion*, 44:51, 2002.

[22] B. V. Chirikov. *Atomnaya Energiya*, 6:630, 1959.

[23] J. W. Connor, T. Fukuda, X. Garbet, C. Gormezano, V. Mukhovatov, and M. Wakatani. *Nucl. Fusion*, 44:R1, 2004.

[24] L. Garcia, B. A. Carreras, V. E. Lynch, M. A. Pedrosa, and C. Hidalgo. *Phys. Plasmas*, 8(9):4111, 2001.

[25] S. Gunter, A. Gude, J. Hobirk, M. Maraschek, S. Saarelma, S. Schade, R. C. Wolf, and ASDEX Upgrade Team. *Nucl. Fusion*, 41:1283, 2001.

[26] X. Garbet, C. Bourdelle, G. T. Hoang, Maget, S. Benkadda, P. Beyer, C. Figarella, I. Voitsekovitch, O. Agullo, and N. Bian. *Phys. Plasmas*, 8:2793, 2001.

[27] Y. Kishimoto, J.-Y Kim, W. Horton, T. Tajima, M. J. LeBrun, S. A. Dettrick, J. Q. Li, and S. Shirai. *Nucl. Fusion*, 40:667, 2000.

[28] X. Garbet, Y. Sarazin, P. Ghendrih, S. Benkadda, P. Beyer, C. Figarella, and I. Voitsekovitch. *Phys. Plasmas*, 9(9):3893, 2002.

[29] M. E. Austin, K. H. Burrell, R. E. Waltz, K. W. Gentle, P. Gohil, C. M. Greenfield, R. J. Groebner, W. W. Heidbrink, Y. Luo, J. E. Kinsey, M. A. Makowski, G. R. McKee, R. Nazikian, C. C. Petty, R. Prater, T. L. Rhodes, M. W. Shafer, and M. A. Van Zeeland. *Phys. Plasmas*, 13:082502, 2006.

[30] R. E. Waltz, M. E. Austin, K. H. Burrell, and J. Candy. *Phys. Plasmas*, 13:052301, 2006.

[31] M. N. Rosenbluth, H. L. Berk, I. Doxas, and W. Horton. *Phys. Fluids*, 30(9):2636, 1987.

[32] O. D. Gurcan, P. H. Diamond, C. J. McDevitt, and M. A. Malkov. Conference Proceedings, 21th IAEA Fusion Energy Conference, Chengdu, China 2006).

[33] R. Z. Sagdeev, V. D. Shapiro, and V. I. Shevchenko. *Sov. J. Plasma Phys*, 4:306, 1978.

[34] H. Okuda, C. Chu, and J. M. Dawson. *Phys. Fluids*, 18:243, 1975.

[35] E. J. Kim and P. H. Diamond. *Phys. Plasmas*, 9(11):4530, 2002.

[36] C. J. McDevitt and P. H. Diamond. *Phys. Plasmas*, 13:032302, 2006.

[37] M. Abramowitz and I. A. Stegun, editors. Dover Publications, Inc., New York, 1972.

[38] L. Garcia, B. A. Carreras, and V. E. Lynch. *Phys. Plasmas*, 6(10):3910, 1999.

[39] F. Romanelli. *Phys. Fluids B*, 1(5):1018, 1988.

[40] A. I. Smolyakov, P. H. Diamond, and M. Malkov. *Phys. Rev. Lett.*, 84:491, 2000.

[41] George M. Zaslavsky. *Hamiltonian Chaos and Fractional Dynamics*. Oxford, University Press, Oxford, 2005.

[42] P. H. Diamond, V. B. Lebedev, Y. M. Liang, A. V. Gruzinov, I. Gruzinova, M. Medvedev, B. A. Carreras, D. E. Newman, L. Charlton, K. L. Sidikman, D. B. Batchelor, E. F Jaeger, C. Y. Wang, G. G. Craddock, N. Mattor, T. S. Hahm, M. Ono, B. LeBlanc, H. Biglari, F. Y. Gang, and D. J. Sigmar. Proceedings of the 15th IAEA International Conference on Plasma Physics and Controlled Nuclear Fusion Research, (IAEA, Seville 1994) Vol. 3, p. 323.

[43] E. J. Kim and P. H. Diamond. *Phys. Rev. Lett.*, 90(18):185006, 2003.

[44] S. I. Itoh, K. Itoh, A. Fukuyama, Y. Miura, and JFT-2M Group. *Phys. Rev. Lett.*, 67(18):2485, 1991.

[45] V. Naulin, J. Juul Rasmussen, and J. Nycander. *Plasma Phys.*, 10:1075, 2003.

[46] B. A. Carreras, K. Sidikman, P. H. Diamond, P. W. Terry, and L. Garcia. *Phys. Fluids B*, 4(10):3115, 1992.

[47] H. R. Wilson, J. W. Connor, R. J. Hastie, and C. C. Hegna. *Phys. Plasmas*, 3:248, 1996.

[48] R. J. La Haye, S. Gunter, D. A. Humphreys, J. Lohr, T. C. Luce, M. E. Maraschek, C. C. Petty, R. Prater, J. T. Scoville, and E. J. Strait. *Phys. Plasmas*, 9:2051, 2002.

[49] A. I. Smolyakov. *Plasma Phys. Control. Fusion*, 35:657, 1993.

[50] C. C. Hegna. *Phys. Plasmas*, 5:1767, 1998.

[51] Z. Chang, J. D. Callen, E. D. Fredrickson, R. V. Budny, C. C. Hegna, K. M. Mcguire, and M. C. Zarnstorff. *Phys. Rev. Lett.*, 74:4663, 1995.

[52] R. Carrera, R. D. hazeltime, and M. Kotschenreuther. *Phys. Fluids*, 29:899, 1986.

[53] E. J. Caramana, R. A. Nebel, and D. D. Schnack. *Phys. Fluids*, 26:1305, 1983.

[54] A. Y. Aydemir and D. C. Barnes. *Phys. Rev. Lett*, 52:930, 1984.

[55] D. D. Schnack, E. J. Caramana, and R. A. Nebel. *Phys. Fluids*, 28:321, 1985.

[56] J. A. Holmes, B. A. Carreras, T. C. Hender, H. R. Hicks, V. E Lynch, Z. G. An, and P. H. Diamond. *Phys. Fluids*, 28:261, 1985.

[57] S. Cappello and D. F. Escande. *Phys. Rev. Lett.*, 85:3838, 2000.

[58] X. Shan and D. Montgomery. *Plasma Phys. Control. Fusion*, 35:1019, 1993.

[59] O. D. Gurcan, P. H. Diamond, T. S. Hahm, and Z. Lin. *Phys. Plasmas*, 12(3):032303, 2005.

[60] T. S. Hahm, P. H. Diamond, Z. Lin, K. Itoh, and S.-I. Itoh. *Plasma Phys. Control. Fusion*, 46:A323, 2004.

[61] Z. Lin and T. S. Hahm. *Phys. Plasmas*, 3:1099, 2004.

[62] P. K. Kaw, E. J. Valeo, and P. H. Rutherford. *Phys. Rev. Lett.*, 43:1398, 1979.

[63] H. R. Strauss. *Phys. Fluids*, 29(11):3668, 1986.

[64] K. Itoh, S-I Itoh, and A. Fukuyama. *Phys. Rev. Lett.*, 69:1050, 1992.

[65] P. H. Diamond, R. D. Hazeltine, Z. G. An, B. A. Carreras, and H. R. Hicks. *Phys. Fluids*, 27(6):1449, 1984.

[66] S.-I. Itoh, K. Itoh, and M. Yagi. *Plasma Phys. Control. Fusion*, 46:123, 2004.

[67] M. Yagi, S. Yoshida, S.-I. Itoh, H. Naitou, H. Nagahara, J.N. Leboeuf, K. Itoh, T. Matsumoto, S. Tokuda, and M. Azumi. *Nucl. Fusion*, 45:900, 2005.

[68] R. Trines, R. Bingham, L. O. Silva, J. T. Mendonca, P. K. Shukla, and W. B. Mori. *Phys. Rev. Lett.*, 94:1650021, 2005.

[69] I. Gruzinov, A. Das, P. H. Diamond, and A. Smolyakov. *Phys. Letters A*, 302:119, 2002.

[70] P. N. Guzdar, R. G. Kleva, A. Das, and P. K. Kaw. *Phys. Rev. Lett.*, 87:1015001, 2001.

[71] A. Bondeson and J. R. Sobel. *Phys. Fluids*, 27(8):2028, 1984.

[72] F. Porcelli. *Phys. Fluids*, 30(6):1734, 1987.

[73] L. D. Pearlstein and H. L. Berk. *Phys. Rev. Lett*, 23(5):220, 1969.

[74] M. N. Rosenbluth and F. L. Hinton. *Phys. Rev. Lett.*, 80(4):724, 1998.

[75] K. C. Shaing, C. C. Hegna, J. D. Callen, and W. A. Houlberg. *Nucl. Fusion*, 43:258, 2003.

[76] M. A. Pedrosa, C. Hidalgo, A. Lopez-Fraguas, B.PH. Van Milligen, R. Balbin, J. A. Jimenez, E. Sanchez, J. Castellano, L. Garcia the TJ-II team, B. A. Carreras, and V. E. Lynch. *Czech J. Phys*, 50(12):1463, 2000.

[77] G. S. Lee and P. H. Diamond. *Phys. Fluids*, 29:3291, 1986.

[78] V. B. Lebedev, P. H. Diamond, V. D. Shapiro, and G. I. Soloviev. *Phys. Plasmas*, 2:4420, 1995.

[79] J. E. Rice, M. Greenwald, I. H. Hutchinson, E. S. Marmar, Y. Takase, S. M. Wolfe, and F. Bombarda. Observation of central toroidal rotation in icrf heated alcator c-mod plasmas. *Nucl. Fusion*, 38:75, 1998.

[80] J. E. Rice, A. Ince-Cushman, J. S. deGrassie, et al. Intermachine comparison of intrinsic rotation. pages EX/p3–12, Vienna, 2006. 21th IAEA Fusion Energy Conference, Chengdu, China, International Atomic Energy Agency.

[81] S. I. Itoh. Anomalous viscosity due to drift wave turbulence. *Phys. Fluids B*, 4(4):796, 1992.

[82] N. Mattor and P. H. Diamond. Momentum and thermal transport in neutral-beam-heated tokamaks. *Phys. Fluids*, 31(5):1180–1189, 1988.

[83] K. C. Shaing. Toroidal momentum confinement in neoclassical quasilinear theory in tokamaks. *Phys. Plasmas*, 8(1):193–198, 2001.

[84] A. G. Peeters, C. Angioni, and D. Strintzi. Toroidal momentum pinch velocity due to the coriolis drift effect on small scale instabilities in a toroidal plasma. *Phys. Rev. Lett.*, 98(26):265003, 2007.

[85] T. S. Hahm, P. H. Diamond, O. D. Gurcan, and G. Rewoldt. Nonlinear gyrokinetic theory of toroidal momentum pinch. *Physics of Plasmas*, 14(7):072302, 2007.

[86] Ö. D. Gürcan, P. H. Diamond, and T. S. Hahm. Turbulent equipartition and homogenization of angular momentum. submitted to Phys. Rev. Lett., 2007.

[87] Ö. D. Gürcan, P. H. Diamond, T. S. Hahm, and R. Singh. Intrinsic rotation and electric field shear. *Phys. Plasmas*, 14:042306, 2007.

[88] Y. B. Kim, P. H. Diamond, Biglari, and P. W. Terry. Theory of resistivity-gradient-driven turbulence in a differentially rotating plasma. *Phys. Fluids B*, 2(9):2143, 1990.

[89] R. R. Dominguez and G. M. Staebler. Anomalous momentum transport from drift wave turbulence. *Phys. Fluids B*, 5:3876–3886, 1993.

[90] P. H. Diamond, V. B. Lebedev, Y. M. Liang, A. V. Gruzinov, I. Gruzinova, and M. Medvedev. Dynamics of the L-H transition, VH-mode evolution, edge localized modes and r.f. driven confinement control in tokamaks. In *Proc. of the 15th IAEA Fusion Energy Conference, Seville, Spain*, pages IAEA–CN–60/D–2–II–6, Vienna, 1994. International Atomic Energy Agency.

[91] X. Garbet, Y. Sarazin, P. Ghendrih, S. Benkadda, P. Beyer, C. Figarella, and I. Voitsekhovitch. Turbulence simulations of transport barriers with toroidal velocity. *Phys. Plasmas*, 9(9):3893–3905, 2002.

[92] J. R. Myra, J. Boedo, B. Coppi, D. A. D'Ippolito, S. I. Krasheninnikov, B. P. LeBlanc, M. Lontano, R. Maqueda, D. A. Russell, D. P. Stotler, M.C. Varischetti, S.J. Zweben, and the NSTX Team. Blob transport models, experiments, and the accretion theory of spontaneous rotation. In *Proc. of the 21th IAEA Fusion Energy Conference, Chengdu, China*, pages IAEA/TH–P6–21, Vienna, 2006. International Atomic Energy Agency.

[93] L. Chen. *Journal of Geophysical Research*, 104:2421, 1999.

[94] R. Z. Sagdeev and A. A. Galeev. *Nonlinear Plasma Theory*. New York, W. A. Benjamin, 1969.

[95] P. H. Diamond and Y.-B. Kim. Theory of mean poloidal flow generation by turbulence. *Phys. Fluids B*, 3(7):1626–1633, 1991.

[96] H. L. Berk and K. Molvig. Nonintrinsic ambipolar diffusion in turbulence theory. *Phys. Fluids*, 26:1385, 1983.

[97] J. Krommes. *Phys. Fluids B*, 5:1066, 1993.